学 位 論 文

A novel insight into the pathogenesis of refractory sight-threatening ocular diseases

（難治性眼疾患に対する新たな病態形成機序の解明）

2020 年 9 月

北 海 道 大 学

呉 迪

Di WU

学 位 論 文

A novel insight into the pathogenesis of refractory sight-threatening ocular diseases

（難治性眼疾患に対する新たな病態形成機序の解明）

2020 年 9 月

北 海 道 大 学

呉 迪

Di WU

Table of Contents

List of Publications and Presentations

A part of this study was published in the following papers.

1. Di Wu, Atsuhiro Kanda, Ye Liu, Satoru Kase, Kousuke Noda, and Susumu Ishida. Galectin-1 promotes choroidal neovascularization and subretinal fibrosis mediated via epithelial-mesenchymal transition. *FASEB J.* 2019;33:2498-2513.
2. Di Wu, Kousuke Noda, Miyuki Murata, Ye Liu, Atsuhiro Kanda, and Susumu Ishida. Regulation of spermine oxidase through hypoxia-inducible factor-1α signaling in retinal glial cells under hypoxic condition. *Invest Ophthalmol Vis Sci*. in press

A part of this study was presented in the following conferences.

1. Di Wu, Atsuhiro Kanda, Miyuki Murata, Susumu Ishida. The vicious cycle of TGF-β autoinduction contributes to VEGF-A expression in Müller glial cells. Association for Research in Vision and Ophthalmology (ARVO) Annual Meeting, May 3 - May 7, 2020, Baltimore, USA. (Poster presentation)
2. Di Wu, Atsuhiro Kanda, Miyuki Murata, Susumu Ishida. TGF-β causes VEGF-A expression forming the vicious cycle of TGF-β autoinduction. 第 124 回日本眼科学会総会, 2020 年 4 月 16 - 19 日，東京. (Poster presentation)
3. Di Wu, Kousuke Noda, Miyuki Murata, Ye Liu, Atsuhiro Kanda, Susumu Ishida. Hypoxia inducible factor-1 regulates spermine oxidase leading to acrolein generation in Müller Glial cells. Association for Research in Vision and Ophthalmology (ARVO) Annual Meeting, Apr 28 - May 2, 2019, Vancouver, Canada. (Poster presentation)
4. Di Wu, Miyuki Murata, Kousuke Noda, Ye Liu, Atsuhiro Kanda, Susumu Ishida. Hypoxia aggravates acrolein generation via HIF-1/SMOX pathway in glial cells. 第 123 回日本眼科学会総会, 2019 年 4 月 18 - 21 日，東京. (Poster presentation)
5. Di Wu, Atsuhiro Kanda, Ye Liu, Kousuke Noda, Susumu Ishida. Galectin-1 promotes choroidal neovascularization and subretinal fibrosis mediated via epithelial-mesenchymal transition. 第 23 回眼科分子生物学研究会, 2019 年 1 月 16 - 17 日，名古屋. (Oral presentation)

6. Di Wu. The involvement of galectin-1/Lgals1 in choroidal neovascularization. 13th Japan-Korea International Symposium in Ophthalmology, November 6, 2018, Sapporo, Japan. (Oral presentation)
7. Di Wu, Atsuhiro Kanda, Ye Liu, Kousuke Noda, Susumu Ishida. The involvement of galectin-1/Lgals1 in choroidal neovascularization. ARVO 2018 Overview Meeting, May 2, 2018, Honolulu, USA. (Oral presentation)
8. Di Wu, Atsuhiro Kanda, Ye Liu, Kousuke Noda, Susumu Ishida. The involvement of galectin-1/Lgals1 in choroidal neovascularization. 第 122 回日本眼科学会総会, 2018 年 4 月 19 - 22 日，大阪. (Oral presentation)
9. Di Wu, Miyuki Murata, Kousuke Noda, Ye Liu, Atsuhiro Kanda, Susumu Ishida. Modulation of spermine oxidation in Müller glial cells under hypoxic condition. ARVO Annual Meeting, May 7 - May 11, 2017, Baltimore, USA. (Poster presentation)
10. Di Wu, Miyuki Murata, Kousuke Noda, Ye Liu, Atsuhiro Kanda, Susumu Ishida. Hypoxia induces hydrogen peroxide generation via spermine oxidase in glial cells. 第 121 回日本眼科学会総会, 2017 年 4 月 6 - 9 日，東京. (Poster presentation)

Summary

Chapter I: Galectin-1 promotes choroidal neovascularization and subretinal fibrosis mediated *via* epithelial-mesenchymal transition

Purpose: Galectin-1, encoded by the *LGALS1* gene, is a recently recognized angiogenic factor associated with diabetic retinopathy. In this study, we investigate the involvement of galectin-1/*Lgals1* in choroidal neovascularization (CNV) and subretinal fibrosis using the mouse model of laser-induced CNV.

Methods: Laser photocoagulation was performed to induce CNV in *Lgals1* knockout and control mice. Seven days after laser treatment, the area of CNV and subretinal fibrosis were evaluated using a flat mount technique. Gene expression levels of *Lgals1* and inflammatory mediators, as well as epithelial-mesenchymal transition (EMT) markers, were evaluated using real-time quantitative PCR. Protein levels of phosphorylated extracellular signal-regulated kinase (p-ERK), phosphorylated SMAD family member (p-SMAD)2 and α-smooth muscle actin (SMA) were analyzed by immunoblot analysis.

Results: Neither deletion nor overexpression of *Lgals1* affected physiological retinal development or visual function. Galectin-1/*Lgals1* was upregulated by CNV induction, while deletion of *Lgals1* suppressed CNV together with vascular endothelial growth factor receptor (VEGFR)2's downstream molecules. Loss of *Lgals1* also attenuated subretinal fibrosis, expression of EMT markers including *Snai1*, and phosphorylation of SMAD2. Supporting these *in vivo* findings, silencing of *LGALS1* in human retinal pigment epithelium (RPE) cells inhibited transforming growth factor (TGF)-β1-induced EMT-related molecules and cell motilities. Conversely, overexpression of *Lgals1* enhanced CNV and subretinal fibrosis. Age-related macular degeneration (AMD) patient specimens demonstrated co-localization of galectin-1 with VEGFR2 in neovascular endothelial cells and with phosphorylated SMAD2 in RPE cells.

Conclusions: These results suggested a biological significance of galectin-1 as a key promotor for both angiogenesis and fibrosis in eyes with AMD.

Chapter II: Regulation of spermine oxidase through hypoxia-inducible factor-1α signaling in retinal glial cells under hypoxic condition

Purpose: Acrolein, a highly reactive unsaturated aldehyde, is known to facilitate glial cell migration, one of the pathological hallmarks in diabetic retinopathy (DR), in an autocrine fashion. However, cellular mechanisms of acrolein generation in retinal glial cells remains elusive. In the present study, we investigated the production mechanism of spermine oxidase (SMOX), which is related to acrolein generation, in retinal Müller glial cells under hypoxic condition.

Methods: Immunofluorescence staining was performed to show the localization of SMOX in glial cells of fibrovascular tissues obtained from patients with proliferative diabetic retinopathy. Rat retinal Müller cell line 5 (TR-MUL5) cells were cultured under either normoxic (20% O_2) or hypoxic (1% O_2) conditions. Expression levels of polyamine oxidation enzymes including SMOX were analyzed using real-time quantitative PCR and enzyme-linked immunosorbent assay (ELISA). Either hypoxia-inducible factor-1α (*Hif1*a) or *Hif2*a were knocked down by siRNA in TR-MUL5 cells. The transcriptional activity of SMOX in TR-MUL5 cells was evaluated using the luciferase assay. Levels of acrolein-conjugated protein, N^{ε}-(3-formyl-3,4-dehydropiperidino) lysine adduct (FDP-Lys), and hydrogen peroxide, were measured.

Results: SMOX was localized in glial cells in fibrovascular tissues. Hypoxia induced SMOX production in TR-MUL5 cells, which were suppressed by silencing of *Hif1*a, but not *Hif2*a. Transcriptional activity of SMOX was regulated through HIF-1 binding to hypoxia response elements 2, 3, and 4 sites in the promoter region of SMOX. Generation of hydrogen peroxide and FDP-Lys increased in TR-MUL5 cells under hypoxic conditions, which were abrogated by MDL72527, a specific inhibitor of SMOX.

Conclusions: The current data demonstrated that hypoxia regulates production of SMOX, which plays a role in the generation of oxidative stress inducers, through HIF-1α signaling in Müller glial cells under hypoxic condition.

Chapter III: Transforming growth factor-β contributes to angiogenesis and Müller glial-mesenchymal transition in the pathogenesis of proliferative diabetic retinopathy

Purpose: TGF-β, a multifunctional protein, regulates various pivotal biological responses and

contributes to the pathogenesis of ocular diseases. This study aimed to investigate the molecular mechanism of TGF-β-induced VEGF-A production in Müller glial cells and the involvement of fibrovascular tissue formation in DR.

Methods: Human Müller glial cells were treated with various pro-fibrotic cytokines including TGF-β1 and -β2, to evaluate changes in gene expression using real-time quantitative PCR. Immunoblot analyses were performed to detect the activation of TGF-β induced downstream signals. Additionally, immunofluorescence analyses were conducted to evaluate the co-localization of VEGF-A and TGF-β1/2, TGF-β receptor (TβR), and myofibroblast markers in fibrovascular tissues obtained from eyes of patients with proliferative DR.

Results: Of various pro-fibrotic cytokines, TGF-β1/2 application to Müller cells exclusively increased mRNA expression of *VEGFA*, which was abolished by pretreatment with anti-TβR-neutralizing antibody and phosphatidylinositol-3 kinase, p38 mitogen-activated protein kinase (MAPK), and SMAD2 inhibitors. Moreover, administration of TGF-β1/2 upregulated *TGFB1* and *TGFB2* mRNA expression in an autocrine manner, which was suppressed by glycogen synthase kinase-3, p38 MAPK and nuclear factor-κB inhibitors. Supporting these findings, the administration of TGF-β1/2 increased the phosphorylation of these intracellular signaling. Fibrovascular tissues from patients with proliferative DR demonstrated co-localization of VEGF-A, TGF-β1/2, TβRI/II, and myofibroblast markers in glial cells.

Conclusions: Our data indicate that the TGF-β/TβR axis activates its downstream signaling pathways in Müller glial cells, causing VEGF-A production (angiogenesis) forming the vicious cycle of TGF-β autoinduction (fibrogenesis) concurrently in DR.

Introduction

Vision loss not only causes suffering to patients, but also brings misfortune to the family and society. As the world's population and average life expectancy have increased, the World Health Organization estimated that 39 million individuals were blind (defined as best-corrected Snellen visual acuity equivalent as 20/400 or worse in the better-seeing eyes) and 246 million suffered from visual impairment (defined as 20/40 to better than 20/400 in the better-seeing eye) in 2020 (Finger et al., 2011; Koberlein et al., 2013). In the past 20 years, cataract, glaucoma, degenerative myopia, age-related macular degeneration (AMD) and diabetic retinopathy (DR) are the most common causes of blindness and vision impairment worldwide (Congdon et al., 2004; Sommer et al., 1991; Yamada et al., 2010). Among them, AMD and DR are frequent retinal degenerative diseases, and responsible for the majority of cases of blindness due to retinal disease. Therefore, to investigate the molecular pathogenesis of AMD and DR are helpful to disclose novel therapeutic targets to those patients suffering from refractory AMD and DR.

AMD is currently considered the leading cause of irreversible visual loss in people aged 65 years and older in the developed countries. It is estimated the globally around 200 million people will have AMD in 2020, increasing to nearly 300 million in 2040 (Wong et al., 2014). AMD is typically classified into two phenotypic categories: non-neovascular (drusen and retinal pigment epithelium abnormalities) and neovascular (choroidal neovascular membrane formation). Although only 10% of patients with AMD have the neovascular form, 90% of AMD patients with significant vision loss have the neovascular form of the disease (Ferris et al., 1984). The early stage of neovascular AMD (nAMD) is recognized by the presence of medium-sized drusen or retinal pigmentary changes in the macular region. Late AMD is defined by the presence of signs indicating either neovascular or atrophic AMD. Choroidal neovascularization (CNV), a form of fibrovascular proliferation beneath the central retina (macula), is a characteristic feature of AMD responsible for severe vision loss and blindness worldwide (Wong et al., 2014). The CNV tissue penetrates Bruch's membrane (type 1 CNV) and the retinal pigment epithelium (RPE) monocellular layer (type 2 CNV), leading eventually to the development of subretinal fibrosis together with permanent photoreceptor

damage and vison loss (Friedlander, 2007; Swaroop et al., 2009) (Fig. 1).

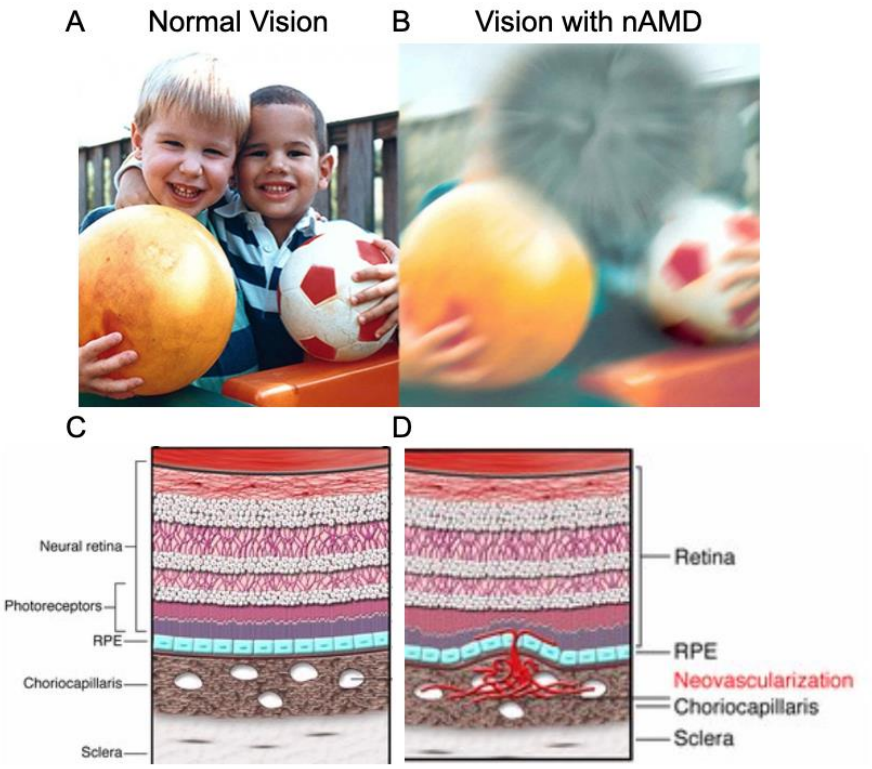

Modified from the Angiogenesis foundation

Figure 1. Schematic of nAMD. Vision field of a healthy person (A) and a nAMD patient (B), with central vision loss and distortion. Schema of the retina and choroid structure of a healthy person (C) and a nAMD patient with CNV (D), which originates from choriocapillaris and extends into the subretinal or sub-RPE space. These immature neovessels can cause subretinal fluid, hemorrhage, and fibrosis, leading to central vision loss and blindness.

Of numerous cytokines and growth factors contributing to the molecular pathogenesis of neovascular AMD, vascular endothelial growth factor (VEGF)-A has proved as a key inflammatory and angiogenic mediator in CNV generation (Miller et al., 2013). To date, anti-VEGF therapy has become the standard treatment for improving visual function in many nAMD patients, unsuccessful treatment outcomes have often been attributed to the progression of subretinal fibrosis (Bloch et al., 2013; Daniel et al., 2014). Therefore, it is necessary to investigate the pathogenic molecules involved in both CNV and subretinal fibrosis formation

in the eye with AMD.

Galectin-1, encoded by lectin, galactoside-binding, soluble (*LGALS*)1 gene, has been shown to play a role in regulating cell growth, migration, and proliferation without having its specific receptors like cytokines do (Camby et al., 2006). Previously, galectin-1 was shown to be an agonistic ligand for VEGF receptor 2, leading its downstream signal transduction in endothelial cells to promote angiogenesis (Croci et al., 2014). Moreover, galectin-1 levels increased in patient eyes along with clinical severity of DR, and were not correlated with elevated VEGF-A levels (Kanda et al., 2017; Kanda et al., 2015). In addition to angiogenesis, galectin-1 was demonstrated to be involved in mesenchymal activity in various cells, including gastric cancer cells, pancreatic stellate cells and fibroblasts (Lim et al., 2014; Tang et al., 2018; Zheng et al., 2016). In the present study, we elucidated galectin-1 involvement in the mouse model of laser-induced CNV and subretinal fibrosis, both of which represent the pathogenesis of AMD. Our present data highlight the biological significance of galectin-1 as a key promotor for both angiogenesis and fibrosis in eyes with AMD. The detailed content of this study is in **Chapter 1**.

DR is a sight-threatening complication of systemic diabetes mellitus, which results from damages to the blood vessels of the retina. It is progressive retinopathy, the severity of which ranges from mild non-proliferative diabetic retinopathy (NPDR) to more advanced proliferative diabetic retinopathy (PDR) (Fig. 2). PDR is characterized by the proliferation of fibrovascular tissue formed by the extension of retinal angiogenesis into the vitreous cavity, and the fibrovascular tissue formation leads to serious complications including traction retinal detachment and vitreous hemorrhage. To date, basic and clinical researches suggest that VEGF-A induced by hypoxia plays a crucial role in retinal neovascularization, which eventually leads to fibrovascular proliferation in late-stage of diabetic retinopathy (Ip et al., 2015; Marhoffer et al., 1994).

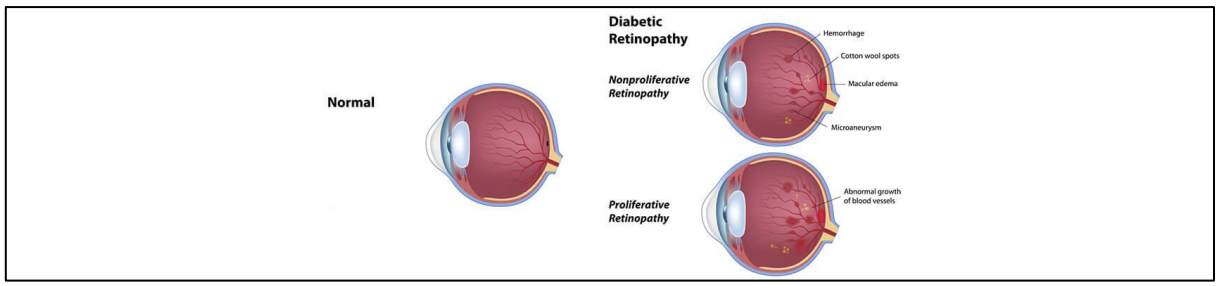

Figure 2. Schematic of normal retina compared with NPDR and PDR. The normal healthy retina includes healthy retinal blood vessels. In contrast, the retina in diabetic retinopathy exhibits multiple abnormalities, including vascular changes.

Acrolein is a highly reactive unsaturated aldehyde that causes dysfunction of multiple proteins. Although acrolein was previously considered as an exogenous pollutant, it has been elucidated that acrolein is also produced endogenously and participates in the pathogenesis of systemic diseases including Alzheimer's disease, brain infarction, cardiovascular diseases, diabetes and others (DeJarnett et al., 2014; Feroe et al., 2016; Huang et al., 2013; Saiki et al., 2009). Previously, our group has reported the pathological role of acrolein in DR and revealed that semicarbazide-sensitive amine oxidase (SSAO) plays a role in acrolein generation in retinal microvascular endothelial cells (Murata et al., 2017; Murata et al., 2019). In addition, we also found that staining signal of acrolein was remarkable in glial cells in fibrovascular tissues obtained from patients with PDR (Dong et al., 2017). However, it is still unknown about the production mechanism of acrolein in glial cells, because glial cells lack SSAO. In the present study, we highlighted that hypoxia regulates the production of spermine oxidase, which plays a role in the generation of oxidative stress inducers, through hypoxia-inducible factor-1 signaling in Müller glial cells under hypoxic conditions. The detailed content of this study is in **Chapter 2**.

VEGF-A, a well-known angiogenic factor, contributes to the principal pathogenic events of DR. Müller glial cells has been demonstrated as the major cellular source of VEGF-A, and involved in the fibrovascular tissue formation in patients with PDR (Adamis et al., 1994; Guidry et al., 2009; Le, 2017). Transforming growth factor (TGF)-β, a multifunctional cytokine, regulates multiple pivotal biological responses, such as proliferation, differentiation, migration and, is regarded as the major trigger of epithelial-mesenchymal transition (EMT) and tissue fibrosis in various organs (Massague, 1998). Activation of TGF-β/its receptor axis induces several cytokines and growth factor expression including VEGF-A, which promotes the inflammatory and angiogenic activity of numerous disorders (Cheon et al., 2002; Qian et al., 2004; Wang et al., 2004). Recently, we reported that TGF-β increases several EMT-related

molecular marker expression and cell motility in human retinal Müller glial cells, induces Müller glial-mesenchymal transition, as an alternative to EMT, in the pathogenesis of idiopathic epiretinal membrane (Kanda et al., 2019). In the present study, we demonstrated the molecular mechanism of TGF-β-induced VEGF-A production in Müller glial cells and the involvement of TGF-β in fibrovascular tissue formation of PDR. The detailed content of this study is in **Chapter 3.**

List of Abbreviations

ACTA2/α-SMA	α-smooth muscle actin
ANOVA	analysis of variance
AMD	age-related macular degeneration
CCL	C-C motif chemokine ligand
CNV	choroidal neovascularization
COL1A1	type I collagen
DAPI	4’,6-diamidine-2’-phenylindole dihydrochloride
DMSO	dimethyl sulfoxide
DR	diabetic retinopathy
EMT	epithelial-mesenchymal transition
ERG	electroretinography
ERK	extracellular signal-regulated kinase
FBS	fetal bovine serum
FGF	fibroblast growth factor
FN1	fibronectin
GAPDH	glyceraldehyde-3-phosphate dehydrogenase
GFAP	glial fibrillary acidic protein
GMT	glial-mesenchymal transition
GS	glutamine synthetase
GSK-3	glycogen synthase kinase
HIF	hypoxia-inducible factor
HRE	hypoxia response elements
ICAM	intercellular adhesion molecule
iERM	idiopathic epiretinal membrane
JNK	c-Jun N-terminal kinase
LGALS	lectin, galactoside-binding, soluble
MAPK	mitogen-activated protein kinase
MCP	monocyte chemotactic protein

NF-κB	nuclear factor-κB
NGF	nerve growth factor
Paox	peroxisomal N(1)-acetyl-spermine/spermidine oxidase
PBS	phosphate-buffered saline
PDGF	platelet-derived growth factor
PDR	proliferative diabetic retinopathy
PI3K	phospharidylinositol-3 kinase
RPE	retinal pigment epithelium
SAT1	spermine N1-acetyltransferase
SEM	standard error of the mean
siRNA	small interfering RNA
SM22	smooth muscle protein 22
SMAD2	SMAD family member 2
SMOX	spermine oxidase
SNAI	Snail family transcriptional repressor
SSAO	semicarbazide-sensitive amine oxidase
TGF-β	transforming growth factor-β
TβR	transforming growth factor-β receptor
VEGF	vascular endothelial growth factor
VEGFR	vascular endothelial growth factor receptor

Chapter 1

Galectin-1 promotes choroidal neovascularization and subretinal fibrosis mediated *via* epithelial-mesenchymal transition

Introduction

Galectin-1, encoded by the lectin, galactoside-binding, soluble (*LGALS1*) gene, is a lectin family protein that recognizes galactose-containing sugar chains and exerts various biological actions through its binding to receptors depending on their glycosylation profile, rather than its specific cognate receptors (Camby et al., 2006). Recently, we and others showed that galectin-1 binds to the *N*-glycans of vascular endothelial growth factor receptor (VEGFR)2, activating its downstream signal transduction in endothelial cells and promoting angiogenesis in cancer and proliferative diabetic retinopathy (PDR) (*i.e.*, neovascular) (Croci et al., 2014; Kanda et al., 2015). Meanwhile, we demonstrated that elevated levels of galectin-1 significantly associated with neovascular pathogenesis of diabetic retinopathy (DR) (Kanda et al., 2015). However, there was no correlation between vascular endothelial growth factor (VEGF)-A and galectin-1 expression levels in PDR eyes, suggesting distinctly different regulatory mechanisms (*i.e.*, upstream stimuli for induction) between galectin-1 and VEGF-A, although these two proangiogenic molecules are hypoxia-induced (Kanda et al., 2015). Indeed, we have recently revealed a hypoxia-independent inflammatory pathway to produce galectin-1 in retinal Müller glial cells, explaining the upregulation of galectin-1 in eyes with DR eyes along with the progression of clinical stages from the pre-ischemic clinical stage with macular edema (Kanda et al., 2017). However, the major cellular participants during choroidal neovascularization (CNV) development are not Müller glial cells but RPE cells, and thus galectin-1 involvement in eyes of age-related macular degeneration (AMD) patients remains unknown.

Subretinal fibrosis, a wound healing response that follow CNV in AMD, is accompanied by destruction of photoreceptors, RPE, and choroidal vessels, leading to severe vision loss (Bloch et al., 2013; Daniel et al., 2014). The epithelial-mesenchymal transition (EMT) plays a physiological role in embryonic development and wound healing, while EMT dysfunction leads to severe pathological reactions, including carcinogenesis and fibrogenesis

(Kalluri and Weinberg, 2009; Lamouille et al., 2014; O'Connor and Gomez, 2014). During EMT, epithelial cells in alignment lose attachment to neighboring cells, acquire elongated morphology, and exhibit increased motility. Transforming growth factor (TGF)-β, a major trigger of EMT in tissue remodeling and fibrosis, has been reported to induced the phosphorylation and translocation of SMAD family proteins, leading to the differentiation of fibroblast into myofibroblast (Kalluri and Weinberg, 2009; Lamouille et al., 2014; O'Connor and Gomez, 2014). Moreover, AMD patient specimens and experimental animal models, previous studies including ours have revealed the involvement of TGF-β-SMAD-driven EMT in RPE cells to the development of subretinal fibrosis (Hirasawa et al., 2011; Iwanishi et al., 2016). In addition to angiogenesis, galectin-1 has also been shown to be involved in mesenchymal activity via the SMAD family member (SMAD)2 signaling in several cells including gastric cancer cells and pancreatic stellate cells as well as fibroblasts (Lim et al., 2014; Tang et al., 2018). Importantly, galectin-1 stimulated the phosphorylation of SMAD2 through its molecular interaction with SMAD2 in lung fibroblasts, thus promoting pulmonary fibrosis (Kathiriya et al., 2017; Tang et al., 2018). As concerns the eye, however, there have been no study reported on the profibrotic role of galectin-1 in fibrogenic disorders such as neovascular AMD.

In the present study, using the mouse model of laser-induced CNV, we elucidated the involvement of galectin-1 in the pathogenesis of CNV and subretinal fibrosis, both of which represent the pathogenesis of AMD.

Methods

Animals

Lgals1$^{+/-}$ mice heterozygously deficient in galectin-1 on C57BL/6J background were purchased from Jackson Laboratory (Bar Harbor, ME), and homozygous *Lgals1*$^{-/-}$ mice were generated via mating for experimental use. Concurrently acquired *Lgals1*$^{+/+}$ littermates served as control mice. *Lgals1*-overexpressing transgenic (*Lgals1*-Tg) mice were generated under control of the cytomegalovirus early enhancer/chicken β-actin promoter (Transgenic Inc., Kobe, Japan). Mouse *Lgals1*-coding region (GenBankTM number NM_008495) with the Kozak consensus sequence was subcloned into a *pCAGGS* vector (Niwa et al., 1991) (Fig. 3). The purified transgene DNA, excluding the vector backbone, was injected into fertilized C57BL/6J mouse oocytes, which were implanted into pseudopregnant females. The founders were bred to C57BL/6J mice (CLEA Japan, Tokyo, Japan) to generate F1 progeny. Their nontransgenic (*Lgals1*-nonTg) littermates served as control mice. All animal experiments were performed following the guidelines of the Association for Research in Vision and Ophthalmology (ARVO) Statement for the Use of Animals in Ophthalmic and Vision Research. The experimental protocols were approved by the Ethics Review Committee for Animal Experimentation of Hokkaido University.

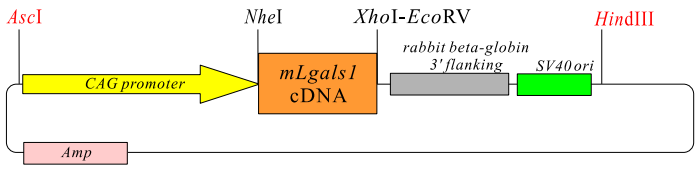

pCAGGS-mLgals1 Expression vector

CAG: cytomegalovirus early enhancer/chicken β-actin promoter

Figure 3. Construction of *pCAGGS-mLgals1* expression vector.

Immunoblot analyses

The tissues and cells were lysed in SDS buffer. After quantifying protein concentrations using BCA reagent (Thermo Fisher Scientific, Waltham, MA), proteins were resolved by SDS-PAGE (polyacrylamide gel electrophoresis) and transferred to polyvinylidene difluoride (PVDF) membrane (Merck Millipore, Burlington, MA) by electroblotting. Membranes were

incubated with the following primary antibodies: goat anti-galectin-1 (1:1,000), mouse anti-α-smooth muscle actin (SMA) (1:1,000; R&D systems, Minneapolis, MN), rabbit anti-extracellular signal-regulated kinase (ERK)1/2 (1:1,000), rabbit anti-phosphorylated ERK1/2 (1:1,000), rabbit anti-SMAD2 (1:1,000), rabbit anti-phosphorylated SMAD2 (1:1,000; Cell Signaling Technology, Danvers, MA, USA), and mouse anti-glyceraldehyde-3-phosphate dehydrogenase (GAPDH) (1:1,000; Thermo Fisher Scientific) antibodies. Horseradish peroxidase-conjugated anti-goat, anti-mouse, and anti-rabbit IgGs (1:4,000, Jackson ImmunoResearch Laboratories) were used as secondary antibodies for chemoluminescence detection (Western Lightning Ultra; Perkin Elmer, Waltham, MA, USA). Signals were obtained by enhanced chemoluminescence (Western Lightning Ultra, Perkin Elmer, Waltham, MA). The bands were analyzed by densitometry using ImageJ software (National Institutes of Health, Bethesda, MD).

Immunofluorescence microscopy

Mouse eyeballs were fixed in 4% paraformaldehyde (PFA) for 1 hour on ice, incubated in an increasing concentration of phosphate buffered saline (PBS)/sucrose (5, 10, 20%), and embedded in Frozen Section compound (Leica, Exton, PA). For antibody staining, sections were washed with PBS containing 0.05% Triton X-100, and then blocked in PBS containing 0.05% Triton X-100 and 5% goat serum. Sections were probed with the following primary antibodies: goat anti-galectin-1 (1:200; R&D systems), mouse anti-rhodopsin (1:500), rabbit anti-cone arrestin (CAR) (1:100), rabbit anti-calbindin (1:100), mouse anti-glutamine synthetase (GS) (1:200; Millipore, Temecula, CA), sheep anti-CHX10 (also known as VSX2, visual system homeobox 2) (1:50; Abcam, Cambridge, MA), mouse anti-paired box protein (PAX6) (1:50; Developmental Studies Hybridoma Bank, Iowa, IA), goat anti-BRN3 (also known as POU4F1, POU class 4 homeobox 1) (1:50, Santa Cruz Biotechnology, Santa Cruz, CA), and isolectin B4-Alexa 488 (1:400; Thermo Fisher Scientific) antibodies. The secondary antibodies for fluorescent detection were Alexa Fluor 488 and 546 (1:200; Thermo Fisher Scientific). Sections were visualized under a FluoView FV1000 confocal microscope (Olympus, Tokyo, Japan).

For whole mounts, eyes were fixed in 4% PFA for 15 min on ice and washed in PBS.

Detaching the retina from the eyecup, retinal cups were post-fixed and stored in methanol at -20 °C. Retinas were pre-incubated with PBS containing 0.3% Triton and 5% goat serum, and probed with isolectin B4-Alexa 488 (1:100; Thermo Fisher Scientific). Vascular parameters were measured using the AngioTool software (National Institute of Health National Cancer Institute, Gaithersburg, MD) (Zudaire et al., 2011).

AMD patient specimens were obtained in our clinic by enucleation due to suspected melanoma from an 82-year-old male with massive subretinal and vitreous hemorrhage secondary to CNV. This study was approved by the Ethics Committee of Hokkaido University Hospital, and written informed consent was obtained from the patient after an explanation of the purpose and consequence of this study. The enucleated globe was fixed with 4% PFA and embedded with paraffin. Sections were deparaffinized and hydrated through exposure with xylene and graded alcohols followed by water. As a pretreatment, microwave-based antigen retrieval was performed in 10 mM citrate buffer (pH 6.0). These slides were incubated with the following primary antibodies: mouse anti-galectin-1 (1:50; Santa Cruz Biotechnology), rabbit anti-CD34 (1:100), mouse anti-RPE65 (1:100), rabbit anti-galectin-1 (1:100; Abcam), goat anti-VEGFR2 (1:100), mouse anti-TGF-β1 (1:50; R&D systems), rabbit anti-phosphorylated SMAD2 (1:100; Cell Signaling Technology), and rabbit anti-type I collagen (1:100; Thermo Fisher Scientific) antibodies. A Keyence BZ-9000 microscope was used for photomicrographs.

Electroretinography (ERG)

ERG recordings were performed with a white light-emitting diode luminescent electrode placed on the cornea (Mayo, Aichi, Japan). The pupils were dilated with a mixed solution of 0.5% tropicamide and 0.5% phenylephrine (Santen, Osaka, Japan). ERG was recorded at 2-month-old mice after anesthetized with an intraperitoneal injection of ketamine at 50 mg/kg body weight (Daiichi-Sankyo, Tokyo, Japan) after animals were dark-adapted for 12-14 hours (overnight) for scotopic ERG and light-adapted for 6-8 hours for photopic ERG. The scotopic ERG (rod-mediated) responses were elicited by a stimulus (10,000 cd/m^2, 1 ms) and differentially amplified and filtered between 0.3 and 500 Hz. The photopic ERG (cone-mediated) responses were elicited by a white light stimulus (10,000 cd/m^2, 0.3 ms) and

differentially amplified and filtered between 0.3 and 500 Hz. Amplitudes were measured from baseline to the a-wave trough for a-waves and from the a-wave trough to the b-wave peak for b-waves.

Real-time quantitative PCR

Total RNA isolation was performed from tissue samples using TRI reagent (Molecular research center, Cincinnati, OH) and from cells using SuperPrep Cell Lysis & RT Kit for qPCR (TOYOBO, Tokyo, Japan), followed by reverse transcription to cDNA using GoScript reverse transcriptase (Promega, Madison, WI) according to the manufacturers' protocols. All primers are listed in Table 1. Real-time quantitative PCR was performed using the GoTaq qPCR Master mix (Promega), THUNDERBIRD Probe qPCR Mix (TOYOBO, Osaka, Japan), and StepOne plus Systems (Thermo Fisher Scientific). Gene expression levels were calculated using the 2^{-ddCt} method, and all experimental samples were normalized using glyceraldehyde-3-phosphate dehydrogenase (*GAPDH*) as an internal control.

Table 1. Primer sequences used in quantitative RT-PCR

Target gene	Sequence
Human	
LGALS1	forward 5'- CGC TAA GAG CTT CGT GCT GAA C -3'
	reverse 5'- CAC ACC TCT GCA ACA CTT CCA G -3'
TGFB1	forward 5'- GCC CTG GAC ACC AAC TAT TG -3'
	reverse 5'- CGT GTC CAG GCT CCA AAT G -3'
ACTA2	forward 5'- TCT GTA AGG CCG GCT TTG C -3'
	reverse 5'- TGT CCC ATT CCC ACC ATC A -3'
COL1A1	forward 5'- GAG GGC CAA GAC GAA GAC ATC -3'
	reverse 5'- CAG ATC ACG TCA TCG CAC AAC -3'
FN1	forward 5'- CAA GTA TGA GAA GCC TGG GTC T -3'
	reverse 5'- TGA AGA TTG GGG TGT GGA AG -3'
SNAI1	forward 5'- TCG GAA GCC TAA CTA CAG CGA -3'
	reverse 5'- AGA TGA GCA TTG GCA GCG AG -3'

SNAI2	forward 5'- CGA ACT GGA CAC ACA TAC AGT G -3'
	reverse 5'- CTG AGG ATC TCT GGT TGT GGT -3'
TWIST1	forward 5'- CGG GAG TCC GCA GTC TTA -3'
	reverse 5'- GCT TGA GGG TCT GAA TCT TG -3'
GAPDH	forward 5'- CCT GGC CAA GGT CAT CCA TG -3'
	reverse 5'- GGA AGG CCA TGC CAG TGA GC -3'
Mouse	
Rho	forward 5'- ATG GGT GTG GTC TTC ACC TG -3'
	reverse 5'- GAA CAT TGC ATG CCC TCA G -3'
Opn1mw	forward 5'- ATC GTG CTC TGC TAC CTC CA -3'
	reverse 5'- TTT CTG TTG CTT TGC CAC TG -3'
Calb	forward 5'- GCT CCG CGC ACT CTC AA -3'
	reverse 5'- TGA CTG CAG GTG GGA TTC TG -3'
Grm6	forward 5'- TGT GCC AGA GAC CTT CAA TG -3'
	reverse 5'- AGT GTG GTC GTT TGG ATG TAG -3'
Pax6	forward 5'- TAC CAG TGT CTA CCA GCC AAT -3'
	reverse 5'- TGC ACG AGT ATG AGG AGG TCT -3'
Thy1	forward 5'- GAG TCC AGA ATC CAA GTC GG -3'
	reverse 5'- AGT CCA GGC GAA GGT TTT G -3'
Glul	forward 5'- GCT GCA AGA CCC GTA CCC T -3'
	reverse 5'- TTC CAC TCA GGT AAC TCT TCC ACA -3'
Lgals1	forward 5'- TCC CCG AAC TTT GAG ACA TTC -3'
	reverse 5'- GTC TCA GGA ATC TCT TCG CTT C -3'
	probe 5'- ACC AGA CCA CAG GCC ATG ATT GAA -3'
Ccl2	forward 5'- TTG GCT CAG CCA GAT GCA -3'
	reverse 5'- CCT ACT CAT TGG GAT CAT CTT GC -3'
Icam1	forward 5'- CCT GTT TCC TGC CTC TGA AG -3'
	reverse 5'- GTC TGC TGA GAC CCC TCT TG -3'
Tgbf1	forward 5'- CAG TGG CTG AAC CAA GGA GAC -3'
	reverse 5'- ATC CCG TTG ATT TCC ACG TG -3'

Acta2	forward 5'- GGA GAA GCC CAG CCA GTC GC -3'
	reverse 5'- AGC CGG CCT TAC AGA GCC A -3'
Col1a1	forward 5'- TGA CTG GAA GAG CGG AGA GT -3'
	reverse 5'- GAC GGC TGA GTA GGG AAC AC -3
Fn1	forward 5'- GTC AGT GTC TCC AGT GTC TAC -3'
	reverse 5'- TGG CTT GCT GGC CAA TCA GT -3'
Snai1	forward 5'- TCG GAA GCC TAA CTA CAG CGA -3'
	reverse 5'- AGA TGA GCA TTG GCA GCG AG -3'
Snai2	forward 5'- CGA ACT GGA CAC ACA TAC AGT G -3'
	reverse 5'- CTG AGG ATC TCT GGT TGT GGT -3'
Twist1	forward 5'- GGA CAA GCT GAG CAA GAT TCA -3'
	reverse 5'- CGG AGA AGG CGT AGC TGA G -3'
Gapdh	forward 5'- AGG TCG GTG TGA ACG GAT TTG -3'
	reverse 5'- TGT AGA CCA TGT AGT TGA GGT CA -3'

Laser-induced CNV model

Since laser-induced CNV model is a well-established model for the investigation of CNV, we therefore generate the CNVs as described previously (Kanda et al., 2015). After male mice (6-8 weeks old) anesthesia, laser photocoagulation (532nm, 180 mw, 50 μm, 50 ms, Novus Spectra; Lumenis, Tokyo, Japan) was performed around the optic disc using a slit-lamp delivery system with a cover glass as a contact lens. Disruption of Bruch's membrane was confirmed by central bubble formation immediately after laser application. Six laser spots for mRNA and protein analysis and four laser spots per eye for immunohistochemistry were set. The schema for laser-induced CNV in mice shows the Bruch's membrane and RPE are ruptured by laser burn in this model, neovascular tissues will then grow into the subretinal space from the choroid at 7-14 days after laser photocoagulation (Fig. 4).

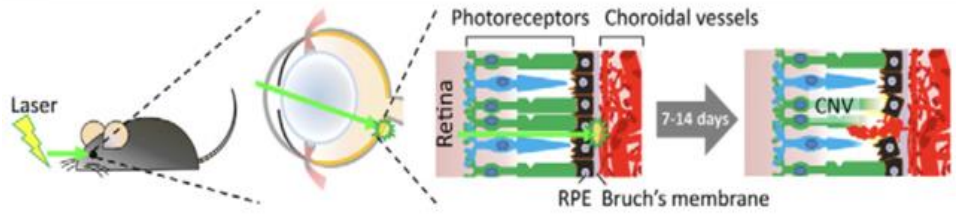

Modified from (Liu et al., 2017)

Figure 4. Schema diagram of the laser-induced CNV model in mice.

Quantification of CNV and subretinal fibrosis

Seven days after laser treatment, eyes were enucleated and fixed in 4% PFA. After removal of the anterior segment and retina, four radial incisions were made, and the remaining RPE-choroid complex were stained with isolectin B4-Alexa 488 (1:100; Thermo Fisher Scientific) and rabbit anti-type I collagen antibody (1:200; Sigma-Aldrich, St. Louis, MO) to detect CNV and subretinal fibrosis, respectively. The secondary antibody for type I collagen was Alexa 546 (1:200; Thermo Fisher Scientific). A Keyence BZ analyzer software (Keyence, Osaka, Japan) was used to measure the areas of CNV and subretinal fibrosis.

Cell cultures and transfection

Human RPE (hTERT-RPE1) cells were obtained from American Type Culture Collection (Manassas, VA) and cultured in DMEM/F-12 (Wako Pure Chemical Industries, Osaka, Japan) supplemented with 10% fetal bovine serum (FBS, Thermo Fisher Scientific) at 37 °C and 5% CO_2. Twenty-four hours after transfection, the composite transfection mixture was removed and replaced with 1% FBS/DMEM/F-12 for 24 hours, followed by application with recombinant human TGF-β1 protein (PeproTech, Rocky Hill, NJ).

Two siRNA oligos for suppressing the gene expression of *LGALS1* (siRNA-1, hs.Ri.LGALS1.13.1; siRNA-2, hs.Ri.LGALS1.13.2) and a negative control siRNA oligo (Ctrl-siRNA, DS NC1) were purchased from Integrated DNA Technologies (Coralville, IA) and used at 10 nM. Cells were transfected with siRNA using Lipofectamine RNAiMAX Reagent (Thermo Fisher Scientific) following the manufacturer's protocol.

Human *LGALS1*-coding region (GenBankTM number NM_002305) was obtained from the DNASU Plasmid Repository (Tempe, AZ) and subcloned into the *pCMV-Tag 3B* vector (Agilent Technologies, Santa Clara, CA). Cells were transfected with plasmid DNA using Lipofectamine LTX with Plus Reagent (Thermo Fisher Scientific) following the manufacturer's protocol. The empty *pCMV-Tag 3B* vector was used for mock transfection as negative controls.

Cell migration assay

RPE cell migration was evaluated with an Oris 96-well cell migration assay kit (Platypus Technologies, Madison, WI), according to the manufacturer's protocol. RPE cells were seeded into each well and transfected with siRNAs. After 1 hour of pretreatment with 1% FBS/DMEM/F-12 containing 10 ng/ml TGF-β1 with 5 mM aphidicolin (Wako Pure Chemical Industries) to inhibit cell division, the stoppers were then removed to allow cells to migrate into the central detection zone. Cells were then incubated for 48 hours and stained with PBS containing calcein AM (Dojindo, Kumamoto, Japan) for 1 hour. The signal intensity of the stained cells that migrated into the detection zone was measured with a Spectra Max M5 microplate reader in the fluorescence mode (Infinite F200 PRO, Tecan, Männedorf, Switzerland) using a fluorescence filter set (excitation 485 and emission 535) with an Oris detection mask attached to the bottom of the plate.

Cell invasion assay

RPE cell invasion was investigated using a BioCoat Matrigel Invasion Chamber (Corning, Bedford, MA), according to the manufacturer's protocol. Chambers were allowed to defrost at room temperature and rehydrated in DMEM/F-12. The siRNA-transfected RPE cells were then seeded onto the upper well, while 10 ng/ml TGF-β1 containing 1% FBS/DMEM/F-12 was applied to the lower well, followed by incubation for 24 hours. The remaining cells in the upper well were removed by wiping. The cells moved to the lower side of the filter were fixed with 100% methanol and stained with Toluidine Blue O. The total number of invading cells was quantified by counting in 5 random fields.

Cell proliferation assay

RPE cell proliferation was assessed using bromodeoxyuridine (BrdU)-ELISA (Roche Applied Science, Indianapolis, IN), according to the manufacturer's protocol. The siRNA-transfected cells were stimulated with 10 ng/ml TGF-β1 containing 1% FBS/ DMEM/F-12 for 24 hours, and incubated with BrdU for 2 hours. The optical density was determined using a microplate reader (Tecan Sunrise, Tecan Inc.).

Immunocytochemistry

RPE cells were cultured in 8-well multichamber slides (Thermo Fisher Scientific). Cells were then washed with PBS, permeabilized with ice-cold methanol for 20 min, and washed again in PBS. After a blocking step with 5% goat serum, the cells were incubated with the following primary antibodies at 4 °C overnight: mouse anti-α-SMA (1:200; R&D systems), rabbit anti-type I collagen (1:200), and mouse anti-fibronectin (1:200; Thermo Fisher Scientific) antibodies followed by secondary antibodies. Nuclei were counterstained with DAPI (4',6-diamidino-2-phenylindole) (Roche Applied Science, Indianapolis, IN), and photomicrographs were taken with a fluorescence microscope (Keyence).

Statistical analyses

All the results are expressed as the mean ± SEM (standard error of the mean). Student's t-test was used for statistical comparison between groups, and one-way analysis of variance (ANOVA) followed by the Tukey-Kramer method as a post-hoc test was used for multiple comparison procedures. Differences between means were considered statistically significant when p values were < 0.05.

Results

Lgals1 deficiency has no effect on retinal structure or function

Galecin-1 has been described to be constitutively expressed in various regions of the mammalian retina (Uehara et al., 2001); however, no study about the physiological role of galectin-1 in the retina has ever been reported. First, immunoblot analyses confirmed a predicted protein band of approximately 14 kDa from the retina and the RPE-choroid complex of *Lgals1*$^{+/+}$ mice (Fig. 5A), and galectin-1 immunoreactivity was localized on the RPE, outer and inner plexiform layers, inner nuclear layer, and ganglion cell layer in the *Lgals1*$^{+/+}$ retina (Fig. 5B), whereas both immunoblot and immunofluorescence signals were abolished in *Lgals1*$^{-/-}$ mice (Figs. 5A, C). Next, to examine whether *Lgals1* deficiency affects retina cellular structure and function loss in mice at 2 months after birth, we performed hematoxylin and eosin (H&E) staining and ERG in the retina of *Lgals1*$^{+/+}$ and *Lgals1*$^{-/-}$ mice. No obvious difference in retinal histology was detected between *Lgals1*$^{+/+}$ and *Lgals1*$^{-/-}$ mice (Figs. 5D, E). Moreover, the amplitudes of scotopic (rod a-wave and b-wave) and photopic (cone a-wave and b-wave) responses were equivalent between *Lgals1*$^{+/+}$ and *Lgals1*$^{-/-}$ mice (Figs. 5F-I). These results suggested that galectin-1/*Lgals1* deficiency did not affect the retinal anatomical structure and visual function.

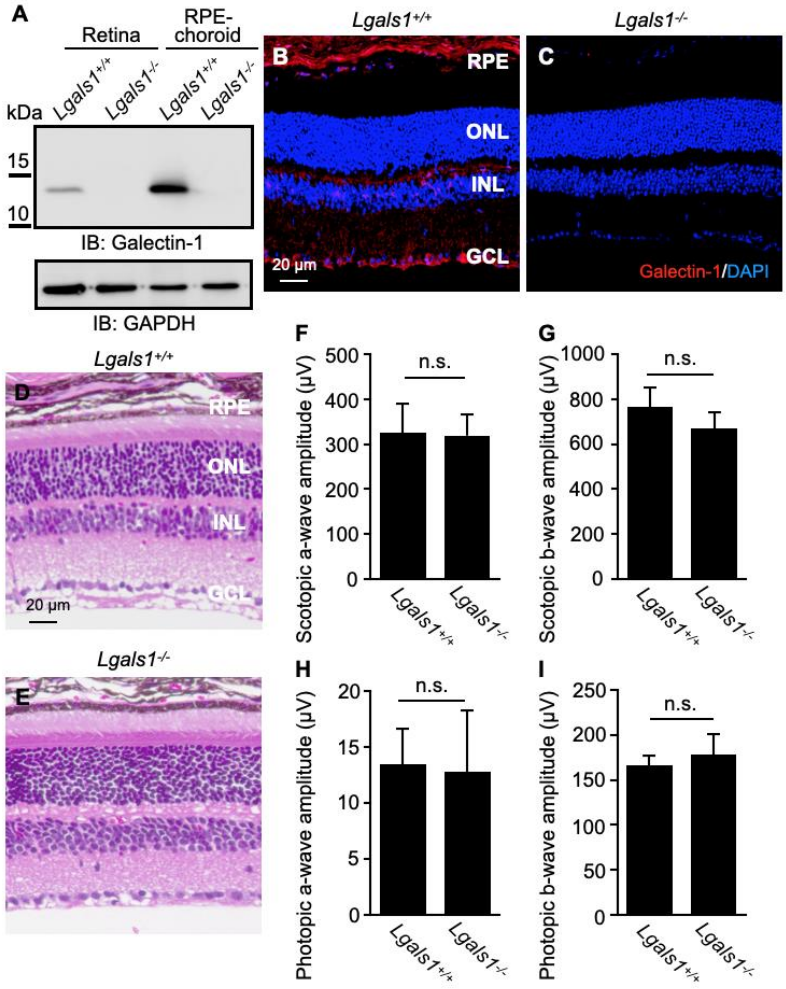

Figure 5. *Lgals1* deficiency has no effect on retinal structure or function. (A-C) Retinal localization and expression of galectin-1 in *Lgals1*$^{+/+}$ and *Lgals1*$^{-/-}$ mice at 2 months. (A) Immunoblot analyses for galectin-1 and GAPDH in the retina and the RPE-choroid complex of *Lgals1*$^{+/+}$ and *Lgals1*$^{-/-}$ mice. (B, C) Galectin-1 immunostaining of the retinas in *Lgals1*$^{+/+}$ (B) and *Lgals1*$^{-/-}$ (C). (D, E) Representative retinal sections stained with HE from *Lgals1*$^{+/+}$ and *Lgals1*$^{-/-}$ mice. RPE, retinal pigment epithelium; ONL, outer nuclear layer; INL, inner nuclear layer; GCL, ganglion cell layer. Scale bar = 20 μm. (F-I) Scotopic (F, G) and photopic (H, I) ERG recordings for comparison of a-wave (F, H) and b-wave (G, I) amplitudes between *Lgals1*$^{+/+}$ and *Lgals1*$^{-/-}$ mice. n.s., not significant; n = 4-10.

***Lgals1* deficiency has no effect on retinal vascular development or neural cell-fate determination**

Previously, we and others demonstrated that galectin-1 binds to the *N*-glycans of VEGFR2, activating its downstream signal transduction and promoting pathological neovascularization (Croci et al., 2014; Kanda et al., 2015). To investigate whether galectin-1/*Lgals1* deficiency affects the development of physiological retinal vasculature, we performed immunostaining for whole-mount retinas with new vessel growth at postnatal day 4 in *Lgals1*$^{+/+}$ and *Lgals1*$^{-/-}$ mice (Figs. 6A, B, A', B'). No significant differences were observed in AngioTool-computed morphometric parameters including vascular area, total vessel length, branching index, and lacunarity between retinas of *Lgals1*$^{+/+}$ and *Lgals1*$^{-/-}$ neonates (Figs. 6C-F).

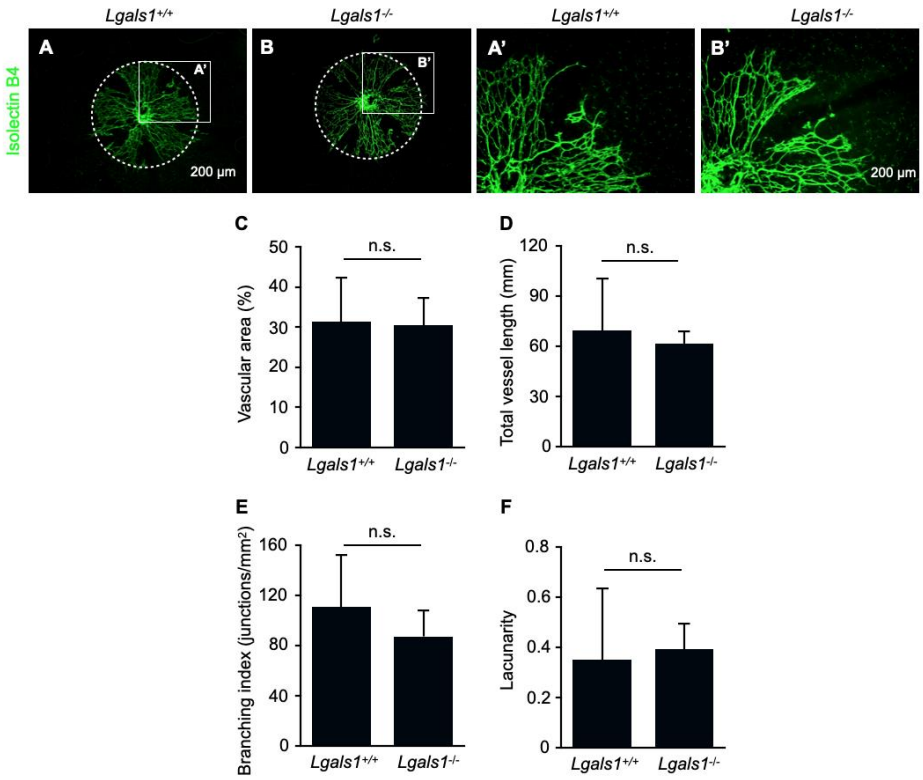

Figure 6. *Lgals1* deficiency has no effect on retinal vascular development. (A, B, A', B') Representative images of whole-mount retinas stained with isolectin B4 from *Lgals1*$^{+/+}$ (A, A') and *Lgals1*$^{-/-}$ (B, B') mice at postnatal day 4. (C-F) Quantitative analyses for the vascular area (C), total vessel length (D), branching index (E), and lacunarity (F) of retinal vasculature in *Lgals1*$^{+/+}$ and *Lgals1*$^{-/-}$ mice at postnatal day 4. n.s., not significant; n = 3. Scale bar = 200 μm.

To determine whether *Lgals1* deficiency affects neural cell fate, we performed immunofluorescence analyses for retinal sections from *Lgals1*$^{+/+}$ and *Lgals1*$^{-/-}$ mice at 2 months after birth, using antibodies against retinal cell type markers (Figs. 7A-L). The *Lgals1*$^{-/-}$ retina exhibited well-organized differentiation and distribution for all types of neural cells including: rod photoreceptor marker (anti-rhodopsin antibody) (Figs. 7A, B), cone photoreceptor marker (anti-CAR antibody) (Figs. 7C, D), horizontal marker (anti-calbindin antibody) (Figs. 7E, F), bipolar marker (anti-CHX10 antibody) (Figs. 7G, H), amacrine and ganglion marker (anti-PAX6 antibody) (Figs. 7I, J), ganglion marker (anti-BRN3 antibody) (Figs. 7K, L), and Müller glial marker (anti-GS antibody) (Figs. 7M, N).

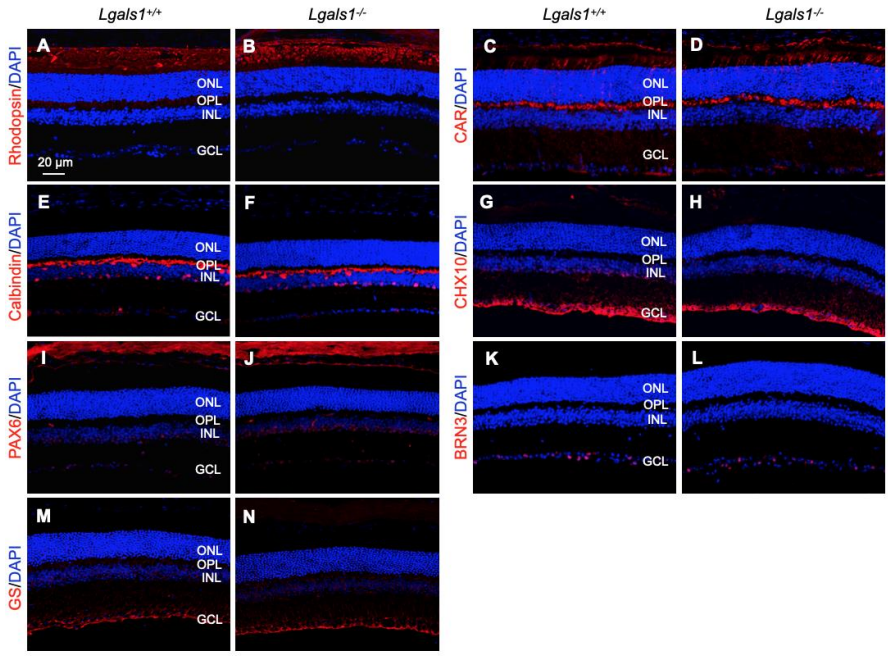

Figure 7. *Lgals1* deficiency causes no impact on retinal neural cell-fate determination. (A-N) Sections of *Lgals1*$^{+/+}$ (A, C, E, G, I, K, M) or *Lgals1*$^{-/-}$ (B, D, F, H, J, L, N) retinas at 2 months stained with antibodies against individual retinal cell-type markers (*red*): rod photoreceptor marker (A, B), cone photoreceptor marker (C, D), horizontal marker (E, F), bipolar marker (G, H), amacrine and ganglion marker (I, J), ganglion marker (K, L), and Müller glial marker (M, N), and counterstained with DAPI (*blue*). Scale bar = 20 μm. ONL, outer nuclear layer; OPL, outer plexiform layer; INL, inner nuclear layer; GCL, ganglion cell layer.

Consistent with these immunohistochemical results, no significant differences were observed between retinas of *Lgals1*$^{+/+}$ and *Lgals1*$^{-/-}$ mice in the gene expression of specific cell markers: rod photoreceptor marker (*Rho*), cone photoreceptor marker (*Opn1mw*), horizontal marker (*Calb*), bipolar marker (*Grm6*), amacrine and ganglion marker (*Pax6*), ganglion marker (*Thy1*), and Müller glial marker (*Glul*) (Fig. 8)

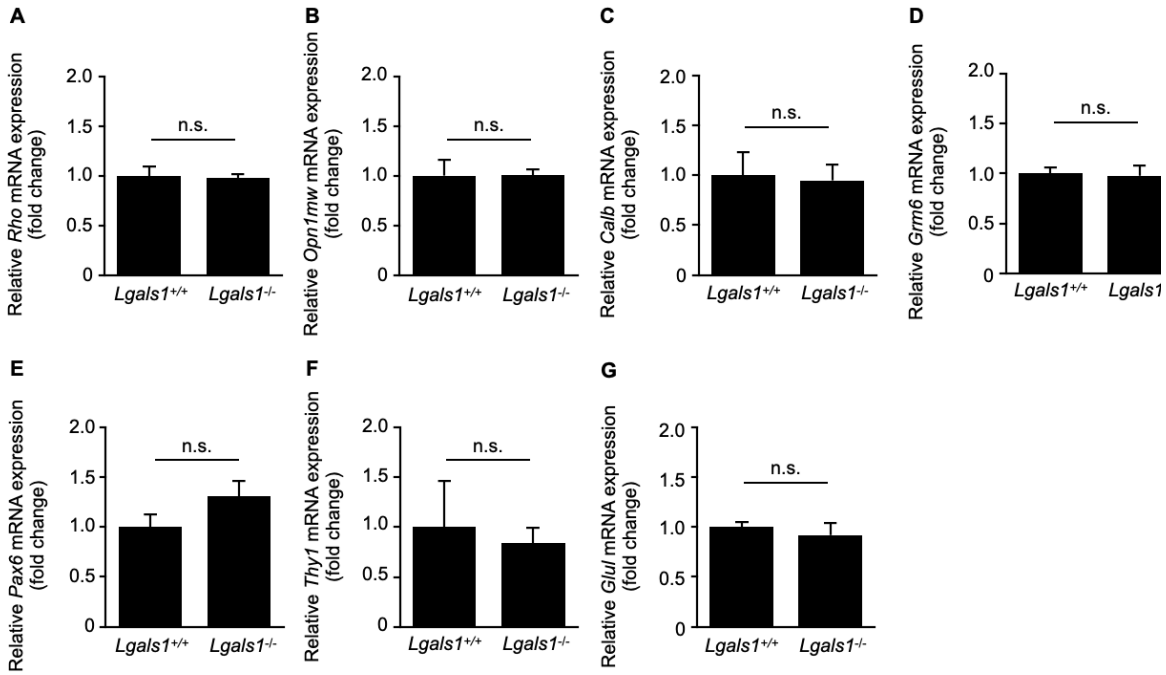

Figure 8. *Lgals1* deficiency causes no impact on retinal neural cell-fate determination. (A-G) Relative mRNA expression of individual retinal cell-type markers: rod photoreceptor marker (A), cone photoreceptor marker (B), horizontal marker (C), bipolar marker (D), amacrine and ganglion marker (E), ganglion marker (F), and Müller glial marker (G) in *Lgals1*$^{+/+}$ and *Lgals1*$^{-/-}$ retinas at 2 months after birth. n.s., not significant; n = 4.

These results demonstrated that galectin-1/*Lgals1* deficiency did not affect physiological vascular and neural architecture in the retina. In concert with the unaffected anatomical and functional phenotypes, galectin-1 was suggested to be physiologically redundant for the homeostasis of the normal retina.

Galectin-1/*Lgals1* expression is upregulated in RPE cells by CNV induction

To examine whether galectin-1 is involved in the formation of CNV, we performed immunostaining for tissue localization and production of galectin-1 with CNV at post-laser day 7. In the CNV tissue, immunostaining for galectin-1 increased mainly in the activated RPE cells, some of which proliferated, migrated, and surrounded isolectin B4-positive new vessels penetrating into the subretinal space, RPE-derived fibroblasts losing melanin pigments (Hirasawa et al., 2011), and part of the invading neovascular endothelial cells (Figs. 9A-H). To confirm these immunofluorescence results, we next examined real-time quantitative PCR to evaluate the expression of *Lgals1* mRNA in the RPE-choroid complex from mice with or without CNV at post-laser day 3. *Lgals1* mRNA levels were significantly upregulated following CNV induction (Fig. 9I), in consistence with elevated galectin-1 protein levels detected via immunoblotting (Fig. 9J). These results indicated that RPE cells are the major source of enhanced galectin-1 production during CNV generation.

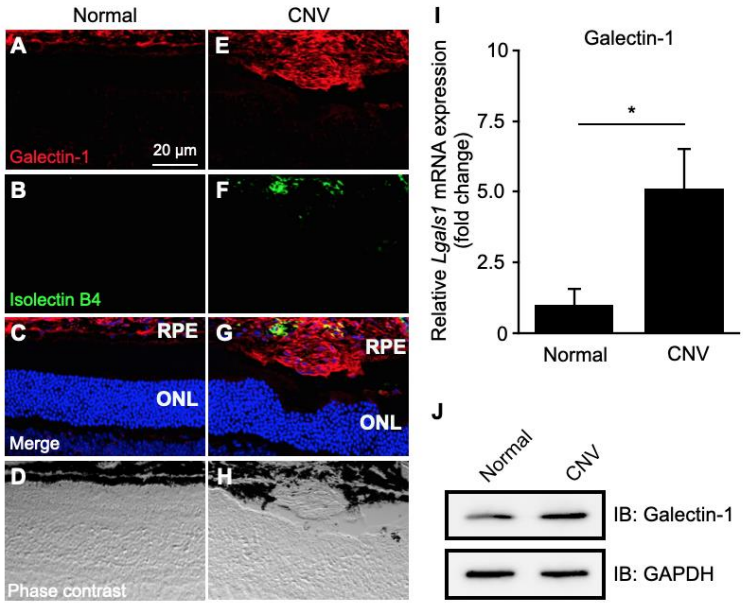

Figure 9. Galectin-1/*Lgals1* expression is upregulated in RPE cells by CNV induction. (A-G) Double labeling of galectin-1 (*red*), isolectin B4 (*green*), and DAPI (*blue*) in normal untreated eyes (A-C), and in eyes with CNV at post-laser day 7 (E-G) from C57BL/6J mice. Scale bar = 20μm. (D, H) Phase contrast images. (I) *Lgals1* mRNA expression in the RPE-choroid complex at post-laser day 3 (fold change = 5.11). * $p < 0.05$, n = 4-5. (J) Immunoblot analyses for galectin-1 in the RPE-choroid complex at post-laser day 3.

***Lgals1* deficiency suppresses CNV together with VEGFR2's downstream molecules**

Next, to determine whether galectin-1 plays a role in the development of CNV, we quantified the CNV area stained by isolectin B4 in the flat mounts of the RPE-choroid complex from *Lgals1*$^{+/+}$ and *Lgals1*$^{-/-}$ mice. The average CNV area at post-laser day 7 was significantly smaller than that of *Lgals1*$^{+/+}$ mice (Figs. 10A-C). To investigate the molecular mechanism by which *Lgals1* deficiency attenuates CNV formation, we focused on monocyte chemotactic protein (MCP)-1, also known as C-C motif chemokine ligand (CCL)2, and intercellular adhesion molecule (ICAM)-1, two major inflammatory cell regulators induced via endothelial VEGFR2 signaling (Kim et al., 2001; Radisavljevic et al., 2000), and also responsible for the pathogenesis of CNV (Sakurai et al., 2003a; Tsutsumi et al., 2003). Compared with *Lgals1*$^{+/+}$ mice, mRNA levels of *Ccl2* and *Icam1* in the RPE-choroid complex significantly increased 3 days after laser photocoagulation (Figs. 10D, E). Importantly, these elevated *Ccl2* and *Icam1* expression levels were significantly reduced in *Lgals1*$^{-/-}$ mice. In addition, galectin-1 increased the phosphorylation of ERK by binding with VEGFR2 (Croci et al., 2014), which also proved to induce the expression of both MCP-1 (Chao et al., 2017; Skiest, 1999) and ICAM-1 (Jiang et al., 2013; Zhong et al., 2012) in vascular endothelial cells. Thus, we next checked whether suppression of CNV in *Lgals1*$^{-/-}$ mice accompanies the inhibition of CNV-associated ERK1/2 activation (*i.e.*, phosphorylation). In accordance with the *Ccl2* and *Icam1* data, CNV-related upregulation of phosphorylated ERK1/2 levels in the of RPE-choroid complex from *Lgals1*$^{+/+}$ mice, which reduced in *Lgals1*$^{-/-}$ mice at post-laser day 3 (Figs. 10F, G). These results suggested that galectin-1 upregulation during CNV formation enhances VEGFR2's downstream ERK1/2 pathway leading to MCP-1 and ICAM-1 expression and subsequent inflammation-related angiogenesis.

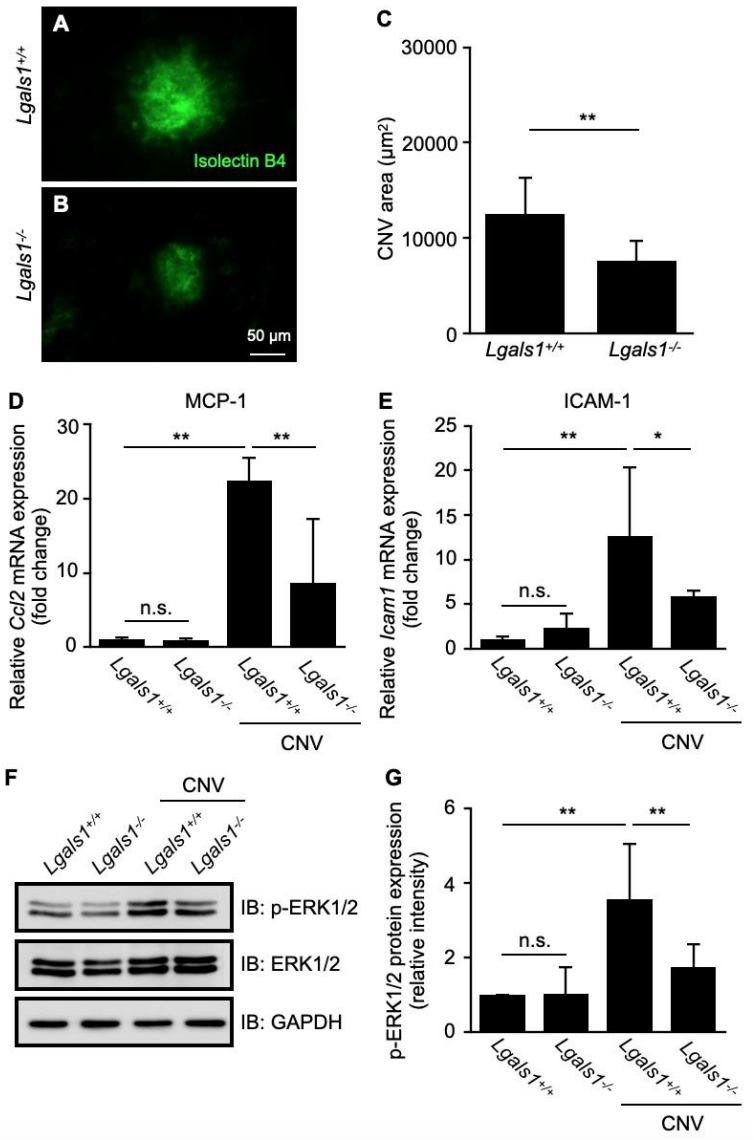

Figure 10. *Lgals1* deficiency suppresses CNV together with VEGFR2's downstream molecules. (A, B) Representative images of CNV lesions in the RPE-choroid flat mounts at post-laser day 7 from *Lgals1*$^{+/+}$ and *Lgals1*$^{-/-}$ mice. Scale bar = 50 μm. (C) Quantitative analyses for the area of CNV. n = 8-9. (D, E) Gene expression levels of *Ccl2* (D) and *Icam1* (E) in the RPE-choroid complex of *Lgals1*$^{+/+}$ and *Lgals1*$^{-/-}$ mice at post-laser day 3. (F) Immunoblot analyses for phosphorylated ERK1/2 and total ERK1/2 in the RPE-choroid complex of *Lgals1*$^{+/+}$ and *Lgals1*$^{-/-}$ mice at day 3 after laser injury. (G) Densitometry values of phosphorylated ERK1/2 normalized to total ERK1/2. * $p < 0.05$, ** $p < 0.01$, n = 4-5.

***Lgals1* deficiency suppresses CNV-associated subretinal fibrosis together with EMT-related molecules**

Subretinal fibrosis, a wound healing response that follow CNV in AMD, is accompanied by destruction of photoreceptors, RPE, and choroidal vessels, leading to severe vision loss (Bloch et al., 2013; Daniel et al., 2014). The EMT plays physiological roles in embryonic development and wound healing, whereas EMT dysfunction causes pathological reactions including carcinogenesis and fibrogenesis (Kalluri and Weinberg, 2009; Lamouille et al., 2014). Galectin-1 was shown to enhance the TGF-β-SMAD pathway, thus leading to the development of pulmonary and pancreatic fibrosis (Lim et al., 2014; Tang et al., 2018). To evaluate whether *Lgals1* deficiency suppresses CNV-associated subretinal fibrosis, composed mainly of type I collagen, we stained flat mounts of the RPE-choroid complex with anti-type I collagen antibody to quantify the size of subretinal fibrosis at 7 days after laser (Figs. 11A, B). The average fibrosis area significantly decreased in *Lgals1*$^{-/-}$ mice compared with *Lgals1*$^{+/+}$ mice (Fig. 11C). To further investigate the molecular mechanism for the attenuation of fibrosis in *Lgals1*$^{-/-}$ mice, we analyzed mRNA expression levels of *Tgfb1* (TGF-β1), *Acta2* (α-SMA), *Col1a1* (type I collagen), and *Fn1* (fibronectin), all of which are representative EMT-related mesenchymal markers (Kalluri and Weinberg, 2009; O'Connor and Gomez, 2014). *Tgfb1*, *Acta2*, *Col1a1,* and *Fn1* mRNA levels significantly elevated at 3 days after laser photocoagulation in the RPE-choroid complex from *Lgals1*$^{+/+}$ mice, were significantly reversed in *Lgals1*$^{-/-}$ mice (Figs. 11D-G).

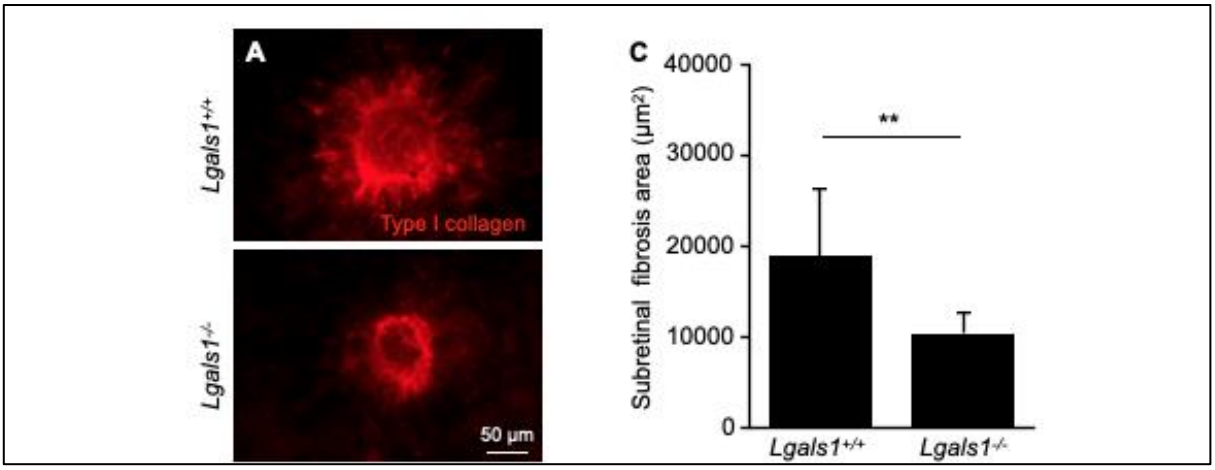

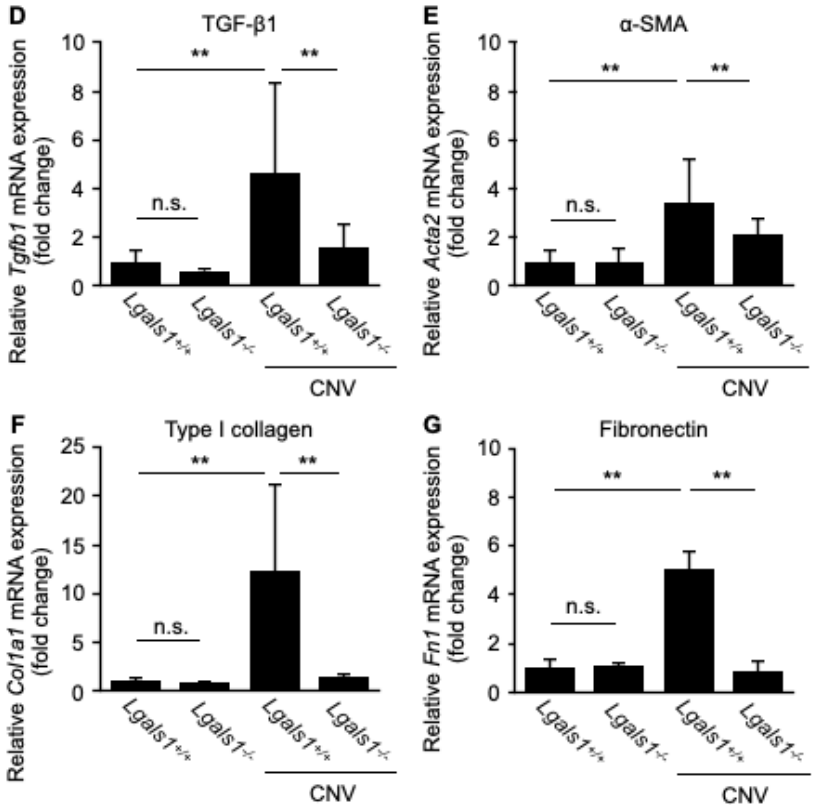

Figure 11. *Lgals1* deficiency suppresses CNV-associated subretinal fibrosis together with EMT-related molecules. (A, B) Representative micrographs of subretinal fibrosis lesions at post-laser day 7 in *Lgals1*$^{+/+}$ and *Lgals1*$^{-/-}$ mice. Scale bar = 50 μm. (C) Quantitative analyses for the area of fibrosis. n = 8-9. (D-H) Gene expression level of *Tgfb1* (D), *Acta2* (E), *Col1a1* (F), and *Fn1* (G) in *Lgals1*$^{+/+}$ and *Lgals1*$^{-/-}$ mice with or without CNV induction at post-laser day 3. n.s., not significant; ** $p < 0.01$, n = 4-5.

Moreover, we examined the EMT-related key transcription factors *Snai1* (SNAIL), *Snai2* (SLUG), and *Twist1* (TWIST) expression levels after CNV induction (Kalluri and Weinberg, 2009; Lamouille et al., 2014). In *Lgals1*$^{+/+}$ mice, mRNA levels of *Snai1,* but not *Snai2* or *Twist1,* significantly upregulated in the RPE-choroid complex at 3 days after laser-induction (Figs. 12A-C), in consistence with our previous data showing the presence of SNAIL, but not SLUG or TWIST, in AMD patient specimens (Hirasawa et al., 2011). Importantly, *Lgals1* deficiency significantly suppressed the CNV-associated upregulation of *Snai1* mRNA expression (Fig. 12A). We next examined the protein levels of α-SMA and phosphorylated

SMAD2, a marker of the TGF-β-transforming growth factor-β receptor (TβR)I/II-SMAD signal activation, in the RPE-choroid complex at post-laser day 3. The protein levels of both α-SMA and phosphorylated SMAD2, elevated in *Lgals1*$^{+/+}$ mice after laser treatment, were significantly reduced in *Lgals1*$^{-/-}$ mice (Figs. 12D-F). Interestingly, *Lgals1* deficiency did not affect any of these EMT-related parameters in mice without CNV induction (Figs. 12D-F). These results suggested that galectin-1 promotes CNV-associated subretinal fibrosis through EMT driven by the pathologically enhanced TGF-β1-SMAD2-SNAIL signaling axis.

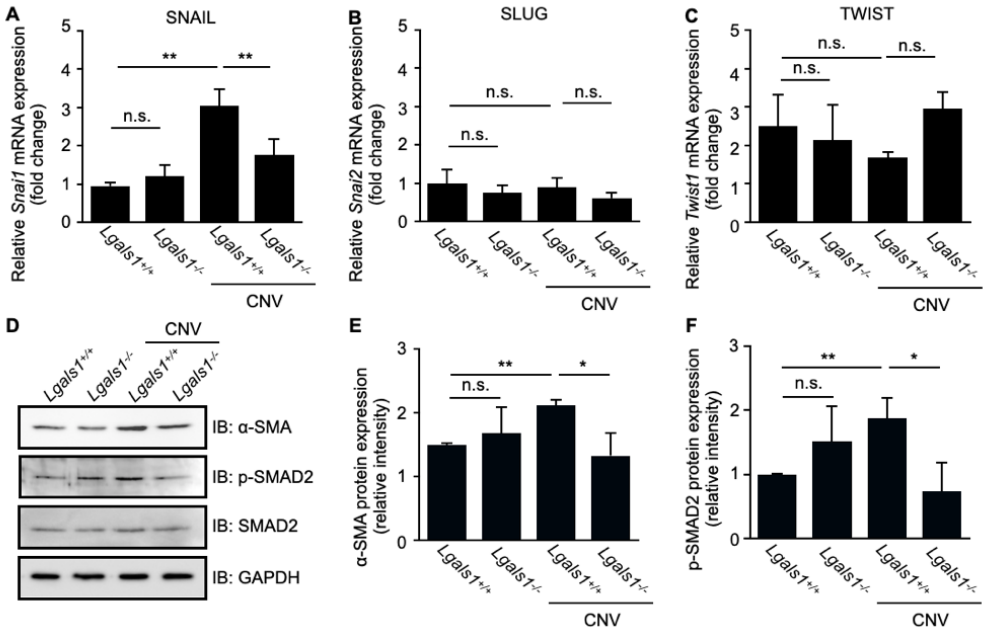

Figure 12. *Lgals1* deficiency suppresses CNV-associated subretinal fibrosis together with EMT-related molecules. (A-C) Gene expression level of *Snai1*(A), *Snail2*(B) and *Twist1*(C) in *Lgals1*$^{+/+}$ and *Lgals1*$^{-/-}$ mice with or without CNV induction at post-laser day 3. n.s., not significant; ** $p < 0.01$, n = 4-5. (D) Immunoblotting for α-SMA, phosphorylated SMAD2 and total SMAD2 in the RPE-choroid complex of *Lgals1*$^{+/+}$ and *Lgals1*$^{-/-}$ mice with or without CNV induction at post-laser day 3. (E, F) Densitometry values of α-SMA (E) and phosphorylated SMAD2 (F) normalized to GAPDH and total SMAD2, respectively. * $p < 0.05$, ** $p < 0.01$, n = 3-4.

Silencing of *LGALS1* suppresses TGF-β1-induced EMT-related molecules in human RPE cells

To further confirm our *in vivo* data, we further investigated whether silencing of *LGALS1* in human RPE cells suppresses EMT changes. In consistence our *in vivo* results, silencing of *LGALS1* significantly prevented TGF-β1-induced expression of the corresponding EMT-related genes *TGFB1*, *ACTA2*, *COL1A1*, *FN1*, and *SNAI1* (Figs. 13A-E), but not *SNAI2* or *TWIST1* (Figs. 13F, G).

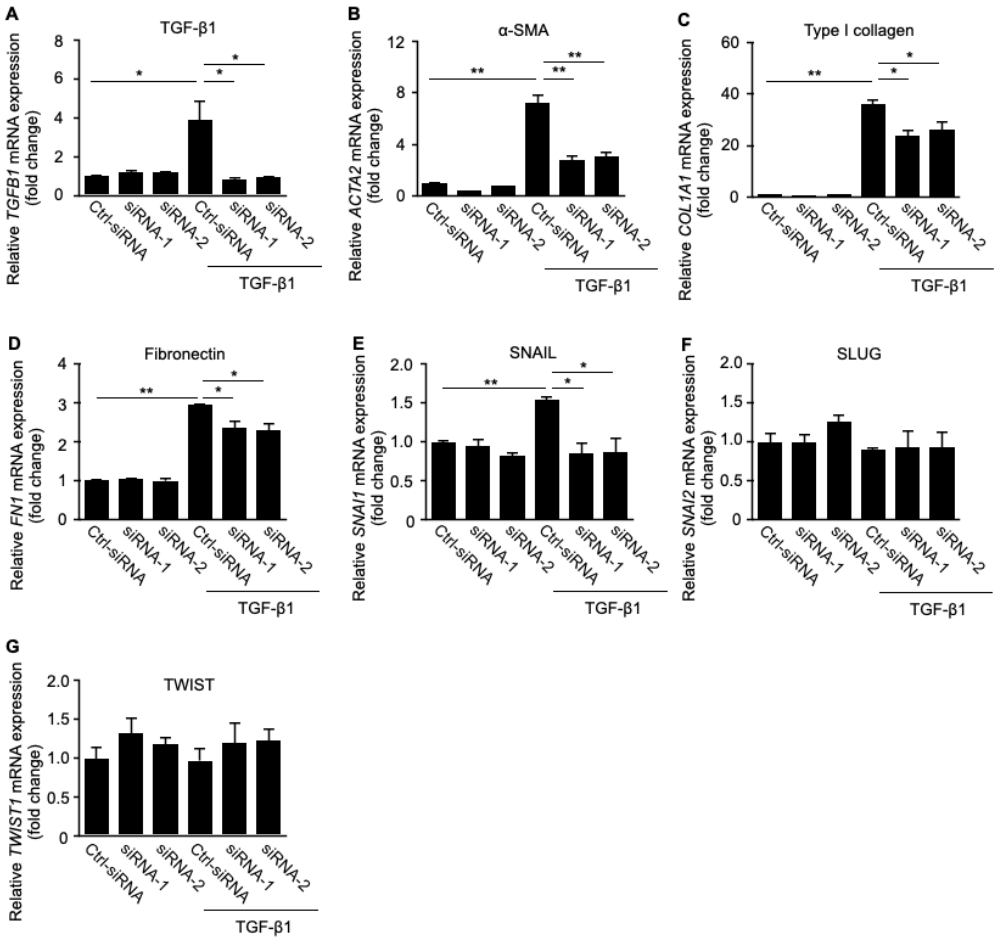

Figure 13. Silencing of *LGALS1* suppresses mRNA levels of TGF-β1-induced EMT-related molecules in human RPE cells. (A-G) Control siRNA-treated (Ctrl-siRNA) and *LGALS1*-knockdown (siRNA-1 and -2) RPE cells were stimulated with or without TGF-β1 at 10 ng/ml for 24 hours. Relative mRNA expression levels of *TGFB1* (A), *ACTA2* (B), *COL1A1* (C), *FN1* (D), *SNAI1* (E), *SNAI2* (F) and *TWIST* (G). $*p < 0.05$, $**p < 0.01$, n = 6-8.

Moreover, TGF-β-induced protein levels of α-SMA and phosphorylated SMAD2 in RPE cells were reduced by silencing of *LGALS1* (Figs. 14A-C), recapitulating the CNV-

associated changes in these proteins in the RPE-choroid complex. In consistence with mice without CNV induction, *LGALS1* knockdown did not affect any of these EMT-related parameters in RPE cells without TGF-β application. These results suggested that galectin-1-mediated subretinal fibrosis depends largely on TGF-β-activated RPE cells undergoing EMT via the SMAD2-SNAIL signal transduction.

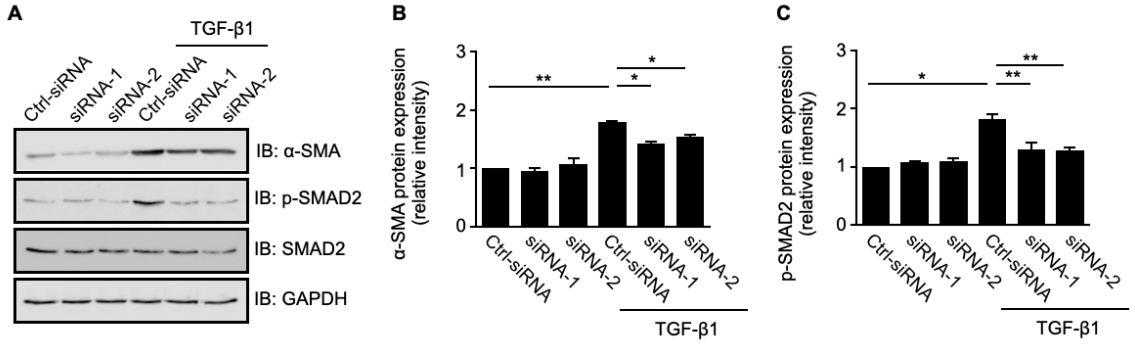

Figure 14. Silencing of *LGALS1* suppresses protein levels of TGF-β1-induced EMT-related molecules in human RPE cells. (A) Immunoblot analyses for α-SMA, phosphorylated SMAD2, total SMAD2, and GAPDH. Densitometry values of α-SMA (B) and phosphorylated SMAD2 (C) normalized to GAPDH and total SMAD2, respectively. * $p < 0.05$, ** $p < 0.01$, n = 3.

Silencing of *LGALS1* suppresses EMT-related cell motilities in human RPE cells

We next investigated whether TGF-β-activated RPE cell motilities, the representative EMT phenotype in parallel with fibrogenesis, are regulated by galectin-1. *LGALS1* knockdown in RPE cells significantly suppressed TGF-β-induced activation of cell motilities including cell migration (Figs. 15A, B), cell invasion (Figs. 15C, D), and cell proliferation (Figs. 15E). These findings suggested that galectin-1 contributes to RPE cell motilities ensuing from TGF-β1-induced EMT changes together with the pro-fibrotic process of extracellular matrix production.

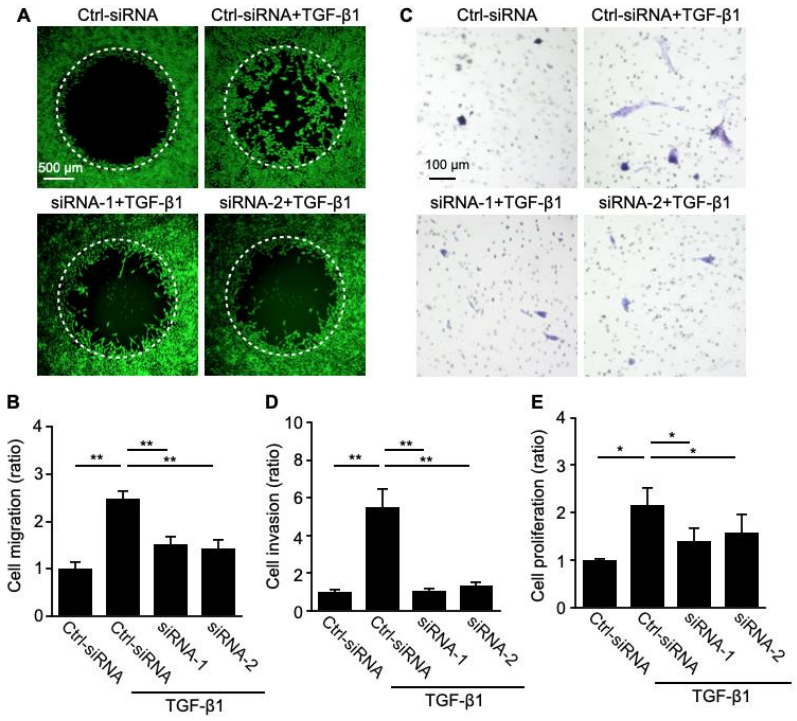

Figure 15. Silencing of *LGALS1* suppresses EMT-related cell motilities in human RPE cells. (A-E) Control siRNA-treated (Ctrl-siRNA) and *LGALS1*-knockdown (siRNA-1 and -2) RPE cells were stimulated with or without TGF-β1 at 10 ng/ml. (A, B) Cell migration assay. Representative images of cells stained with calcein AM (A). The signal intensity of stained cells having migrated within the detection zones (white dotted circles) after 48 hours was measured (B). ** $p < 0.01$, n = 7-10. Scale bar = 500 μm. (C, D) Cell invasion assay. Representative images of cells stained with Toluidine Blue O (C). The number of stained cells having invaded on the bottom side of Matrigel-coated filter after 24 hours was counted (D). ** $p < 0.01$, n = 3. Scale bar = 100 μm. (E) Cell proliferation assay. The optical density for BrdU incorporation after 24 hours was measured. *$p <$ 0.05, **$p < 0.01$, n = 8.

Lgals1 overexpression enhances CNV and subretinal fibrosis

To further confirm our current findings on *Lgals1* deficiency in mice, we generated *Lgals1*-Tg mice, and explored whether galectin-1 overexpression affects angiogenesis and fibrosis in the CNV model. Preliminary results confirmed significant increases in mRNA and protein levels of *Lgals1*/galectin-1 in the retina and the RPE-choroid complex from *Lgals1*-Tg mice compared

with *Lgals1*-nonTg mice (Figs. 16A, B). On histology and ERG, retinal structure and function appeared to be unaffected by the *Lgals1* transgene (Figs. 16C-H).

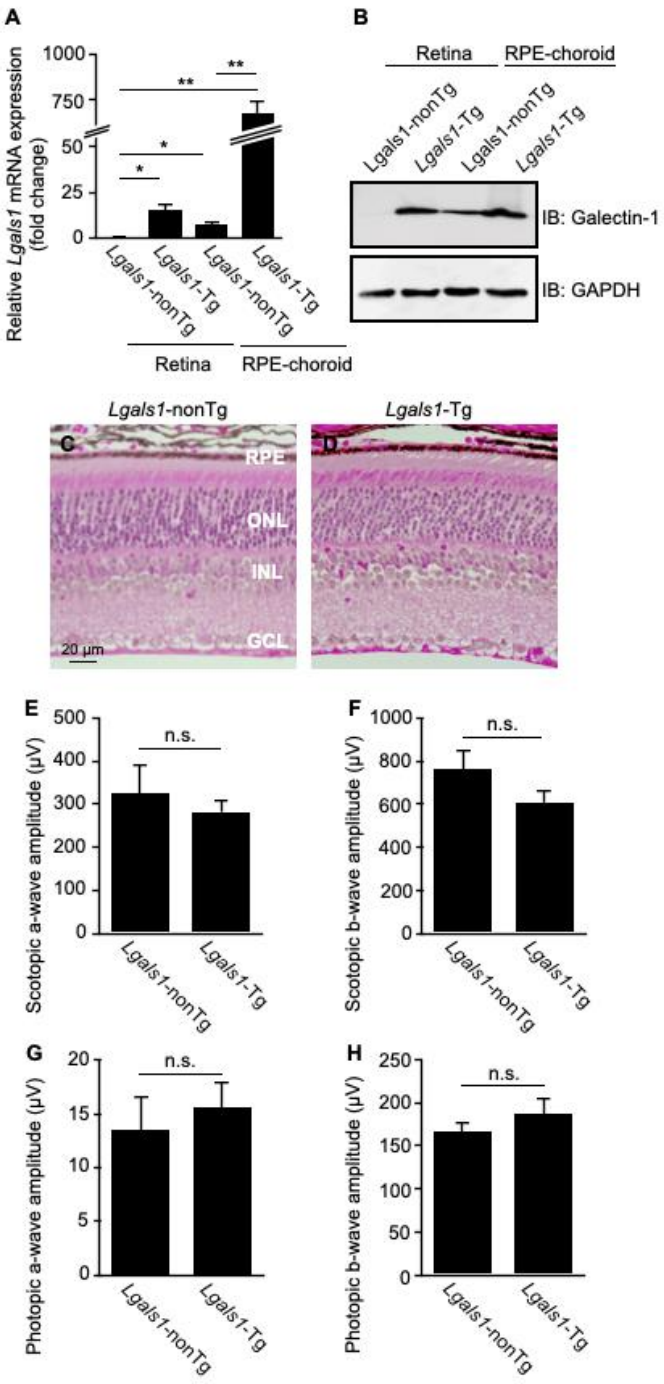

Figure 16. *Lgals1* overexpression causes no impact on retinal structure or function. (A-H) *Lgals1*-nonTg and *Lgals1*-Tg mice were evaluated at 2 months after birth. (A) Gene expression of *Lgals1* in the retina and the RPE-choroid complex. n = 6. (B) Immunoblot analyses for galectin-1 and GAPDH in the retina and the RPE-choroid complex. (C, D)

Representative retinal sections stained with hematoxylin and eosin from *Lgals1*-nonTg (C) and *Lgals1*-Tg (D) mice. RPE, retinal pigment epithelium; ONL, outer nuclear layer; INL, inner nuclear layer; GCL, ganglion cell layer. Scale bar = 20 μm. (E-H) Scotopic (E, F) and photopic (G, H) ERG recordings for comparison of a-wave (E, G) and b-wave (F, H) amplitudes between *Lgals1*-nonTg and *Lgals1*-Tg mice. n.s., not significant; * $p < 0.05$, ** $p < 0.01$, n = 4.

We next carried out whether galectin-1 overexpression affects angiogenesis and fibrosis in the CNV model (Figs. 17A-F). Quantitative analyses revealed both CNV (Fig. 17G) and fibrosis area (Fig. 17H) were significantly upregulated in *Lgals1*-Tg mice compared with *Lgals1*-nonTg mice, which were completely opposite findings due to *Lgals1* deficiency.

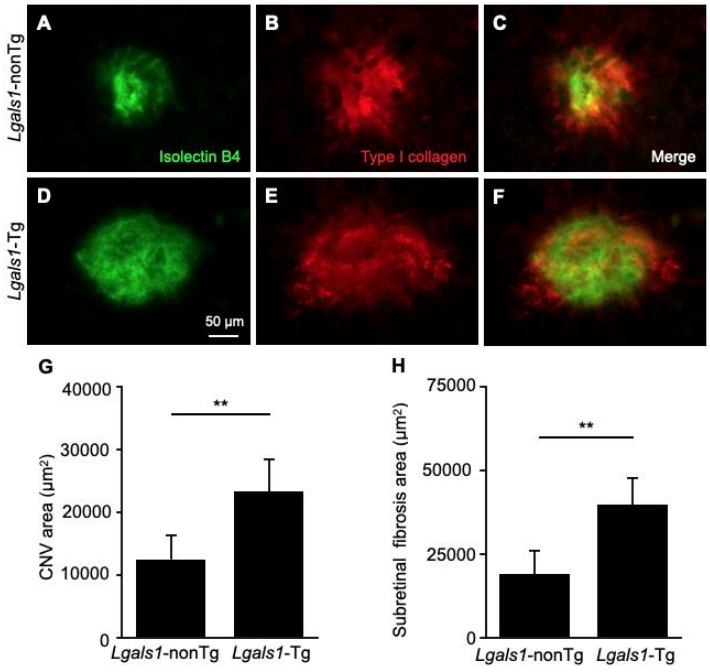

Figure 17. *Lgals1* overexpression enhances CNV and subretinal fibrosis. (A-F) Representative images of CNV (isolectin B4, *green*) and subretinal fibrosis (type I collagen, *red*) lesions in the RPE-choroid complex of *Lgals1*-nonTg and *Lgals1*-Tg mice at post-laser day 7. Scale bar = 50 μm. (G, H) Quantitative analyses for the area of CNV and subretinal fibrosis. ** $p < 0.01$, n = 6-9.

Consistent with these *in vivo* results, overexpression of *LGALS1* in plasmid DNA-

transfected RPE cells synergistically increased TGF-β1-stimulated upregulation of *ACTA2*, *COL1A1*, and *FN1* mRNA expression, as compared with mock-transfected RPE cells (Figs. 18A-D).

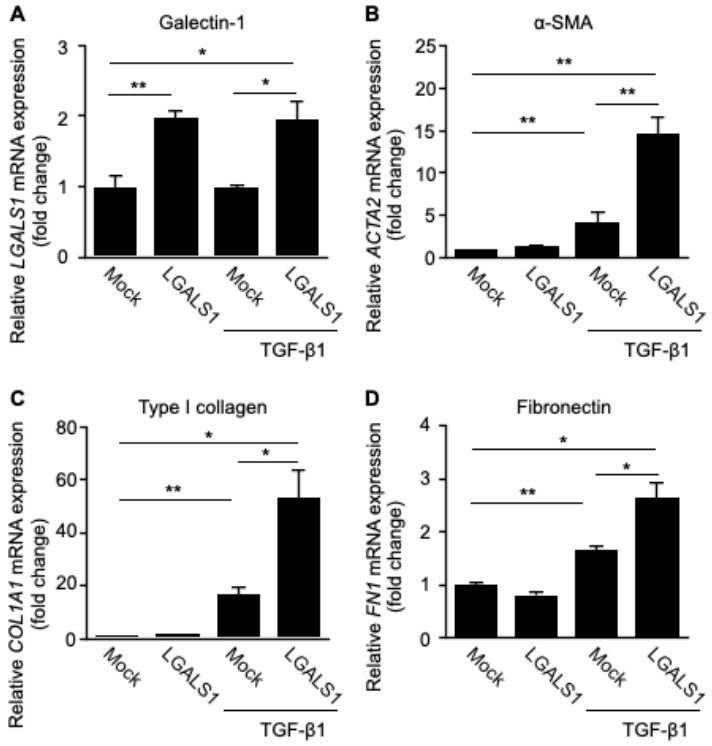

Figure 18. *LGALS1* overexpression induces TGF-β1-induced EMT markers in human RPE cells. (A-D) Gene expression levels of *LGALS1* (A), *ACTA2* (B), *COL1A1* (C), and *FN1* (D) in mock-transfected and *LGALS1*-transfected RPE cells treated with or without TGF-β1 at 10 ng/ml for 24 hours. * $p < 0.05$, ** $p < 0.01$, n = 4.

Galectin-1 co-localizes with VEGFR2 and phosphorylated SMAD2 in AMD patient specimens

Previously, we demonstrated Galectin-1 co-localization with VEGFR2-expressing in neovascular endothelial cells in the fibrovascular tissue from eyes with PDR (Kanda et al., 2015), however, no data on AMD patient samples have been reported. To explore the tissue localization and expression of galectin-1 and related molecules, we performed immunofluorescence for the CNV tissue of AMD patient specimens. Double-staining experiments demonstrated co-localization of galectin-1 with CD34 (vascular endothelial cell marker) (Figs. 19A-C), VEGFR2 (Figs. 19D-F), RPE65 (RPE cell marker) (Figs. 19G-I),

phosphorylated SMAD2 (Figs. 19J-L), TGF-β1(Figs. 19M-O), and type I collagen (Figs. 19P-R) in the CNV tissue. Moreover, Galectin-1 co-localization with phosphorylated SMAD2 within RPE cells is supported by previous data showing that galectin-1 enhances SMAD2 phosphorylation via its molecular binding with SMAD2 (Lim et al., 2014). These results suggested the VEGFR2- and SMAD2-mediated pathogenic role of galectin-1 in CNV and subretinal fibrosis in human AMD.

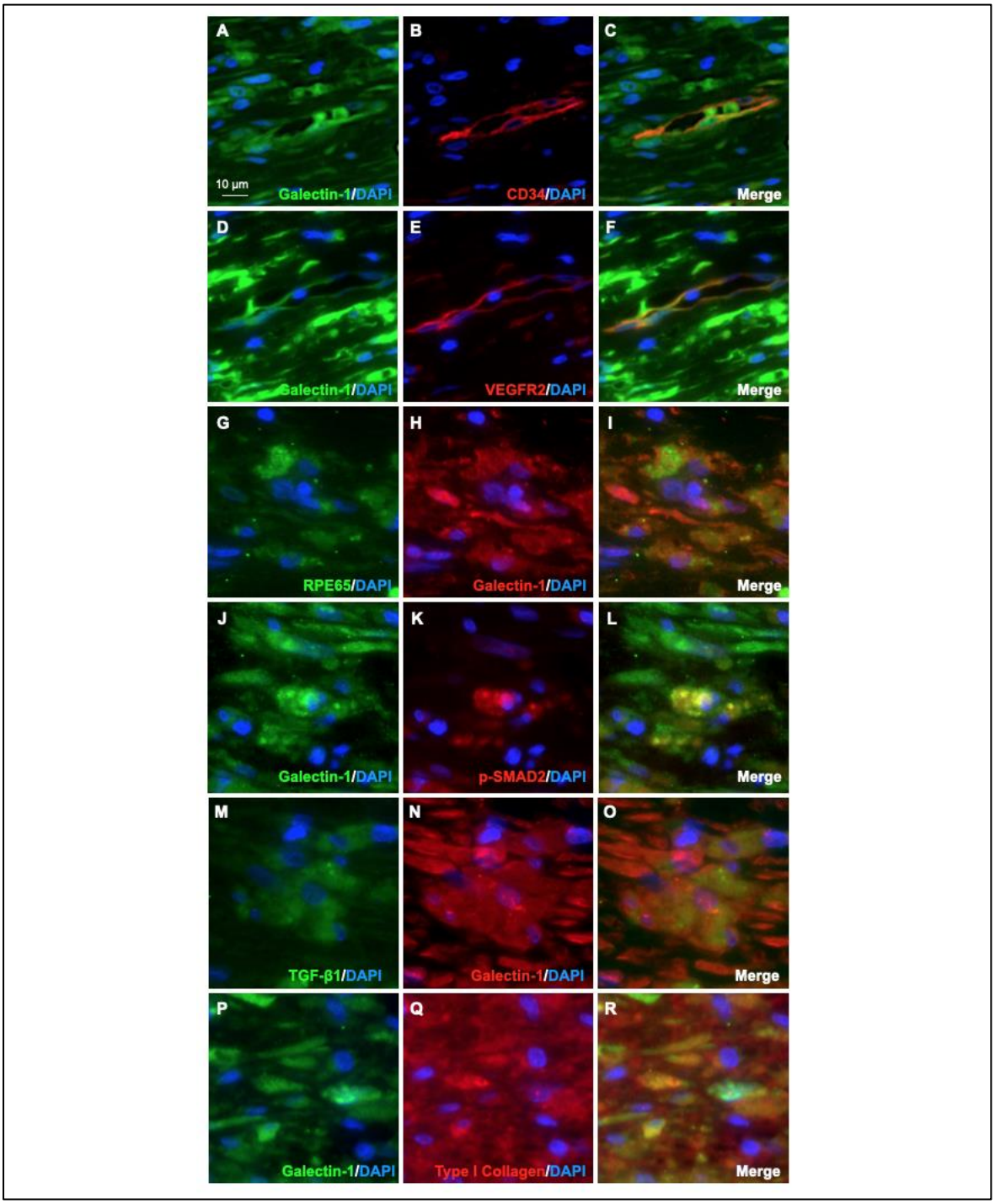

Figure 19. Galectin-1 co-localizes with VEGFR2, phosphorylated SMAD2, TGF-ß1 and type I collagen in AMD patient specimens. (A-L) Double labeling of galectin-1 (*green*), CD34 (*red*), and DAPI (*blue*) (A-C); galectin-1 (*green*), VEGFR2 (*red*), and DAPI (*blue*) (D-F); RPE65 (*green*), galectin-1 (*red*), and DAPI (*blue*) (G-I); galectin-1 (*green*), phosphorylated SMAD2 (*red*), and DAPI (*blue*) (J-L); TGF-ß1 (*green*), galectin-1 (*red*), and DAPI (*blue*) (M-O); galectin-1 (*green*), type I collagen (*red*), and DAPI (*blue*) (P-R) in the CNV tissue specimens. Scale bar = 10 μm.

Discussion

The current study reveals, for the first time, the involvement of galectin-1 in the pathogenesis of CNV and subretinal fibrosis. The following findings showed: i) *Lgals1* deficiency in mice has no effect on retinal structure, visual function, physiological development of retinal vascular and neural architecture. ii) *Lgals1*/galectin-1 was upregulated by induction of CNV at both mRNA and protein levels, and CNV-related parameters (*i.e.,* the area of CNV, phosphorylation of ERK1/2, and expression of *Ccl2* and *Icam1*) were attenuated in *Lgals1*-deficient mice compared with control animals. iii) *Lgals1*-deficient mice also exhibited a significant decrease in the area of subretinal fibrosis together with downregulation of EMT-related genes and phosphorylation of SMAD2. iv) In consistence with the *in vivo* findings, silencing of *LGALS1* in human RPE cells suppressed TGF-β1-induced EMT molecular markers and cell motilities. v) Overexpression of *Lgals1* facilitated CNV and subretinal fibrosis. vi) Importantly, AMD patient specimens demonstrated the presence of galectin-1 in neovascular endothelial cells and RPE cells together with its co-localization with VEGFR2 and phosphorylated SMAD2. These results suggest that the significant involvement of galectin-1 modified VEGF-A and TGF-β1 receptor signaling pathways in promoting CNV and fibrosis, respectively (Fig. 20).

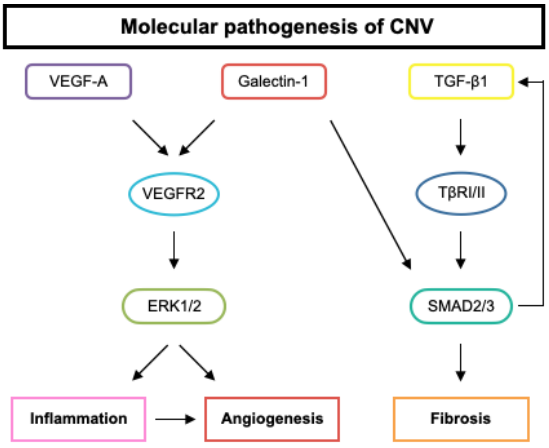

Figure 20. A schema showing galectin-1 involvement in the molecular pathogenesis of CNV via modification of VEGF-A and TGF-β1 signaling pathways to enhance inflammation-related angiogenesis and fibrosis, respectively.

A number of studies have shown that galectin-1, a key pro-angiogenic factor in tumor

growth and progression, activates multiple signaling pathways such as the mitogen-activated protein kinase (MAPK)-ERK kinase-ERK cascade, and induces two key steps in tumor angiogenesis, *i.e.*, endothelial cell proliferation and migration (Chung et al., 2012; Elad-Sfadia et al., 2002; Thijssen et al., 2010; Thijssen et al., 2006). Supporting these findings, binding of galectin-1 to VEGFR2 has recently been shown to mediate its downstream signal transduction (*e.g.,* phosphorylation of ERK1/2) in human umbilical vein and retinal microvascular endothelial cells, thereby promoting angiogenesis in cancer and proliferative diabetic retinopathy (Croci et al., 2014; Kanda et al., 2015). Furthermore, using a mouse model of oxygen-induced retinopathy, inhibition of hypoxia-induced galectin-1 was showed to suppress retinal neovascularization (Ridano et al., 2017; Yang et al., 2017), in which VEGF-A-mediated inflammation is required for pathological, but not physiological, vessel growth (Ishida et al., 2003). CNV is an inflammatory disorder that depends on endothelial production of CCL2/MCP-1 (Sakurai et al., 2003b) and ICAM-1 (Tsutsumi et al., 2003), both of which proved to be regulated under VEGFR2 (Kim et al., 2001; Marumo et al., 1999; Radisavljevic et al., 2000) as well as ERK1/2 (Chao et al., 2017; Jiang et al., 2013) and responsible for the recruitment of pro-angiogenic macrophages (Ishida et al., 2003; Sakurai et al., 2003a). Our present study showed that galectin-1/*Lgals1* deficiency suppressed inflammatory cytokines (*i.e.*, *Mcp-1* and *Icam-1*) and phosphorylation of Erk1/2 after laser treatment, suggest that galectin-1 regulates CNV formation via Erk1/2 pathway.

In the long-term management of nAMD, subretinal fibrosis has recently been regarded as a key pathological event in CNV, basically a form of fibrovascular proliferation consisting of both vascular and fibrous components, the latter of which would theoretically be and actually seemed to be resistant to anti-VEGF therapy (Bloch et al., 2013; Daniel et al., 2014). Previous studies showed AMD patient specimens the potent immunoreactivity of TGF-β1 in CNV-associated RPE cells, and the process of CNV-associated subretinal fibrosis was shown to be mainly mediated by TGF-β1-SMAD2/3 signal transduction, leading to SNAIL-mediated EMT changes in RPE cells (Hirasawa et al., 2011; Ishikawa et al., 2016; Iwanishi et al., 2016). Our current *in vivo* and *in vitro* data showing TGF-β1-induced *SNAI1*, but not *SNAI2* or *TWIST1*, are comparable with the previously shown positive immunostaining of SNAIL, but not SLUG or TWIST, within α-SMA-positive RPE cells having migrated into

the CNV tissue collected from AMD patients (Hirasawa et al., 2011). Interestingly, TGF-β1 was reported to induce the expression of TGF-β1 via its own downstream SMAD pathway in an autocrine manner and generate the TGF-β1-SMAD2/3-TGF-β1 vicious cycle during fibrogenesis (Ashcroft et al., 1999; Iwanishi et al., 2016; Piek et al., 2001). This mechanism of autoinduction for TGF-β1 was repeatedly confirmed in a variety of cell types including monocytes, keratinocytes, and fibroblasts (Piek et al., 2001). The current *in vitro* results are the first to show the TGF-β1 autoinduction in RPE cells, supporting a recent finding on the significant reduction of CNV-induced TGF-β1 in SMAD3-deficient mice (Iwanishi et al., 2016). AMD patient specimens previously demonstrated the potent immunoreactivity of TGF-β1 in CNV-associated RPE cells (Amin et al., 1994). Importantly, we revealed that galectin-1 was expressed in RPE cells together with its co-localization with phosphorylated SMAD2 and fibrotic markers in the CNV tissue of AMD patient specimens. Taken together, subretinal fibrosis may theoretically be the result of SNAIL-induced EMT changes in RPE cells driven by the TGF-β1-TβRI/II-SMAD2/3-TGF-β1 auto-amplifying loop.

In the present study, *Lgals1* deficiency led to significant suppression of CNV-associated subretinal fibrosis, the mechanism of which was suggested to inhibit the TGF-β1 auto-induction and subsequent SMAD2-SNAIL signal amplification to accelerate EMT changes in RPE cells. Interestingly, neither *Lgals1* deficiency nor *LGALS1* knockdown changed *Tgfb1* expression in the RPE-choroid tissue in mice without CNV induction or basal levels of *TGFB1* expression as well as EMT markers in non-stimulated RPE cells. Moreover, *LGALS1* overexpression in RPE cells did not affect EMT-related molecules, but further enhanced TGF-β1-induced upregulation of these EMT markers, suggesting that galectin-1 cannot facilitate EMT without the TGF-β1 auto-amplifying loop. These results indicate the possible involvement of galectin-1 selectively in the pathological (*i.e.*, auto-amplifying and thus pro-fibrotic), but not physiological, regulation of TGF-β1, in accordance with no requirement of galectin-1 for the physiological vascular and neural development. Previously, immunoreactive staining for AMD patients specimens demonstrated localization of TGF-β1in CNV-associated RPE cells (Amin et al., 1994), and the process of CNV-associated subretinal fibrosis was caused by TGF-β1-SMAD2/3 signal transduction, leading to SNAIL-mediated EMT changes in RPE cells (Hirasawa et al., 2011; Ishikawa et al., 2016). Moreover, galectin-

1 was shown to induce the activation of the pathway by phosphorylating SMAD2 via molecular interaction between galectin-1 and SMAD2 in lung fibroblasts to promote pulmonary fibrosis (Lim et al., 2014). Indeed, AMD patient specimens exhibited the co-localization of galectin-1 with phosphorylated SMAD2 translocated into the nucleus of RPE cells. Accordingly, the upregulation of galectin-1 in RPE cells following CNV induction, in concert with the presence of galectin-1 and TGF-β1 in neovascular AMD specimens, implies that galectin-1 enhances the TGF-β1-SMAD2-TGF-β1 vicious cycle by phosphorylating SMAD2 in RPE cells.

Co-existence of galectin-1 with VEGFR2 expressed on the surface of neovascular endothelial cells is known to stem from its lectin activity in the extracellular milieu (Croci et al., 2014), whereas galectin-1-modified SMAD2 phosphorylation in RPE cells would be listed as one of its diverse signaling interactions that typically take place intracellularly in a carbohydrate-independent manner (Camby et al., 2006). As for its additional but related property of potentially mimicking VEGF-A and TGF-β1 functions, galectin-1 has also proven to possess glycosylation-dependent binding capacity with neuropilin-1, a co-receptor for both VEGFR2 and TβRI/II, thus activating their downstream MAPK and SMAD2/3 signaling pathways, respectively (Hsieh et al., 2008; Xu et al., 2016). Interestingly, TGF-β1 was shown to induce galectin-1 via various non-canonical (*i.e.*, SMAD-independent) pathways such as p38 MAPK, phosphatidylinositol 3-kinase, and focal adhesion kinase-1 in embryonic skin fibroblasts and lung epithelial cells (Lim et al., 2014; Zheng et al., 2016). In the present study, however, RPE cells did not respond to TGF-β1 to cause the upregulation of *LGALS1* expression, suggesting the distinctly different cause-effect relationships between galectin-1 and TGF-β1 depending on individual cell species.

Supporting our current findings, previously reported pre-clinical results on Matrigel-induced CNV in rats showed the inhibitory effects of aflibercept (formerly known as VEGF Trap), which also binds to and neutralizes galectin-1 (Kanda et al., 2015), on leukocyte infiltration, CNV generation, and collagen deposition, thereby suggesting its efficacy as anti-inflammatory, -angiogenic, and -fibrotic actions (Cao et al., 2010), all of which are attributable, at least in part, to galectin-1's bioactivity. However, no clinical trials have so far clarified the anti-fibrotic property of aflibercept for the treatment of neovascular AMD patients. Nevertheless, this study highlights new insights on the molecular pathogenesis of CNV,

focusing on the role of galectin-1 in modifying VEGF-A and TGF-β1 receptor signaling to promote inflammation-related angiogenesis and fibrosis.

Chapter 2

Regulation of spermine oxidase through hypoxia-inducible factor-1α signaling in retinal glial cells under hypoxic condition

Introduction

Acrolein is a highly reactive unsaturated aldehyde that preferentially reacts with cysteine, lysine, and histidine residues in peptide chains to preserve aldehyde functionality (Aldini et al., 2011; Stevens and Maier, 2008). Our previous study demonstrated that the acrolein-conjugated protein (4-dehydropiperidino)lysine adduct (FDP-Lys) accumulates in glial cells of fibrovascular tissues of patients with PDR (Dong et al., 2017). Furthermore, subsequent analyses revealed that the acrolein production is catalyzed by SSAO, a copper-containing enzyme that deaminates aromatic and aliphatic amines, in retinal microvascular endothelial cells (Murata et al., 2017). In addition, accumulation of acrolein reduced level of glutathione (GSH) production and consequently increased the generation of reactive oxygen species (ROS) (Murata et al., 2017). The imbalance between ROS production and the antioxidant defense system activates several oxidative stress-related mechanisms that promote the pathogenesis of DR (Li et al., 2017). Moreover, we recently elucidated that acrolein increases oxidative stress by reducing the antioxidant GSH in cultured Müller glial cells and accelerates its cellular motility by inducing chemokine (CXC motif) ligand 1 in an autocrine fashion (Murata et al., 2019). Müller glial cells, as a major cellular source of VEGF, has been demonstrated that migrate into the retina and toward the vitreoretinal surface in patients with PDR (Nork et al., 1987; Ohira and de Juan, 1990). Thus, evidence indicates that acrolein is a causative factor for glial cell migration in diabetic retinopathy, and cellular machinery of acrolein generation in retinal glial cells, which lack SSAO, is yet to be understood.

Polyamines including putrescine, spermidine, and spermine are naturally occurring polycationic alkylamines that are involved in various biological processes, including cell proliferation and differentiation (Heby, 1981; Pegg, 2013). Of these, spermine possesses the highest biological activity, and conversion of spermine to spermidine occurs through one of two distinct pathways (Aikens et al., 1983). The catabolism of spermine to spermidine, spermine oxidation, is mediated via either the one-step enzymatic reaction of spermine oxidase (SMOX) or the two-step process of spermidine/spermine N1-acetyltransferase (SAT1) coupled with the

peroxisomal enzyme N1-acetylpolyamine oxidase (PAOX) (Gawandi and Fitzpatrick, 2007). Both catabolic pathways produced hydrogen peroxide and aldehydes (Casero and Pegg, 2009) (Fig. 21).

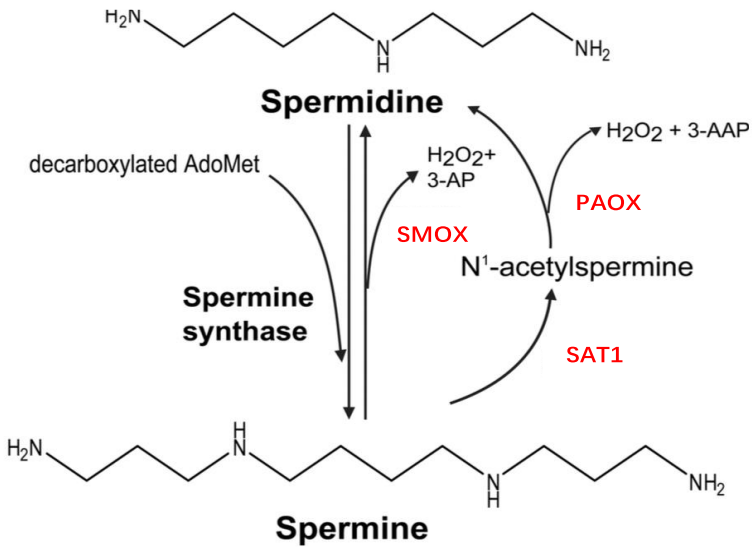

Polyamine metabolism

Figure 21. The polyamine metabolism. Either two-steps process of spermidine/spermine N1-acetyltransferase (SAT1) coupled with the peroxisomal enzyme N1-acetylpolyamine oxidase (PAOX) or directly from spermine to spermidine by spermine oxidase (SMOX).

SMOX is a flavin adenine dinucleotide-containing enzyme that catalyzes the oxidative degradation of spermine, a polyamine, to produce spermidine, hydrogen peroxides, and 3-aminopropanal that is, as aforementioned, non-enzymatically converted to acrolein. Müller glial cells are the cellular components of the mammalian retina that contain endogenous spermine (Biedermann et al., 1998). Moreover, a study showed that the level of spermine in the vitreous was approximately 15 times higher in patients with PDR than in those without DR (Nicoletti et al., 2003). Therefore, it is possible that spermine and its related products are involved in the pathogenesis of DR. However, spermine metabolism in retinal glial cells, which is likely to be important for further understanding of the pathogenesis of DR, has not fully been investigated.

In this study, we explored the effect of hypoxia on SMOX production and its regulatory mechanism in retinal glial cells under hypoxic conditions.

Methods

Cell culture

Conditionally immortalized rat retinal Müller cell line 5 (TR-MUL5) from transgenic rats harboring the temperature-sensitive simian virus 40 large T-antigen gene was provided by Fact Inc (Sendai, Japan) (Tomi et al., 2003). TR-MUL5 cells were cultured in DMEM containing 10% FBS and incubated at 33°C. The following experiments were performed at a 5% CO_2 with either 20% O_2 for normoxia or 1% O_2 balanced with N_2 for hypoxia at 37°C. All experiments were performed with cells in a subconfluent state and at passages 25–40.

Immunofluorescence microscopy

Fibrovascular tissues were collected from patients with PDR, including two men and one woman, with a mean age of 52.7 ± 4.0 years, and embedded in paraffin after fixation in 4% paraformaldehyde and stored at 4°C. This study was conducted in accordance with the tenets of the Declaration of Helsinki. The study protocol was approved by the institutional review committee of the Hokkaido University Hospital (#014-0293).

Sections were deparaffinized in xylene, dehydrated through a graded alcohol series, and subsequently rehydrated in deionized water. After microwave-based antigen retrieval with 10 mM citrate buffer (pH 6.0) for 15 min, sections were blocked in 10% normal goat serum (Thermo Fisher Scientific) for 1 h. At 4°C, sections were probed overnight with the following primary antibodies: rabbit anti-SMOX (1:100; Proteintech, Chicago, IL), rabbit anti-spermidine/spermine-N(1)-acetyl transferase (SAT1; 1:100; Thermo Fisher Scientific), rabbit anti-peroxisomal N(1)-acetyl-spermine/spermidine oxidase (PAOX; 1:100; Proteintech), and mouse anti-glial fibrillary acid protein (GFAP) (1:100; Leica Microsystems, Exton, PA). The secondary antibodies Alexa Fluor 488 and 546 (1:200; Thermo Fisher Scientific) were used for fluorescence detection. Normal rabbit IgG (1:100; R&D systems) and normal mouse IgG (1:100; Dako) were used as a negative control. Nuclei were counterstained with DAPI, and sections were visualized under a fluorescence microscope (Keyence).

For immunofluorescence staining of vimentin in TR-MUL5, the cells were cultured in 6-well plate with sterile glasses, fixed with 4% PFA for 10 min, and permeabilized with 0.2% Triton X-100 for 15 min. Subsequently, cells were blocked with 5% normal goat serum and

incubated overnight at 4℃ with mouse anti-vimentin (1:50; Thermo Fisher Scientific) antibody. Normal mouse IgG (1:50; Dako) in place of the primary antibody was used as a negative control. The secondary antibodies for fluorescent detection were Alexa Fluor 546 (1:200; Thermo Fisher Scientific). Nuclei were counterstained with DAPI and stained sections were visualized using fluorescence microscope (Keyence).

Real-time quantitative PCR

Following the manufacturers' instructions, total RNA was isolated using TRI Reagent (Molecular Research Center, Inc.), and reverse transcription was then performed to cDNA with GoScript reverse transcriptase (Promega). All primers are listed in Table 2. Real-time qPCR was performed using the GoTaq qPCR Master Mix (Promega) and StepOne Plus Systems (Thermo Fisher Scientific). Gene expression levels were calculated using the 2^{-ddCt} method, and all experimental samples were normalized using *Actb* as the internal control.

Table 2. Primer sequences used in quantitative RT-PCR

Target gene	Sequence
Smox	forward 5'- CGG GGA AAA TGG AAA CGT CAG -3'
	reverse 5'- ACT TTG CAT ACC GTC CGT ACT -3'
Sat1	forward 5'- CCT GGT TGC AGA AGT GCC TAA -3'
	reverse 5'- GTA CAT GGC AAA ACC AAC AAT GC-3'
Paox	forward 5'- TGG GCC CTC CCA TTA GAC AG -3'
	reverse 5'- GTC CTG CTG AGG GTT CAA G -3'
Vegfa	forward 5'- AGC AGA TGT GAA TGC AGA CCA AAG A-3'
	reverse 5'- TGG CTC ACC GCC TTG GCT T-3'
Actb	forward 5'- GGG AAA TCG TGC GTG ACA TT-3'
	reverse 5'- GCG GCA TGG CCA TCT C-3'

Enzyme-linked immunosorbent assay (ELISA)

TR-MUL5 cells were cultured under normoxic or hypoxic conditions for 24 h. Levels of SMOX protein in the cell lysate were analyzed using ELISA kits for rat SMOX (MyBioSource, San Diego, CA) following the manufacturer's protocol. Absorbance was read at 450 nm on a microplate reader (Tecan Sunrise). SMOX concentration was normalized by total protein concentration of cell lysates measured by BCA kit (Thermo Fisher Scientific).

Cell viability assay

TR-MUL5 cells were seeded into a 96-well plate and incubated for 24 h at 33℃ in the atmosphere of 95% air and 5% CO_2. The cells were cultured under normoxic or hypoxic conditions for 6 h or 24 h. Cell viability was assessed using CellTiter-Glo 2.0 (Promega), according to the manufacturer's instruction. Luminescence was measured by an Infinite 200 PRO micro-plate reader (Tecan Sunrise).

RNA interference

TR-MUL5 cells were transfected with a 5-nM final concentration of various Dicer-substrate siRNA (DsiRNA) for suppressing the gene expression of hypoxia-inducible factor-1α (*Hif1*a*)* or Hif-2α (*Hif2*a*)* (*Hif1*a siRNA-1, rn.Ri.Hif1a.13.1; *Hif1*a siRNA-2, rn.Ri.Hif1a.13.2; *Hif2*a siRNA-1, rn.Ri.Hif2a.13.1; *Hif2*a siRNA-2, rn.Ri.Hif2a.13.2) (Integrated DNA Technologies, Inc.), and negative control siRNA (Ctrl-siRNA). Transfections were performed using the Lipofectamine RNAiMAX reagent (Thermo Fisher Scientific). The composite transfection mixture was replaced with 10% FBS/DMEM 24 h after the transfection, and the cells were exposed to hypoxic stimulation.

Transient transfection and luciferase assay

TR-MUL5 cells were seeded in a 96-well plate at 1.5×10^4 cells/well containing 65 μL of 10% FBS/DMEM. After incubation for 24 h, cells were co-transfected with the X-tremeGENE HP DNA transfection reagent (Sigma-Aldrich) containing the pGL4.10 luciferase vector (Firefly-expressing plasmid, Promega), with the *Smox* promoter (-1067~ +122bp from transcriptional start site of *Smox*), and pRL-CMV vector (Renilla-expressing plasmid, Promega). Firefly and

Renilla luciferase activities were determined using the Dual-Glo luciferase assay system (Promega), and the luciferase activity (a Firefly: Renilla luciferase ratio) was measured according to the manufacturer's instructions. The promoter sequence analysis revealed six putative hypoxia response elements (HREs), 5'-A/GCGTG-3', over the *Smox* promoter region. Subsequently, the *Smox* promoter reporter with each of the six mutant sites was modified into a pGL4.10 luciferase vector using PrimeSTAR Mutagenesis Basal Kit (Takara Bio, Shiga, Japan). The HRE wild-type or mutated constructs, together with pRL-CMV, were transiently co-transfected into TR-MUL5 cells, followed by treatment with hypoxia, and the luciferase activity was measured.

Measurement of hydrogen peroxide and FDP-Lys production

TR-MUL5 cells were cultured with or without 50μM SMOX inhibitor (MDL72527, Sigma-Aldrich) for 24 h with or without hypoxia stimulation. Subsequently, cells were incubated in phosphate buffered saline at 37°C for 3 h, and the concentration of hydrogen peroxide in the supernatant was measured using the Hydrogen Peroxide Detection Kit (Cell Technology, Inc., Fremont, CA), according to the manufacturer's protocol.

FDP-Lys concentration in supernatant was evaluated using the ELISA kit (MK-150, Takara Bio), according to the manufacturer's instructions. Protein concentration of the supernatant was measured using the Quick Start Bradford 1× Dye Reagent (Bio-Rad, Hercules, CA) and used for normalization of FDP-Lys concentration.

Statistical analyses

Data are expressed as mean ± SEM for three to six individual experiments. Differences between two groups were compared using Student's *t*-test. For comparisons of multiple groups, the one-way analysis of variance and Tukey's honestly significant difference multiple comparisons test were used. A *P*-value less than 0.05 was considered statistically significant.

Results

Hypoxic upregulation of *SMOX* expression in TR-MUL5 cells

To investigate whether polyamine catabolic enzymes are involved in TR-MUL5 cells under hypoxic condition, we examined the mRNA expression levels of *Smox*, *Sat1*, and *Paox*. Under hypoxic condition, the mRNA expression of *Smox* was significantly upregulated in TR-MUL5 cells at 6 h, and followed with a slight upregulation at 24 h (Fig. 22A). In contrast, no significant upregulations were observed in mRNA expressions of *Sat1* and *Paox* in TR-MUL5 cells (Figs. 22B, C). The mRNA expression level of *Vegfa,* which was used as a positive control, significantly increased under hypoxic conditions (Fig. 22D).

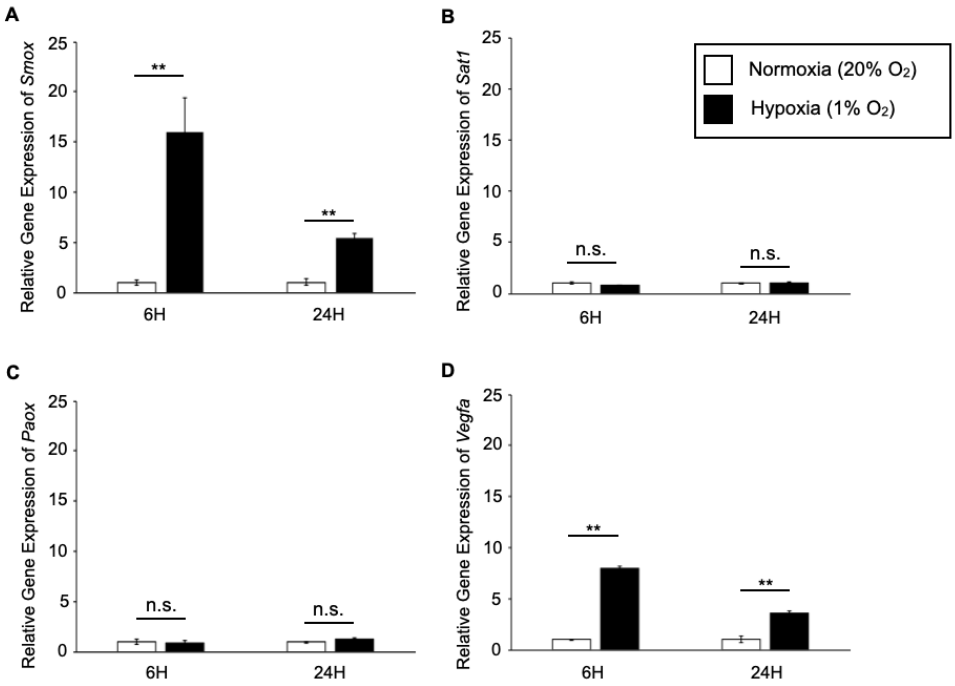

Figure 22. Gene expression levels of polyamine catabolic enzymes in TR-MUL5 cells under hypoxic conditions. (A-C) Real-time qPCR analysis for *Smox*, *Sat1* and *Paox* in TR-MUL5 cells. (D) Real-time qPCR analysis for *Vegfa* as a positive control. $n = 3$ in each group. $^{**}P < 0.01$, n.s., not significant.

Next, we investigate whether cell viability and structure were affected under hypoxic condition, we performed cell viability assay and immunofluorescent signal of vimentin under hypoxic condition. As shown in Figure 23A, hypoxic condition reduced the cell viability of

TR-MUL5 when cultured for 24 h, but not at 6 h. In addition, immunofluorescence was more intense in TR-MUL5 cells cultured under hypoxic condition than those under normoxic condition (Figs. 23B, C), indicating the presence of cellular stress at 24 h after hypoxic stimulation, which reduced *Smox* mRNA upregulation with time.

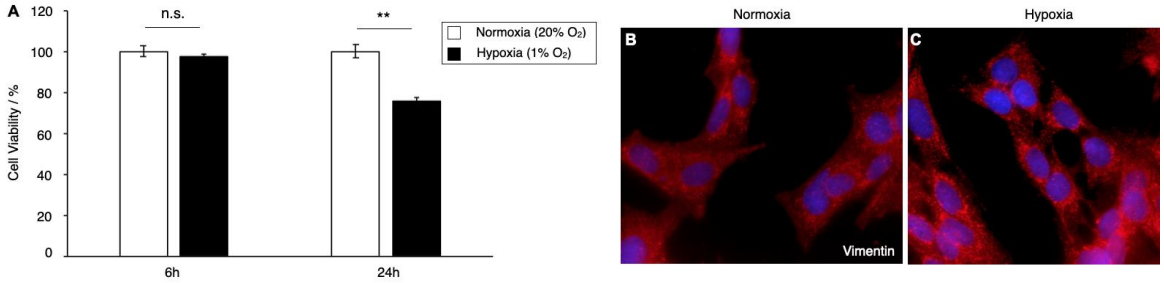

Figure 23. Cell viability assay in TR-MUL5 cells under hypoxic conditions. (A) Cell viability analysis of TR-MUL5 cells under hypoxic condition in 6 and 24 h. (B, C) Immunofluorescence staining for vimentin. SMOX protein levels in TR-MUL5 cells under hypoxic condition (1% O_2). n = 3 in each group. *P<0.05., **P <0.01, n.s., not significant.

Consistent with the mRNA data, protein concentration of SMOX under hypoxic conditions significantly increased to 1.5 times (P < 0.05) of that under normoxic conditions (Fig. 24). The current data demonstrated that hypoxia upregulates SMOX in retinal glial cells.

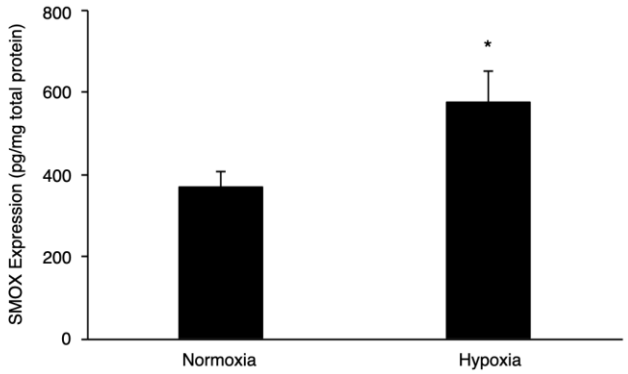

Figure 24. SMOX protein levels in TR-MUL5 cells under hypoxic condition (1% O_2). n = 3 in each group. *P<0.05.

Localization of SMOX, SAT1, and PAOX in fibrovascular tissues

To further confirm in vitro study, we performed immunofluorescent staining for polyamine oxidase enzymes to investigate the tissue localization of SMOX, SAT1, and PAOX in fibrovascular tissues of patients with PDR. Immunofluorescence staining showed that SMOX signals were intensely localized in the nucleus of TR-MUL5 cells (GFAP-positive cells) of the fibrovascular tissues (Fig. 25A). However, SAT1 and PAOX signals were weakly detected in glial cells (Figs. 25B, C). The staining data suggested that SMOX predominantly plays a role in spermine oxidation in retinal glial cells of fibrovascular tissues, which supported our in vitro study.

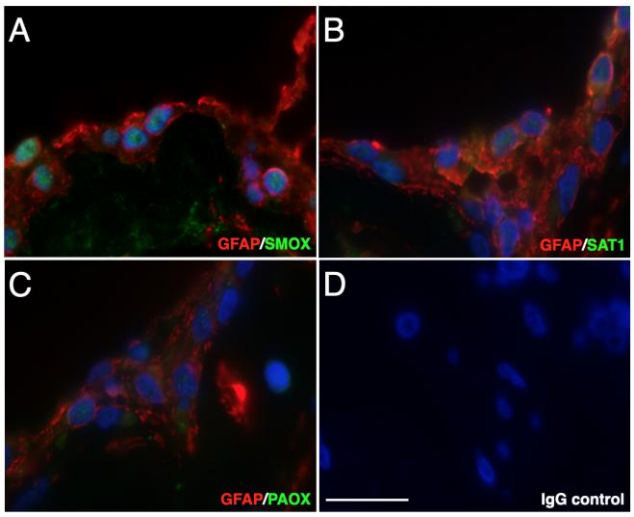

Figure 25. Immunofluorescence staining of spermine oxidase (SMOX), SAT1, and PAOX in fibrovascular tissues of patients with PDR. (A) Green, SMOX (Alexa Fluor 488); Red, glial fibrillary acid protein (GFAP) (Alexa Fluor 546). (B) Green, SAT1; Red, GFAP. (C) Green, PAOX; Red, GFAP. (D) Negative control (rabbit and mouse normal IgG) in sequential sections. Scale bar = 20μm.

HIF-1α modulation of the SMOX expression level in TR-MUL5 cells under hypoxic conditions

HIF, a transcriptional factor, is responsible for cellular responses to hypoxia and regulates various genes that are required for adaptation to hypoxia. To explore whether HIF mediates *Smox* expression under hypoxic conditions, we examined the expression level of *Smox mRNA* with silencing of either *Hif1*a or *Hif2*a. As shown in Figure 26A, expression of *Smox* was

significantly reduced by *Hif1*a siRNAs, but not by *Hif2*a siRNAs. In accordance with the gene expression data, the protein level of SMOX increased under hypoxic conditions and was reduced by *Hif1*a knockdown (Fig. 26B). Meanwhile, cell viability showed no reduction with silencing of either *Hif1*a or *Hif2*a (Fig. 26C). These results indicated that HIF-1α, but not HIF-2α, is a primary mediator that regulates SMOX production in TR-MUL5 cells under hypoxic conditions.

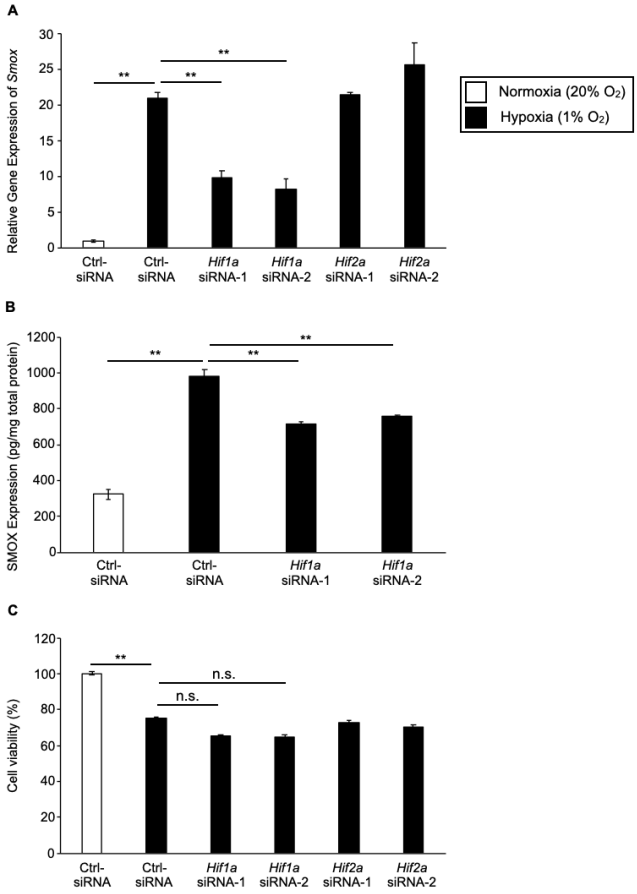

Figure 26. Expression and production of SMOX in TR-MUL5 cells with silencing of *Hif-1*a or *Hif-2*a under hypoxic condition (1% O_2). TR-MUL5 cells were transfected with control siRNA (Ctrl-siRNA), siRNAs for *Hif-1*a (*Hif-1*a siRNA-1 and -2), or siRNAs for *Hif-2*a (*Hif-2*a siRNA-1 and -2) and cultivated with or without hypoxic stimulation. (A) Real-time qPCR analysis for *Smox* mRNA expression 6 h after hypoxic stimulation. (B) SMOX protein levels in TR-MUL5 cells measured by ELISA 24 h after hypoxia stimulation. (C) Cell viability assay. $n = 3$ in each group. $^{**}P < 0.01$.

Functional HRE sites in the SMOX promoter region under hypoxic conditions

Next, we investigated whether the hypoxic induction of *Smox* is regulated at the transcriptional level. An analysis of the genomic sequences of rat *Smox* (NCBI: NC_005102.4) revealed six HRE sites within the promoter region (Fig. 27A). Based on the locations of HRE sites, sequences from -1067 to +122 of the *Smox* encoding region were cloned into the pGL4.10 luciferase reporter plasmid (rsmox-1067.pGL4.10). To evaluate the functional activity of the *Smox* promoter, transfection experiments were performed using *Smox* promoter–reporter vector constructs in TR-MUL5 cells under normoxic or hypoxic condition. As shown in Figure 27B, transcriptional activity of constructs containing rsmox-1067.pGL4.10 were higher under hypoxic conditions compared to cells co-transfected with the empty pGL4.10 vector. To further examine whether hypoxia regulates *Smox* transcriptional activity via HIF-1α, we evaluated luciferase activity after co-transfecting the *Smox* promoter–reporter vector with *Hif1a* siRNA. As a result, the transcriptional activation of *Smox* was significantly suppressed by silencing of *Hif1a* (Fig. 27C), indicating that *Hif1a* is involved in the hypoxic regulation of *Smox* transcriptional activity.

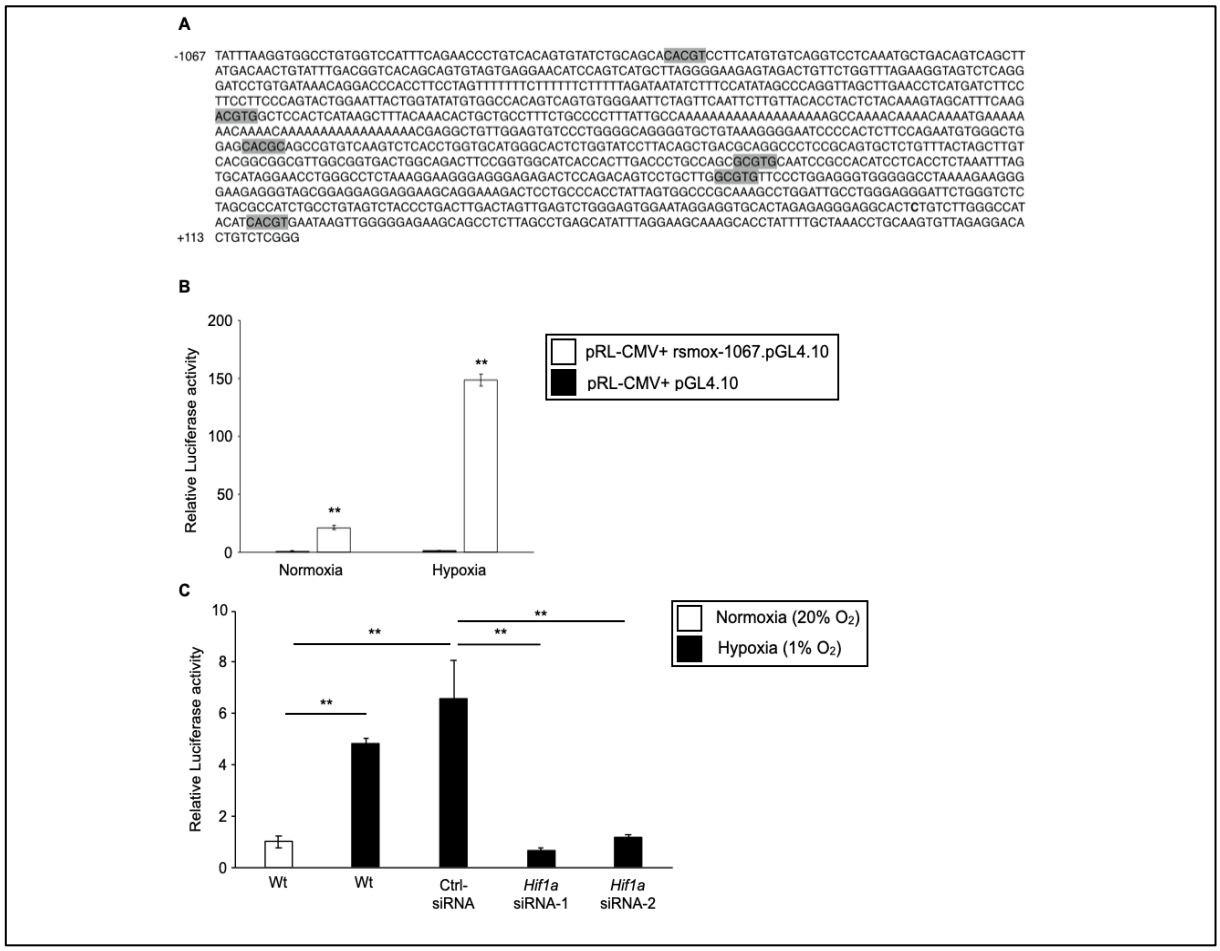

Figure 27. Identification of HRE sites in the SMOX promoter. (A) Six potential HRE sites were located in the rat Smox promoter in the sequence analysis. (B) The luciferase analysis showed that the transcriptional activity of the Smox promoter in TR-MUL5 cells was significantly enhanced by hypoxia incubation. (C) The transcriptional activity of the Smox promoter was reduced by silencing of HIF-1α under hypoxic conditions. **P <0.01.

To investigate the respective activity of the six HRE sites, we generated mutant reporter constructs using site-directed mutagenesis (Fig. 28A). As shown in Figure 28B, the HRE mutant sites (mHRE) 2, 3, and 4 exhibited significant decrease in luciferase activity compared to the non-mutated control, suggesting that these three HRE sites in the *Smox* promoter contribute to the transcriptional activation of *Smox*. The current results suggest that hypoxia regulates *Smox* transcriptional activity via HIF-1α binding to HRE2, HRE3, and HRE4 sites in the *Smox* promoter.

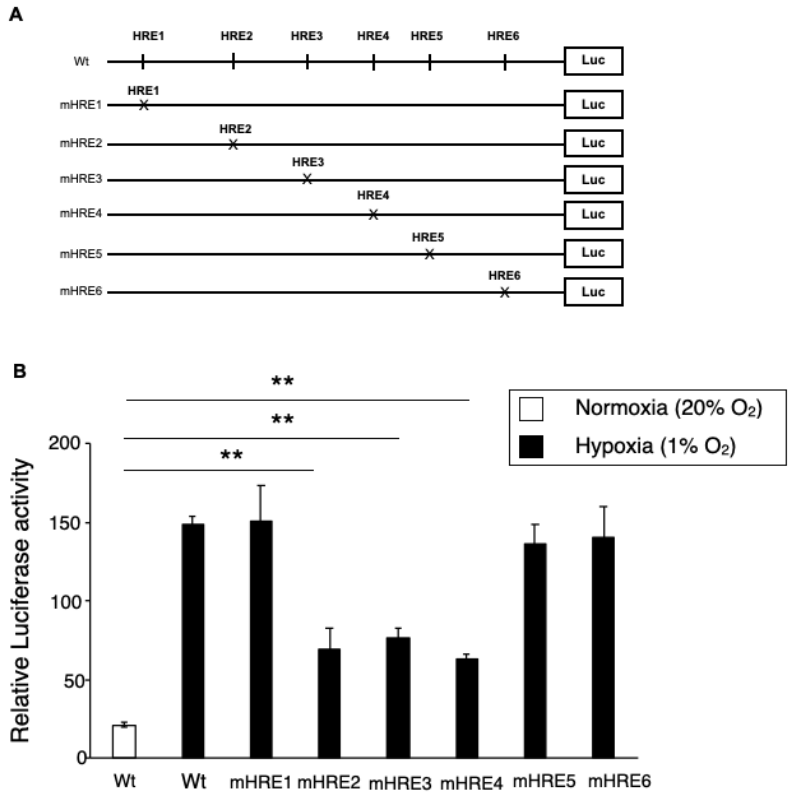

Figure 28. The regulation of HRE sites in the SMOX promoter under hypoxic condition. (A) Mutant luciferase constructs were designed for each of the six HRE sites via site-direct

mutagenesis using the -1067 Luc reporter plasmid as a backbone. (B) Mutant HRE2, HRE3, and HRE4 of the Smox promoter reduced the Smox transcript activity under hypoxic conditions. (n = 6 in each group). **P <0.01.

Production of Hydrogen Peroxide and FDP-Lys Mediated by SMOX under Hypoxic Conditions in TR-MUL5 cells

To examine the role of SMOX in Müller glial cells under hypoxic conditions, we measured the concentration of hydrogen peroxide and FDP-Lys, acrolein-conjugated protein, with or without the SMOX inhibitor (MDL72527) under hypoxic conditions in TR-MUL5 cells. The concentration of hydrogen peroxide significantly increased in the supernatants of the TR-MUL5 cells under hypoxic conditions (3 h), while their production was reduced by the SMOX inhibitor (Fig. 29A). In addition, FDP-Lys production significantly increased under hypoxic conditions (24 h), which was suppressed by the SMOX inhibitor (Fig. 29B). These data indicated that SMOX induced by hypoxia participates in the production of hydrogen peroxide and FDP-Lys in retinal glial cell.

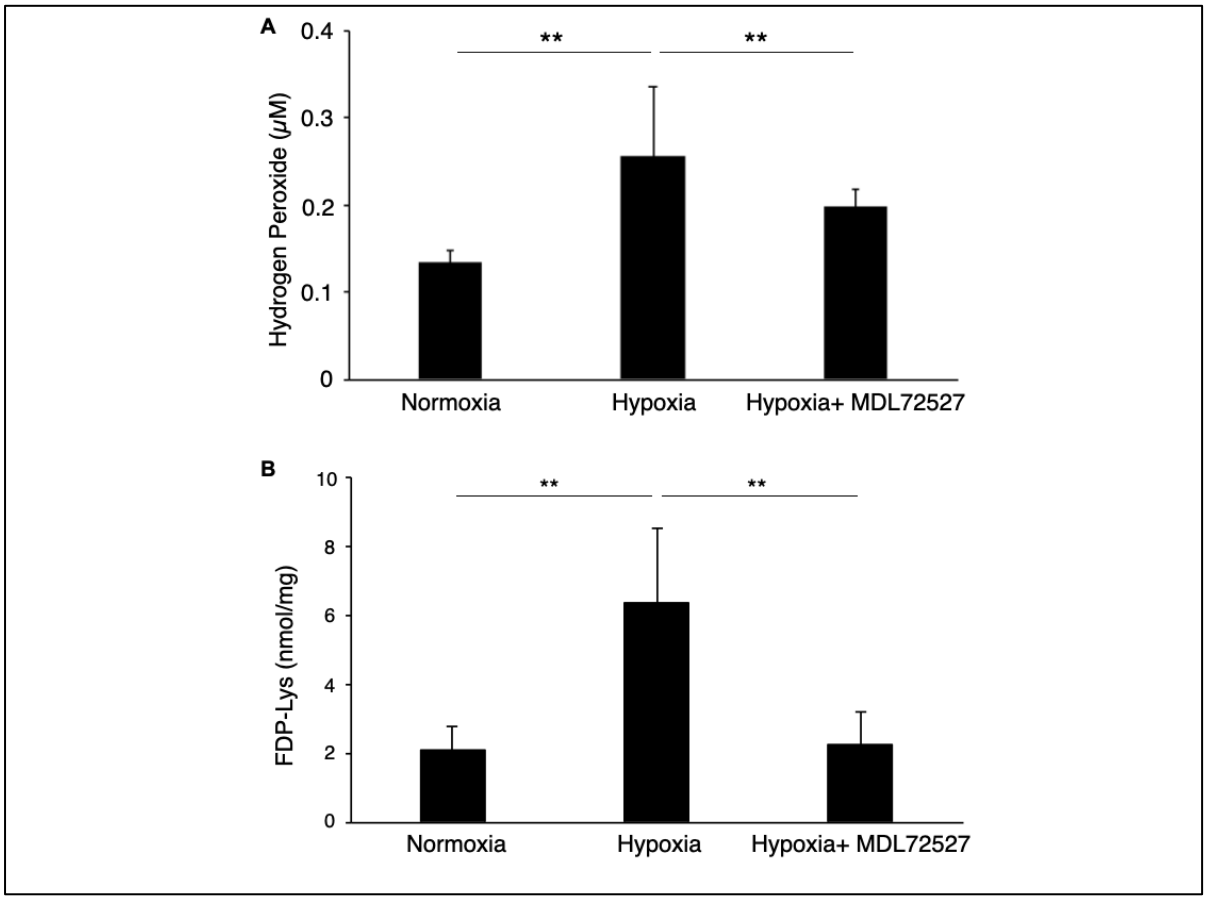

Figure 29. Hydrogen peroxide and acrolein generation via SMOX under hypoxic conditions in TR-MUL5 cells. The production of hydrogen peroxide and FDP-Lys were analyzed when incubated with or without the SMOX inhibitor (MDL72527) under hypoxic conditions. (A, B) Hypoxia-induced hydrogen peroxide (A) and FDP-Lys (B) secretion were inhibited in the presence of MDL72527. (n = 6 in each group). **P <0.01.

Discussion

In the present study, we demonstrated for the first time that the significant involvement of SMOX, a polyamine oxidase enzyme, in PDR. SMOX was upregulated by hypoxic stimulation at mRNA and protein levels in retinal glial cells (Figs. 22-24). Among polyamine oxidase enzymes, SMOX primarily localized in retinal glial cells of fibrovascular tissues (Fig. 25). In hypoxic condition, HIF-1α was the mainly regulator to mediate SMOX production (Figs. 26-28), following the hydrogen peroxide and acrolein production in retinal glial cells (Fig. 29). These results suggest that hypoxia induces SMOX via HIF-1α signaling in retinal glial cells, presumably participating in fibrovascular proliferation in eyes with PDR.

PDR is still a main cause of visual impairment, despite the recent progress in vitreoretinal surgery. It is characterized by proliferation of fibrovascular tissue formed by the extension of retinal angiogenesis into the vitreous cavity, and the fibrovascular tissue formation caused severe complications, such as vitreous hemorrhage and tractional retinal detachment, and irreversible vision loss. Müller glial cells are the principal glial cell type in the retina that contribute to structural support and maintenance of the complex metabolism (Bringmann et al., 2006; Willbold and Layer, 1998). In addition, they provoke fibrovascular proliferation with propensities for migration (Nork et al., 1987; Ohira and de Juan, 1990), fibroblastic transdifferentiation (Guidry et al., 2003), and angiogenic activity (Ishida et al., 2000; Noda et al., 2005) in PDR. Therefore, the activation mechanism of Müller glial cells in diabetic retinopathy should be investigated. In the present study, we primarily focused on SMOX induction in retinal glial cells since SMOX enzymatically generates 3-aminopropanal, the precursor of unsaturated aldehyde acrolein, which promotes cellular motility of cultured Müller glial cells during spermine oxidation (Murata et al., 2019).

In the current study, RT-PCR and ELISA data demonstrated the all the polyamine oxidation enzymes are expressed in culture Müller glial cells, and hypoxic stimulation exclusively upregulates SMOX alone in cultured glial cells. Consistent with the RT-PCR and ELISA data, the immunofluorescence staining showed that SMOX was predominantly localized in glial cells of the fibrovascular tissues from patients with PDR, The current data indicated that SMOX is a primary enzyme for spermine oxidation in glial cells migrated into fibrovascular tissues.

SMOX is a highly inducible enzyme in the polyamine catabolism cascade. SMOX expression is upregulated by inflammatory cytokines, including tumor necrosis factor-α and interleukin-6 (Babbar and Casero, 2006; Cervelli et al., 2010). In addition, dysregulation of SMOX alters intracellular polyamine levels and is associated with the progression of various human diseases, such as cancer (Goodwin et al., 2008; Snezhkina et al., 2016), ulcerative colitis (Hong et al., 2010), stroke (Tomitori et al., 2005), and diabetes (Seghieri et al., 1990). With respect to ocular diseases, SMOX expression is upregulated in the retinal tissue of streptozotocin-induced diabetic mice (Liu et al., 2020). Additionally, the current study elucidated that hypoxia enhances SMOX production in retinal glial cells. In general, polyamines, including spermine, have been recognized as essential components for various cellular functions. Conversely, recent studies have revealed that polyamines are implicated in cell apoptosis and autophagy (Chae and Kim, 2014; Lasbury et al., 2007; Pignatti et al., 2004). Several studies showed that excessive spermine exerts cellular toxicity (Del Rio et al., 2018; Kaneko et al., 2007). Spermine oxidation by SMOX could be a common trigger for pathological changes in various diseases, including diabetic retinopathy.

Cellular activities in response to hypoxia, for instance, angiogenesis and erythropoiesis, are regulated via the highly conserved HIF family, consisting of heterodimers composed of one of the three α-subunits (HIF-1α, HIF-2α, or HIF-3α) and a β-subunit known as the aryl hydrocarbon nuclear translocator (Zamudio et al., 2007). Of these, HIF-1 is a heterodimeric basic helix-loop-helix transcription factor composed of two subunits, HIF-1α and HIF-1β (Wang et al., 1995). The HIF-1 complex recognizes HRE motifs in the promoter of a broad range of target genes (Zhong et al., 1999). In the present study, *Hif1*a knockdown using the siRNA technique suppressed the increase in SMOX transcription whereas *Hif2*a knockdown showed no suppressive effect on SMOX transcription, indicating that HIF-1, but not HIF-2, regulates transcriptional activity of *SMOX* in glial cells exposed to hypoxia. Furthermore, using luciferase assay, we also justified that HIF binding sites in the promoter region of SMOX are HRE2, HRE3, and HRE4. The luciferase assay data also supported that HIF-1 is a mediator of SMOX transcription in retinal glial cells under hypoxic conditions.

Finally, the role of hypoxia-induced SMOX in retinal glial cells was elucidated in the present study. Hypoxic stimulation to cultured glial cells elevated the levels of hydrogen

peroxide and FDP-lys, both of which were abrogated by the potent SMOX inhibitor MDL72527, indicating that SMOX produces the two oxidative stress inducers through the enzymatic conversion of spermine to spermidine in retinal glial cells under hypoxic conditions. In eyes with PDR, FDP-Lys, a reactive intermediate that can covalently bind to thiols, including GSH, through the retained electrophilic carbonyl moiety, accumulates in the vitreous (Murata et al., 2019) and glial clusters of fibrovascular tissues (Dong et al., 2017) in patients with PDR. Collectively, the previous and current data indicated that SMOX participates in the pathogenesis of PDR via deterioration of oxidative stress.

In conclusion, the current data indicated that HIF-1 regulates SMOX production, leading to acrolein and hydrogen peroxide generation in Müller glial cells under hypoxic condition. One scientific significance of the present research is that it implies the involvement of SMOX in ischemic retinopathies, including retinal vein occlusion, retinopathy of prematurity, and DR. To date, these diseases have been treated as vascular diseases; however, much attention has recently been paid to the neurodegenerative aspects of the diseases. Since SMOX has been recognized as a potential molecular target to prevent neurodegeneration in diabetic retinopathy (Narayanan et al., 2019), SMOX inhibition may have the potential for simultaneous therapeutic intervention, neuroprotection, and fibrovascular proliferation prevention in DR.

Chapter 3

Transforming growth factor-β contributes to angiogenesis and Müller glial-mesenchymal transition in the pathogenesis of proliferative diabetic retinopathy

Introduction

To date, basic and clinical reports have exhibited that vascular endothelial growth factor (VEGF)-A, a key proangiogenic factor, contributes to the principal pathogenic events (*e.g.,* retinal neovascularization and inflammation) of DR (Adamis et al., 1994; Aiello et al., 1994). Hypoxia is one of the key activators for VEGF-A expression; this explains why hyperglycemia-induced capillary loss leads to progressive retinal hypoxia, and an increase in retinal vascular permeability and VEGF-A expression. Indeed, hypoxia-responsive elements are identified in the promoter region of *VEGFA*, indicating that hypoxia regulates *VEGFA* transcription through transcriptional regulation by the hypoxia-inducible factor (HIF)-1 (Forsythe et al., 1996). In addition to hypoxia, several cytokines and growth factors have been demonstrated to regulate VEGF-A expression via various activated transcription factors (*e.g.,* activator protein-1 and stimulator protein-1) that bind to the *VEGFA* promoter region (Loureiro and D'Amore, 2005; Pages and Pouyssegur, 2005). In the eyes, among various retinal cell types including astrocytes, ganglion cells, retinal pigment epithelium (RPE), and vascular endothelium involved in the production of VEGF-A (Penn et al., 2008), Müller glial cells, the primary glia of the retina, are the major source of VEGF-A, and contribute to the fibrovascular tissue formation as cellular components in the eyes of patients with PDR (Guidry et al., 2009; Le, 2017). Müller cell-derived fibroblasts are one of the cell populations capable of generating tractional force against the fibrovascular tissue (Guidry et al., 2003). Therefore, the molecular mechanisms underlying VEGF-A production and fibrovascular proliferation in Müller glial cells as well as in DR is of great practical interest; however, still remains unknown.

Transforming growth factor (TGF)-β, a multifunctional secreted protein, regulates various critical biological responses, such as differentiation, migration, and proliferation, and is regarded as the key initiator of epithelial-mesenchymal transition (EMT) and tissue fibrosis in numerous organs (Massague, 1998). The TGF-β ligand triggers downstream signal transductions by binding to membrane receptors bearing serine/threonine kinase activity, namely type I TGF-β receptor (TβRI) and type II TGF-β receptor (TβRII), and its cellular

signaling is translocated to the nucleus through SMAD-independent (noncanonical) and SMAD-dependent (canonical) pathways (Seystahl et al., 2015; Shi and Massague, 2003; Vander Ark et al., 2018). Activation of TGF-β/TβR axis induces several cytokines and growth factor expression including VEGF-A, which promotes the inflammatory and angiogenic activity of numerous disorders (Fang et al., 2020; Qian et al., 2004; Wang et al., 2004). Recently, we reported that TGF-β increases the expression of several EMT-related molecular markers and cell motility in human retinal Müller glial cells, which induces Müller glial-mesenchymal transition (GMT), as an alternative to EMT, in the pathogenesis of idiopathic epiretinal membrane (iERM) (Kanda et al., 2019). However, concerning PDR, there have been no reports on the pro-angiogenic and fibrotic roles of TGF-β in Müller glial cells.

In the present study, we demonstrated the molecular mechanism of TGF-β-induced VEGF-A production in Müller glial cells and the involvement of TGF-β in fibrovascular tissue formation of PDR.

Methods

Cell Culture and Reagents

The human Müller glial cell line Moorfields/Institute of Ophthalmology-Müller 1 (MIO-M1) was provided from Dr. G. Astrid Limb (UCL Institute of Ophthalmology, London, United Kingdom) (Limb et al., 2002). MIO-M1 were cultured in DMEM (FUJIFILM Wako Pure Chemical Corporation, Osaka, Japan) containing 10% fetal bovine serum (Thermo Fisher Scientific, Waltham, MA, USA) at 37°C incubator.

Recombinant human TGF-β1, TGF-β2, connective tissue growth factor (CTGF), fibroblast growth factor (FGF)2, nerve growth factor (NGF) and platelet-derived growth factor (PDGF)-BB proteins were purchased from PeproTech (Rocky Hill, NJ, USA), and VEGF-A was from R&D systems (Minneapolis, MN, USA). To block intracellular signaling pathways, the following inhibitors were used: U0126 for extracellular signal-regulated kinase (ERK)1/2 (Promega, Madison, WI, USA); JSH-23 for nuclear factor (NF)-κB (Sigma-Aldrich, St. Louis, MO, USA); LY294002 for phosphatidylinositol-3 kinase (PI3K) (FUJIFILM Wako Pure Chemical Corporation); SP600125 for c-Jun N-terminal kinase (JNK) (Millipore, Temecula, CA, USA); SB203580 for p38 mitogen-activated protein kinase (MAPK) (Cell Signaling Technology, Danvers, MA, USA); SB216763 for glycogen synthase kinase (GSK)-3 (ChemScence, Monmouth Junction, NJ, USA), and SB431542 for TβRI kinase (Cayman Chemical, Ann Arbor, MI, USA). Rabbit anti-TβRI, goat anti-TβRII neutralizing antibodies, and normal rabbit and goat IgGs were purchased from R&D systems. Two siRNA oligos for suppressing the gene expression of *SMAD2* (siRNA-1, hs.Ri.SMAD2.13.1; siRNA-2, hs.Ri.SMAD2.13.2) (Integrated DNA Technologies, Coralville, IA, USA) and negative control siRNA oligo (Ctrl-siRNA, Mission SIC-001, Sigma-Aldrich) were used at 10 nM for transfection. Transfections were performed using the Lipofectamine RNAiMAX Reagent (Thermo Fisher Scientific), following the manufacturer's protocol.

Real-time quantitative PCR

Total RNA was isolated by using TRI reagent (Molecular Research Center, Cincinnati, OH, USA) and reverse transcription to cDNA using GoScript reverse transcriptase (Promega, Madison, WI, USA), according to the manufacturer's instructions. All primers are listed in

Table 3. Real-time qPCR was performed with the GoTaq qPCR Master Mix (Promega) and StepOne Plus Systems (Thermo Fisher Scientific). Gene expression levels were calculated using the 2^{-ddCt} method, and all experimental samples were normalized using *glyceraldehyde-3-phosphate dehydrogenase* (*GAPDH*) as an internal control.

Table 3. The list of primers used in the present study

Target gene	Sequence
VEGFA	forward 5'- CAG ATT ATG CGG ATC AAA CCT CA -3'
	reverse 5'- CAA GGC CCA CAG GGA TTT TC -3'
TGFB1	forward 5'- AAG GAC CTC GGC TGG AAG TG -3'
	reverse 5'- CCG GGT TAT GCT GGT TGT A-3'
TGFB2	forward 5'- TTG TTG CCC TCC TAC AGA CTG G -3'
	reverse 5'- GTA AAG AGG GCG AAG GCA GCA A-3'
SMAD2	forward 5'- ACC GAA ATG CCA CGG TAG AA -3'
	reverse 5'- TGG GGC TCT GCA CAA AGA T-3'
TGFBR1	forward 5'- GGA ATT CAT GAA GAT TAC CAA C-3'
	reverse 5'- AGA GTT CAG GCA AAG CTG TAG A-3'
TGFBR2	forward 5'- GCG GGA GCA CCC CTG TGT C-3'
	reverse 5'- CCC GAG AGC CTG TCC AGA TGC-3'
GAPDH	forward 5'- CCT GGC CAA GGT CAT CCA TG -3'
	reverse 5'- GGA AGG CCA TGC CAG TGA GC -3'

ELISA

Protein levels of VEGF-A in the supernatant were determined with ELISA kits for human VEGF (R&D Systems) according to the manufacturer's protocols. The optical density was measured using a microplate reader (Sunrise).

Human Surgical Samples and Immunofluorescence Microscopy

During vitrectomy for traction retinal detachment, 4 fibrovascular tissues were excised from PDR eyes and used for immunohistochemistry. This study was conducted in accordance with the tenets of the Declaration of Helsinki and after receiving approval from the institutional review board of Hokkaido University Hospital. Written informed consent was obtained from all patients after explanation of the purpose and procedures of this study.

Immunofluorescence analyses were performed as described previously (Kanda et al.,

2020; Kanda et al., 2019; Wu et al., 2019). Sections were deparaffinized in xylene, dehydrated through a graded alcohol series, and subsequently rehydrated in deionized water. After microwave-based antigen retrieval with 10 mM citrate buffer (pH 6.0), sections were blocked in 5% normal goat or donkey serum for 1h. Sections were incubated overnight at 4°C with the following primary antibodies: rabbit anti-glial fibrillary acidic protein (GFAP) (1:2000; DAKO, Tokyo, Japan), mouse anti-GFAP (1:100; Leica, Exton, PA, USA), mouse anti-TGF-β1 (1:10), rabbit anti-TGF-β2 (1:50), goat anti-TβRII (1:40), mouse anti-α-smooth muscle actin (SMA) (1:50; R&D system), rabbit anti-TβRI (1:50), mouse anti-VEGF-A (1:200; Abcam, Cambridge, UK), mouse anti-glutamine synthetase (GS) (1:100; Sigma-Aldrich), rabbit anti-smooth muscle protein (SM)22 (1:100; Thermo Fisher Scientific) antibodies. The secondary antibodies Alexa Fluor 488 and 546 (1:200; Thermo Fisher Scientific) were used for fluorescence detection. Nuclei were counterstained with DAPI (4',6-diamidino-2-phenylindole), and sections were examined using a Biorevo BZ-9000 microscope (Keyence).

Immunoblot Analyses

Collected cells were lysed in SDS buffer. After quantifying protein concentrations using BCA reagent (Thermo Fisher Scientific), proteins were resolved by SDS-PAGE and transferred to PVDF membrane by electroblot analysis. Membranes were blocked in Tris-buffered saline containing 5% skim milk and 0.05% Tween-20 and incubated with the following primary antibody: rabbit anti-phosphorylated AKT (1:1000), rabbit anti-AKT (1:1000), mouse anti-phosphorylated p38 MAPK (1:1000), rabbit anti-p38 MAPK (1:1000), rabbit anti-phosphorylated SMAD2 (1:1000), rabbit anti-SMAD2 (1:1000), rabbit anti-phosphorylated GSK-3α/β (1:1000), rabbit anti-phosphorylated NF-κB p65 (1:1000), rabbit anti-NF-κB p65 (1:1000; Cell signaling Technology), mouse anti-GSK-3α/β (1:1000; Santa Cruz Biotechnology) and mouse anti-GAPDH (1:1000; Thermo Fisher Scientific) antibodies. Horseradish peroxidase-conjugated anti-mouse and rabbit IgGs (1:4000; Jackson ImmunoResearch Laboratories, West Grove, PA, USA) were used as secondary antibodies for chemiluminescence detection. Signals were visualized by enhanced chemiluminescence (iBright 1500 Imaging System, Thermo Fisher Scientific).

Statistical Analyses

All the results are expressed as the mean ± SEM (standard error of the mean). Student's t-test was used for statistical comparison between groups, and one-way analysis of variance (ANOVA) followed by the Tukey-Kramer method as a post-hoc test was used for multiple comparison procedures. Differences between means were considered statistically significant when p values were < 0.05.

Results

TGF-β1 as well as TGF-β2 alone stimulates the expression of *VEGFA* in Müller glial cells

Hypoxia induces the VEGF-A production in Müller glial cells and accelerates pathological neovascularization in PDR (Kanda et al., 2020; Stone et al., 1995), as well as various pro-fibrotic cytokines and growth factors, are known to be upregulated in the eyes of patients with PDR (Dai et al., 2014; Kuiper et al., 2008; Praidou et al., 2011). The upregulated cytokines and growth factors-induced VEGF-A levels in other organs (Liu et al., 2014; Tsai et al., 1995; Wang et al., 2016), led us to hypothesize that *VEGFA* expression can be increased not only by hypoxia but also by the pro-fibrotic molecules in human Müller glial cells. Of various stimuli including TGF-β1/2, CTGF, FGF2, NGF, and PDGF-BB, all of which are reported to be increased in the eyes of patients with PDR (Dai et al., 2014; Kuiper et al., 2008; Praidou et al., 2011), TGF-β1 as well as TGF-β2 alone significantly elevated the mRNA expression levels of *VEGFA* in Müller glial cells, as compared to PBS control (Fig. 30A). The administration of TGF-β1/2 to Müller glial cells upregulated *VEGFA* mRNA level in a time- and dose-dependent manner (Figs. 30B, C). Consistent with the mRNA expression results, the protein levels of VEGF-A in the culture medium elevated by TGF-β1/2 stimulation in a dose-dependent manner (Fig. 30D).

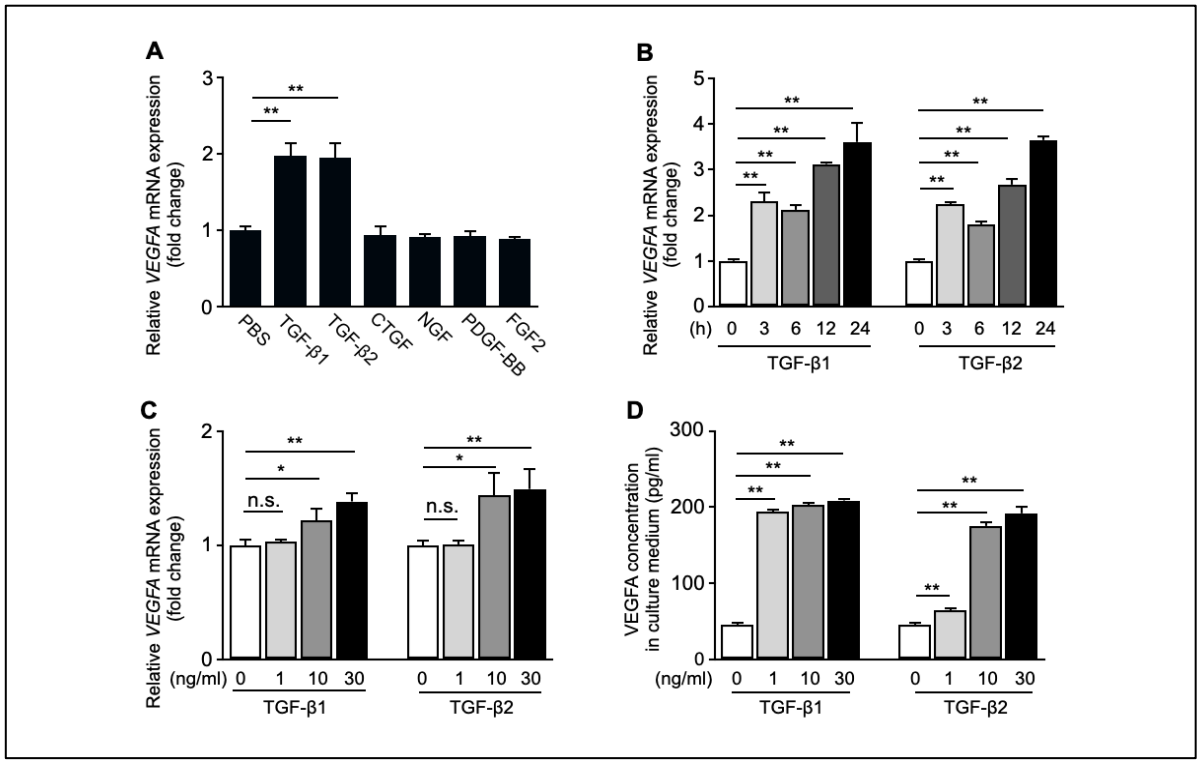

Figure 30. TGF-β1 as well as TGF-β2 alone stimulate the expression of *VEGFA* in Müller glial cells. (A) Müller glial cells were treated with TGF-β1, TGF-β2, CTGF, NGF, PDGF-BB and FGF2 at the dose of 10 ng/ml for 24 hours, and *VEGFA* expression were analyzed. (B-D) Müller glial cells were incubated with TGF-β1 or TGF-β2 in different time- or dose-point, and the mRNA and protein expression levels of *VEGFA* were analyzed. n = 3, **P* < 0.05, ***P* < 0.01, n.s., not significant.

Furthermore, we investigated whether VEGF-A contributes to the molecular mechanism of TGF-β1/2 expression in Müller glial cells; however, the mRNA levels of *TGFB1* and *TGFB2* were not changed with VEGF-A incubation (Fig. 31).

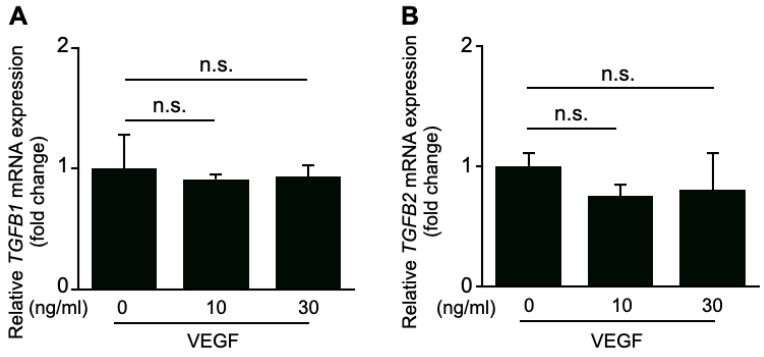

Figure 31. Administration of VEGF-A unelevated the expression of *TGFB1* and *TGFB2* in Müller glial cells. (A, B) Müller glial cells were incubated with VEGF-A (10 or 30 ng/ml) for 24 hours, and the mRNA expression level of *TGFB1* (A) and *TGFB2* (B) were analyzed. n = 3, n.s., not significant.

TGF-β1 and TGF-β2 upregulate the expression of *VEGFA* via TβR

Upon TGF-β1/2 binding to TβRII, TβRI is recruited and phosphorylated to stimulate the downstream signaling pathway (Massague, 1998). To check the involvement of TβR in TGF-β1/2-induced VEGF-A expression, we further performed blocking experiments using neutralizing antibodies and chemical inhibitor. Compared to normal IgG or DMSO controls, pretreatment with anti-TβRI neutralizing antibody, TβRI kinase inhibitor (SB431542), and anti-TβRII neutralizing antibody significantly blocked the TGF-β1/2-induced upregulation of

VEGFA mRNA expression levels (Figs. 32A, B). These data suggest that the TGF-β/TβR axis participates in the production of VEGFA in Müller glial cells.

To validate the *in vitro* TGF-β/TβR-mediated regulation of VEGF-A, we carried out immunofluorescence analyses to investigate the existence of TGF-β1/2, TβRI/II and VEGF-A in human samples surgically excised from the eyes of patients with PDR. Double-staining experiments for serial sections exhibited co-localization of GFAP, a marker for glial cells, with TGF-β1 (Figs. 32C-E), TβRI (Figs. 32F-H), and VEGF-A (Figs. 32I-K), as well as TGF-β2 (Figs. 32L-N) and TβRII (Figs. 32O-Q). Moreover, VEGFA-positive glial cells co-localized with TβRI (Figs. 32R-T) and TβRII (Figs. 32U-W) in the fibrovascular tissues, suggesting the TGF-β-induced production of VEGF-A protein via the TβR axis in Müller glial cells.

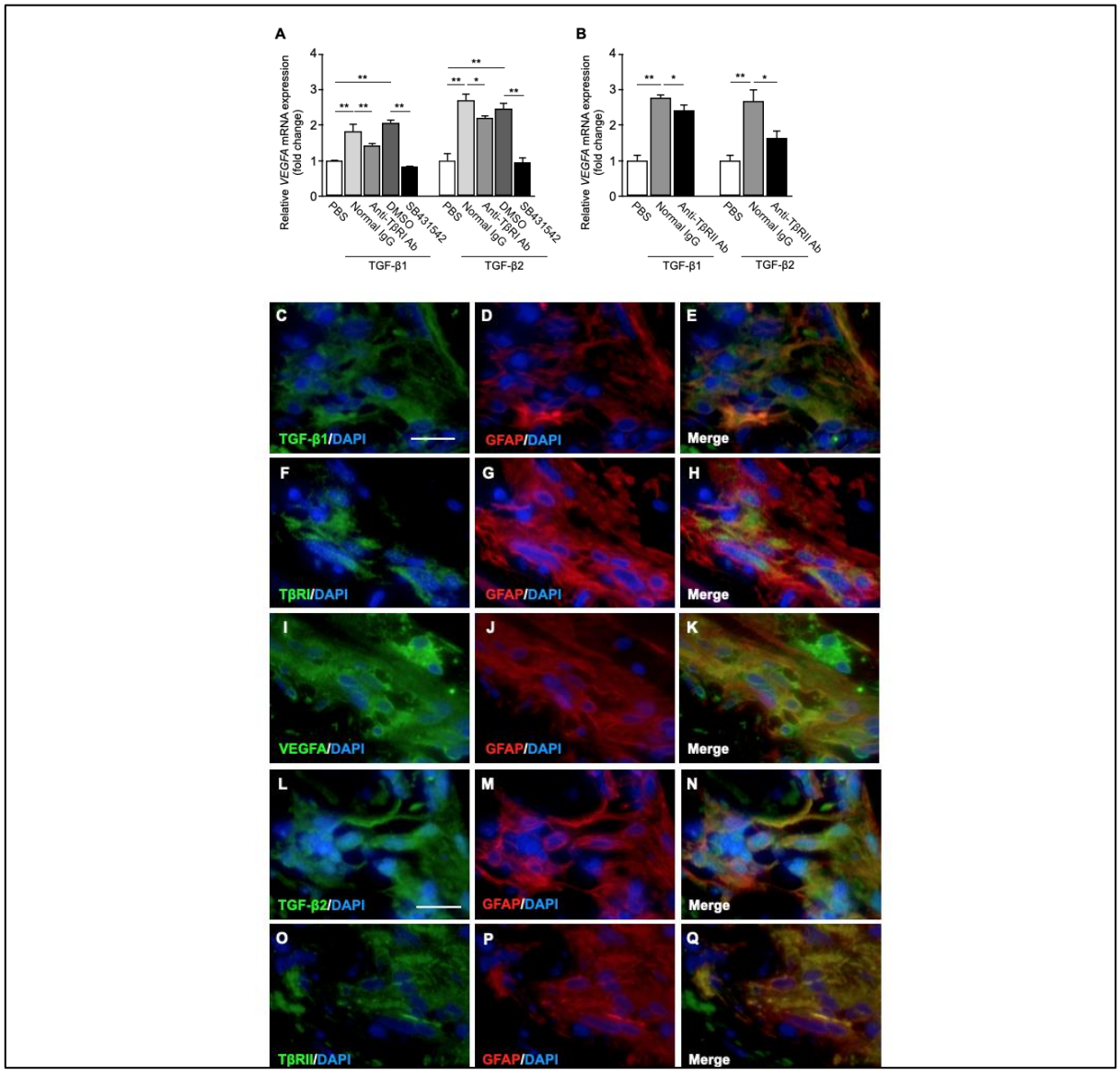

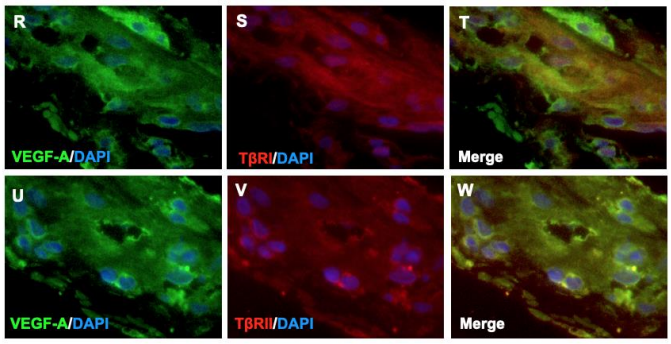

Figure 32. TGF-β1 and TGF-β2 upregulate the expression of *VEGFA* via TβR. (A, B) Müller glial cells were pre-treated with normal IgG (1 mg/ml), anti-TβRI antibody (300 ng/ml), TβRI kinase inhibitor SB431542 (10 μg/ml), or anti-TβRII antibody (250 ng/ml) for 30 minutes followed by treatment with TGF-β1 or TGF-β2 (30 ng/ml) for 24 hours, and *VEGFA* mRNA expression levels were analyzed. n = 3, $*P < 0.05$, $**P < 0.01$. (C-W) Double labeling of TGF-β1 (*green*) and GFAP (*red*) (C-E), TβRI (*green*) and GFAP (*red*) (F-H), VEGF-A (*green*) and GFAP (*red*) (I-K), TGF-β2 (*green*) and GFAP (*red*) (L-N), TβRII (*green*) and GFAP (*red*) (O-Q), VEGF-A (*green*) and TβRII (*red*) (R-T) and VEGF-A (*green*) and TβRI (*red*) (U-W) in PDR fibrovascular tissues with DAPI (*blue*) counterstain to nuclei. Scale bar = 20 μm.

TGF-β1 and TGF-β2 require the activation of canonical and non-canonical signaling pathways to regulate VEGF-A secretion

TGF-β-dependent signaling regulates target gene expression through the activation of SMAD-independent (non-canonical) and -dependent (canonical) pathways (Seystahl et al., 2015; Shi and Massague, 2003; Vander Ark et al., 2018). To further determine its downstream intracellular signaling, the mRNA expression levels of *VEGFA* were evaluated after pretreatment with specific inhibitors for ERK1/2 (U0126), NF-κB (JSH-23), PI3K (LY294002), JNK (SP600125), p38 MAPK (SB203580), and GSK-3 (SB216763). TGF-β1/2-induced *VEGFA* mRNA levels were significantly reversed by PI3K and p38 MAPK inhibitors, but in contrast significantly enhanced by JNK and GSK-3 inhibitors (Fig. 33A). The siRNA-based silencing of *SMAD2* mRNA significantly suppressed TGF-β1/2-mediated upregulation of *VEGFA* transcript (Fig. 33B). Treatment with SP600125 or SB216763 alone also increased

VEGFA expression (Figs. 33C, D), indicating that the regulation of *VEGFA* transcription was positively regulated via PI3K, p38 MAPK and SMAD2, and negatively via JNK and GSK-3 in Müller glial cells.

Furthermore, we verified the impact of PI3K, p38 MAPK, and SMAD2 inhibitors on TGF-β1/2-induced VEGF-A protein levels as well (Figs. 33E, F). Importantly, the phosphorylation of AKT, p38, and SMAD2 were shown to be increased significantly following 10 minutes to 24 hours TGF-β1/2 incubation (Fig. 33G). Additionally, we examined whether TGF-β1/2-activated PI3K and p38 MAPK signaling regulate the activation of SMAD2. The blockade of p38 MAPK signaling pathway with SB203580 was reduced the phosphorylated levels of SMAD2, but not LY294002 for PI3K (Fig. 33H), suggesting a facilitatory role of p38 MAPK/SMAD2 pathways in TGF-β-induced VEGF-A expression in Müller glial cells.

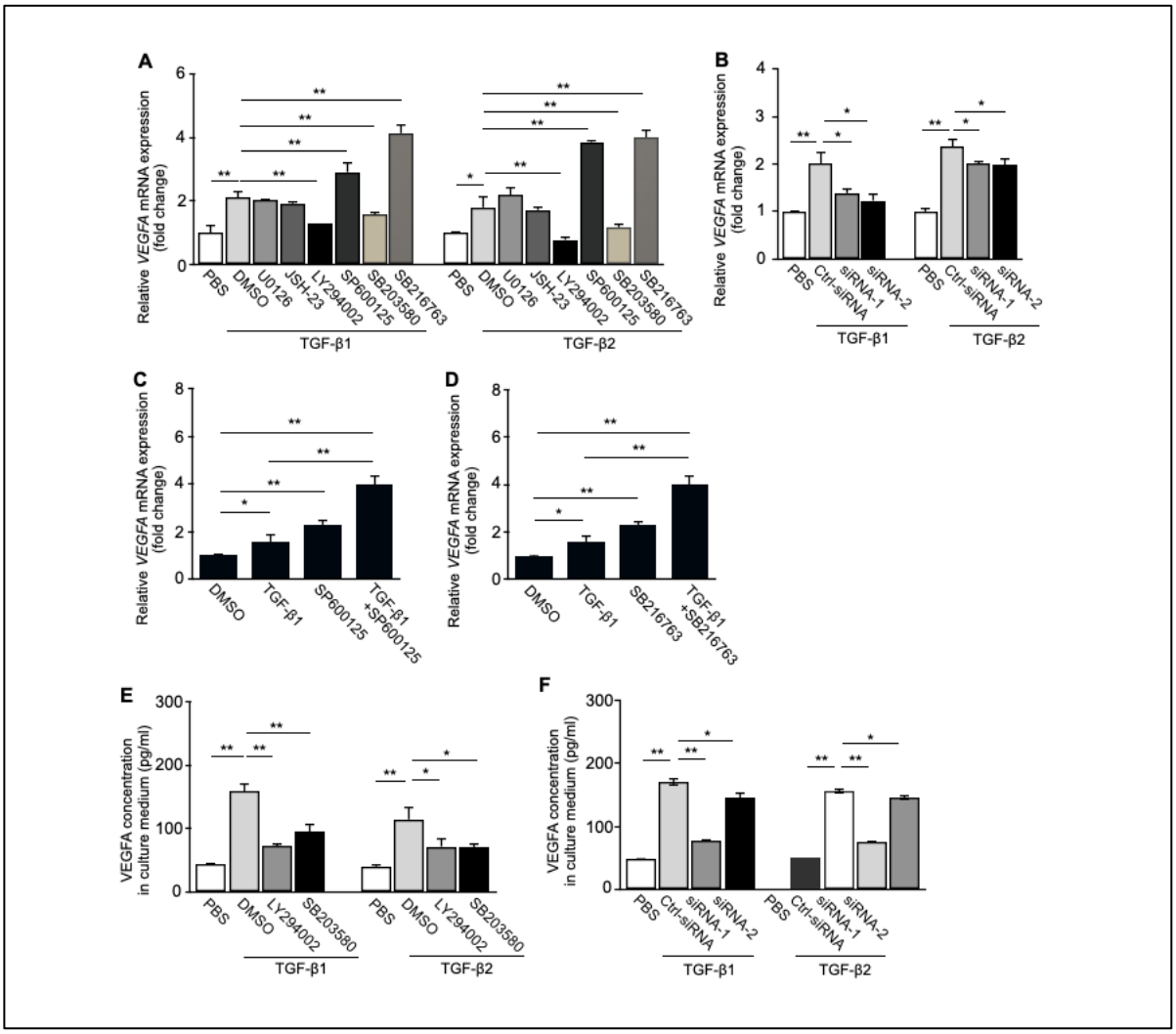

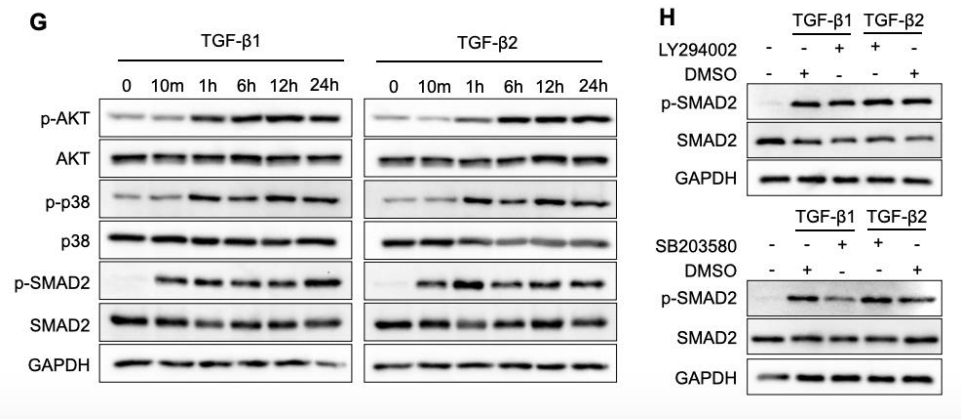

Figure 33. TGF-β1 and TGF-β2 require the activation of canonical and non-canonical signaling pathways to regulate VEGFA secretion. (A) Müller glial cells were pre-treated with each inhibitor at 10 μM for 30 minutes before cultured with TGF-β1 or TGF-β2 (30 ng/ml) for 24 hours, and *VEGFA* gene expression levels were analyzed. (B) Control siRNA-treated (Ctrl-siRNA) and *SMAD2*-knockdown (siRNA-1 and siRNA-2) Müller glial cells were stimulated with TGF-β1 or TGF-β2 (30 ng/ml) for 24 hours, and *VEGFA* gene expression levels were analyzed. (C, D) Müller glial cells were pre-treated with SP600125, SB216763 (10 μM) for 30 minutes before stimulation with or without TGF-β1 (30 ng/ml) for 24 hours, and the mRNA levels of *VEGFA* expression were analyzed. (E, F) Müller glial cells were pre-treated with each inhibitors (E), and siRNAs against *SMAD2* (F) before stimulation with TGF-β1 or TGF-β2 (30 ng/ml) for 48 hours, and protein levels of VEGF-A were analyzed. n = 3, $*P < 0.05$, $**P < 0.01$. (G) Müller glial cells were incubated with TGF-β1 or TGF-β2 (30 ng/ml) for various times, and protein levels of phosphorylated and total forms of AKT, p38 and SMAD2 were analyzed. (H) Müller glial cells were pre-treated with each inhibitor before stimulation with TGF-β1 or TGF-β2 (30 ng/ml) for 1 hours, and protein levels of phosphorylated and total forms of SMAD2 were analyzed.

TGF-β1 and TGF-β2 produce autoinduction via non-canonical pathway

Given that TGF-β activates the expression of TGF-β via multiple TβR-activated pathways in an autocrine manner in several tissues and induces the TGF-β-TβR-TGF-β vicious cycle during pathogenesis changes such as fibrosis (Dumont et al., 2003; Zhang et al., 2006), we next investigated whether the administration of TGF-β1/2 changes TGF-β production as an autocrine

manner in human Müller glial cells. TGF-β1 or TGF-β2 applications to Müller glial cells significantly elevated the mRNA levels of both *TGFB1* and *TGFB2* (Figs. 34A, B). Next, to better understand the downstream signaling pathway of TGF-β1 and TGF-β2 autocrine, we studied the mRNA expression levels of *TGFB1* and *TGFB2* after pretreatment with various potential signaling pathway inhibitors. The upregulated mRNA expression levels of *TGFB1* and *TGFB2* were significantly reduced by NF-κB, p38 MAPK, and GSK-3 inhibitors (Figs. 34C, D), whereas the PI3K inhibitor enhanced its expression. Inhibition of PI3K synergistically increased TGF-β1/2-induced *TGFB1* and *TGFB2* expression (Figs. 34E, F). Interestingly, silencing *SMAD2* did not cancel TGF-β1-induced *TGFB1* and *TGFB2* expression (Figs. 34G, 4H). In addition to the increase of phosphorylated p38 (Fig. 33G), the phosphorylation of NF-κB and GSK-3α/β were shown to be increased (peak at 6 hours or later) following 10 minutes to 24 hours of TGF-β1/2 treatment (Fig. 34 I).

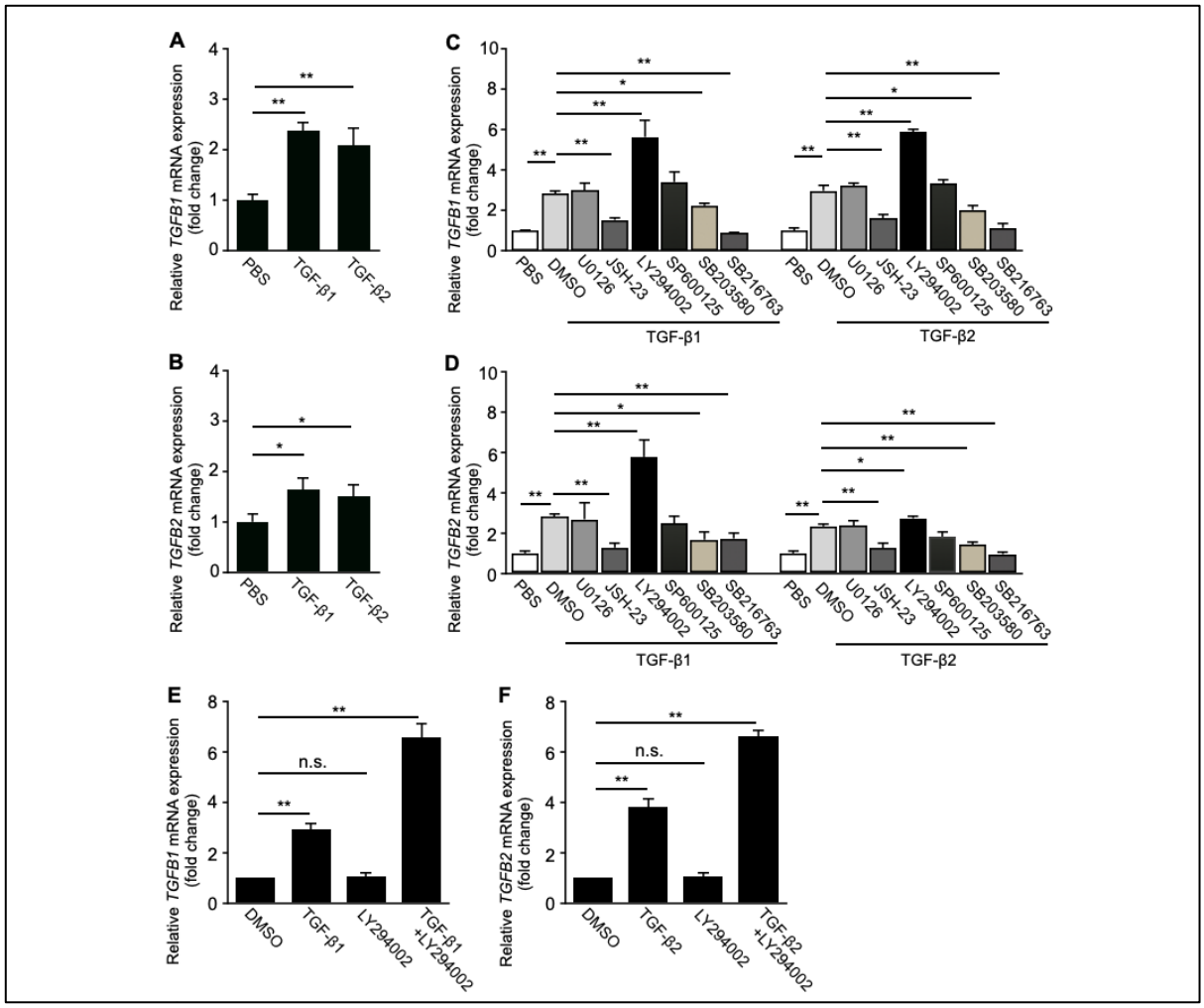

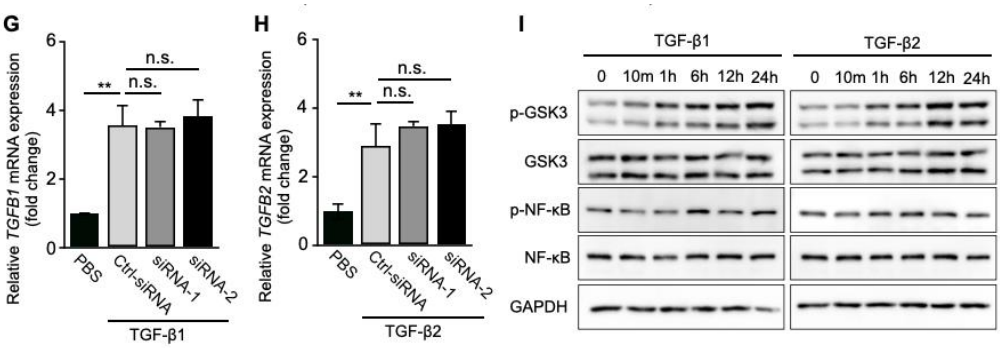

Figure 34. TGF-β1 and TGF-β2 produce autoinduction via non-canonical pathway. (A-D) Müller glial cells were pre-treated with each inhibitor at 10 μM for 30 minutes before cultured with TGF-β1 or TGF-β2 (30 ng/ml) for 24 hours, and *TGFB1* or *TGFB2* gene expression levels were analyzed. (E, F) Müller glial cells were pre-treated with LY294002 (10 μM) for 30 minutes before stimulation with or without TGF-β1 or TGF-β2 (30 ng/ml) for 24 hours, and the mRNA levels of *TGFB1* and *TGFB2* expression were analyzed. (G, H) Control siRNA-treated (Ctrl-siRNA) and *SMAD2*-knockdown (siRNA-1 and siRNA-2) Müller glial cells were stimulated with TGF-β1 or TGF-β2, and *TGFB1* and *TGFB2* gene expression levels were analyzed. n = 3, **P* < 0.05, ***P* < 0.01, n.s., not significant. (I) Müller glial cells were incubated with TGF-β1 or TGF-β2 for various times, and protein levels of phosphorylated and total forms of GSK-3α/β and NF-κB were analyzed.

Moreover, real-time qPCR analysis showed that mRNA levels of TGF-β receptors, *TGFBR1* and *TGFBR2* gene expression levels were increased after TGF-β1/2 stimulation (Figs. 35). These data suggest that TGF-β1 and TGF-β2 autoinduction are positively regulated by NF-κB, p38 MAPK, and GSK-3 in Müller glial cells.

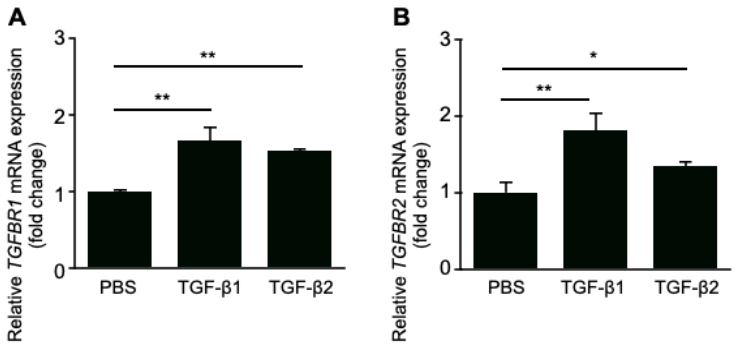

Figure 35. TGF-β1 and TGF-β2 upregulate the expression of *TGFBR1* and *TGFBR2* in Müller glial cells. (A, B) Müller glial cells were incubated with TGF-β1 or TGF-β2 (30 ng/ml) for 24 hours, and the mRNA levels of *TGFBR1* and *TGFBR2* expression were analyzed. n = 3, **P* < 0.05, ***P* < 0.01.

TGF-β induces Müller glial-mesenchymal transition in fibrovascular tissues excised from human eyes with PDR

Recently, we reported that TGF-β induces the expression of EMT-related molecules such as SM22 and α-SMA in human Müller glial cells, and leads to GMT to promote the formation of iERM, which is a vision-threatening disease characterized by fibrocellular proliferation and contraction on the inner surface of the retina (Kanda et al., 2019). To investigate the involvement of GMT in the formation of fibrovascular tissues in PDR, we carried out immunofluorescence analyses to investigate the existence of EMT-related molecular markers. Co-localization of GFAP with TβRI (Figs. 33A-C), SM22 (Figs. 33D-F), and α-SMA (Figs. 33G-I) immunoactivity were observed in serial sections from PDR patients. Supporting these results, SM22 co-localized with GS (Figs. 33J-L), a known specific Müller glial marker, indicating that TGF-β-mediated GMT promotes the formation of fibrovascular tissues in PDR patients.

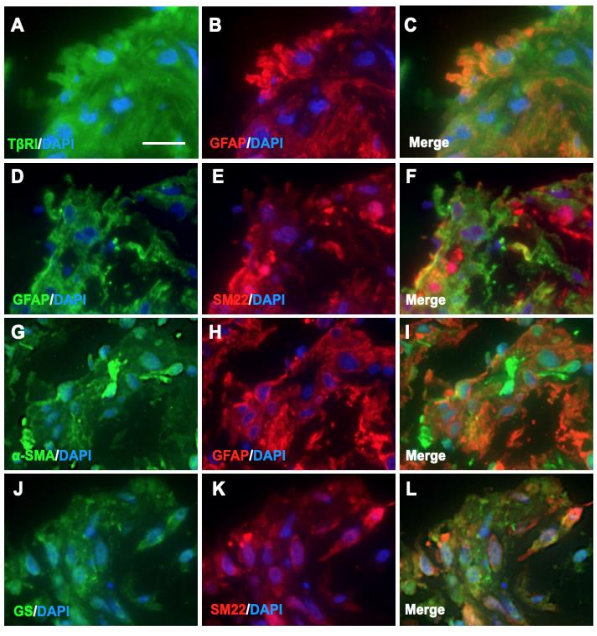

Figure 36. TGF-β induce Müller glial-mesenchymal transition fibrovascular tissues in PDR. (A-L) Double labeling of TβRI (*green*) and GFAP (*red*) (A-C), GFAP (*green*) and SAM22 (*red*) (D-F), α-SMA (*green*) and GFAP (*red*) (G-I), and GS (*green*) and SM22 (*red*) (J-L) in PDR fibrovascular tissues with DAPI (*blue*) counterstain to nuclei. Scale bar = 20 μm.

Discussion

Müller glia cells, the principal glial cell type in the retina, participate in retinal structure and homeostasis. However, dysfunction of Müller glial cells affects in the pathogenesis of various diseases as the key source of VEGF-A overproduction. Our current study presented novel data regarding the exogenous TGF-β modulates angiogenesis via VEGF-A release in Müller glial cells. Among several pro-fibrotic cytokines examined, only TGF-β1/2 application to human Müller glial cells enhanced the expression of VEGF-A via TβRI/II (Figs. 30-32). Both SMAD-independent (PI3K/AKT and p38 MAPK) and -dependent (SMAD2) pathways were involved in the TGF-β-induced VEGF-A production in Müller glial cells (Fig. 33). TGF-β1 and -β2 caused autoinduction in Müller glial cells through NF-κB, p38 MAPK, and GSK-3 signaling pathways, thereby enhancing the TGF-β1 and TGF-β2 responses (Fig. 34, 35). Immunofluorescence analyses demonstrated co-localization of TGF-β, VEGF-A and EMT-related molecular markers in GFAP- and TβRI/II-positive glial cells in fibrovascular tissues from PDR patients (Figs. 32, 36). The molecular mechanism of TGF-β1/2-induced VEGF-A production and TGF-β1/2 autoinduction via SMAD-independent and -dependent pathways plays important roles in angiogenesis and Müller GMT in the pathogenesis of PDR (Fig. 37).

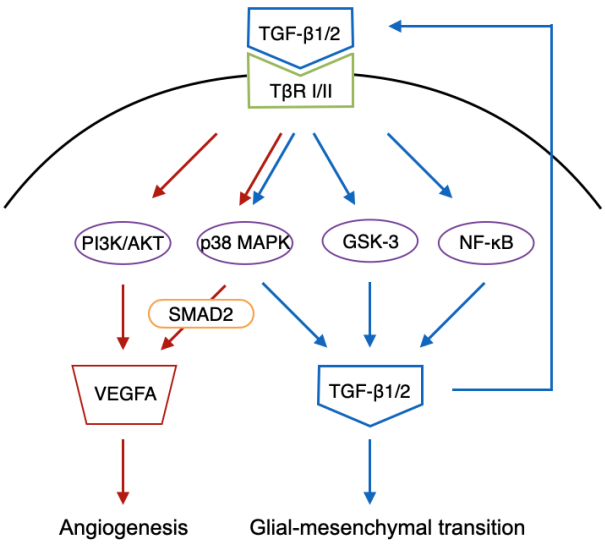

Figure 37. A schema showing the involvement of TGF-β in VEGF-A production and TGF-β autoinduction in Müller glial cells of the molecular pathogenesis of PDR.

Besides the HIF-1 regulatory mechanism of VEGF-A expression, accumulating evidence has shown that *VEGFA* mRNA expression increased through the phosphorylation of intracellular signaling pathways (*e.g.,* ERK1/2, PI3K/AKT, p38 MAPK), following to the activation of tyrosine kinase receptors including the insulin, FGF, and PDGF receptors (Chang et al., 2006; Miele et al., 2000; Willems-Widyastuti et al., 2013). The activated intracellular signaling pathways transduce the signals from the cell membrane to the nucleus, and phosphorylate various transcription factors. Subsequently, the functional transcription factors bind to the transcription factor binding sites on the *VEGFA* promoter region and induce its transcriptional activity (Pages and Pouyssegur, 2005). The TGF-β superfamily, a large number of multifunctional proteins that participate in various diverse biological processes, interacts with membrane receptors bearing serine/threonine kinase activity, and signals through many pathways. Previous reports demonstrated that the activation of TGF-β/TβR axis induces VEGF-A expression via intracellular signaling pathways (Fang et al., 2020; Qian et al., 2004; Wang et al., 2004); furthermore, TGF-β1-activated SMAD2 was revealed to directly bind to the *VEGFA* promoter region and regulate angiogenesis by increasing VEGF-A production (Clifford et al., 2008). Moreover, the TGF-β-activated SMAD-dependent signaling pathway is integrated into a complex network of cross-talk with other signaling pathways, particularly the MAPK signaling pathways (*i.e.,* ERK1/2, JNK, and p38 MAPK) (Dziembowska et al., 2007; Vander Ark et al., 2018). Consistent with previous reports, we demonstrated that TGF-β1/2, but not other pro-fibrotic molecules, induced VEGF-A expression through the activation of multiple pathways (PI3K/AKT, p38 MAPK, and SMAD2) via TβRI/II, and cross-talk between SMAD-dependent and -independent signaling pathways in Müller glial cells. Furthermore, we showed that VEGF-A was expressed in Müller glial cells and co-localized with TGF-β1/2 and TβRI/II in the fibrovascular tissue of PDR patients. Importantly, it has been reported that the protein levels of TGF-β1 and TGF-β2 in the vitreous fluid were higher in the eyes of patients with PDR than in non-diabetic control eyes, and correlated significantly with elevated vitreous VEGF-A levels (Dai et al., 2014). Supporting our findings, TβRI kinase inhibitor suppressed choroid neovascularization in the RPE-choroid complex of mice through SMAD2/VEGF-A signaling (Wang et al., 2017). The current study is the first to show the contribution of the TGF-β/TβR axis in the induction of VEGF-A expression in Müller glial cells, implying the

molecular regulation of VEGF-A by two interacting pathways necessary for retinal angiogenesis in the fibrovascular tissue of PDR.

An autoinduction mechanism of TGF-β production has been observed to induce the expression of TGF-β via its own downstream pathways, both SMAD-independent (*e.g.,* p38 MAPK and PI3K/AKT) and -dependent pathways in an autocrine manner, and to generate a vicious cycle during fibrogenesis (Dumont et al., 2003; Zhang et al., 2006). Moreover, previous reports disclosed that TGF-β induced TβR expression levels and caused a rapid increase of TβR on the cell surface by amplifying its own response, indicating that the increased levels of TβRI/II confers increased responsiveness to autocrine TGF-β signaling (Duan and Derynck, 2019). Indeed, we revealed that TGF-β1/2 induced *TGFB1/2* and *TGFBR1/2* mRNA expression levels in Müller glial cells, exhibiting detailed molecular mechanisms by TGF-β-mediated TGF-β expression via its own downstream pathways. Taken together, the paracrine or autocrine release of growth factors, including TGF-β cooperates with facilitating VEGF-A secretion in the microenvironment.

In a previous oncologic report, GMT change was first proposed in malignant glioma cells of brain astrocytic (*i.e.*, non-epithelial) origin, which exhibited irradiation-induced mesenchymal (EMT-like) features (Mahabir et al., 2014). We recently revealed that the administration of TGF-β1 to human Müller glial cells exclusively enhanced several EMT-related molecular marker expression and cell motility. Supporting our *in vitro* findings, iERM patient specimens demonstrated the tissue co-localization of TGF-β ligand-receptor system in Müller glial cells undergoing myofibroblastic differentiation with EMT-related molecules (*e.g.,* SM22 and α-SMA) expression. This implies that Müller GMT is driven by the TGF-β/TβR axis in Müller glial cells with myofibroblastic differentiation, leading to the generation of fibrocellular membrane and contraction on the inner surface of the retina (Kanda et al., 2019). The present study revealed co-localization of GFAP with TβR, SM22 and α-SMA in fibrovascular tissues from patients with PDR. Importantly, in PDR, Müller glial cells have been shown to participate in fibrovascular tissue formation (*i.e.*, fibroblastic transdifferentiation), which results in retinal traction and detachment (Guidry et al., 2003). These results suggest that activation of the TGF-β/TβR axis in Müller GMT contributes to the formation of fibrovascular tissues in PDR. Of course, other cell types such as vascular cells,

fibrocytes, and hyalocytes are involved in the origin of myofibroblasts during the fibrogenesis of PDR (Snead et al., 2008). The fibrovascular tissue surgically excised from patients with PDR showed myofibroblastic differentiation from vascular endothelial cells and fibrocytes (Abu El-Asrar et al., 2015; Tamaki et al., 2016), which can secrete various angiogenic growth factors including VEGF-A. These variety type of cells participate in the induction of neovascularization and fibrosis in PDR, leading to vitreous hemorrhage and tractional retinal detachment, both of which eventually result in irreversible vision loss in patients with PDR.

Anti-VEGF therapy has become the standard of care for the management of DR; however, DR is a complicated disorder and anti-VEGF refractory cases have been observed in clinical practice, suggesting that multiple other molecules contribute to the pathogenesis of DR. In conclusion, our previous (Kanda et al., 2019) and current findings indicate that TGF-β plays crucial roles in the pathogenesis of both VEGF-A-driven angiogenesis and Müller GMT-driven fibrovascular tissue formation in PDR, and also provide evidence that a blockade of TGF-β may be a potential therapeutic target for DR.

Summary and conclusions

Chapter I

We revealed the biological significance of galectin-1 as a key promotor for both angiogenesis and fibrosis in eyes with AMD.

Chapter II

We sought to elucidate the mechanism by which acrolein is produced in retinal glial cells with polyamine metabolism via SMOX.

Chapter III

Our data indicate that the TGF-β/TβR axis activates its downstream signal pathways in Müller glial cells, causing VEGF-A production (angiogenesis) forming the vicious cycle of TGF-β autoinduction (fibrogenesis) concurrently in DR.

Taken all together, our current studies highlight new insights on the molecular pathogenesis of CNV and DR, both of which are refractory sight-threating diseases.

Acknowledgements

I would like to express my sincere gratitude to my advisors Professor Susumu Ishida, Associate Professor Kousuke Noda, Assistant Professor Atsuhiro Kanda, and Assistant Professor Miyuki Murata, for their supervision, guidance, support and encouragement throughout my PhD period. I owe great thanks to Ikuyo Hirose and Shiho Yoshida for their kind help in the research laboratory. Throughout my study, I received very insightful and helpful ideas from my seniors, juniors in graduate school and I am sincerely grateful to them. Special thanks to my family for their continued support and encouragement. I greatly appreciate the funding received through the Otsuka Toshimi Scholarship Foundation to undertake my 2 years PhD study.

Disclosure of Conflict of Interest

The author declares no conflict of interest.

References

Abu El-Asrar, A.M., De Hertogh, G., van den Eynde, K., Alam, K., Van Raemdonck, K., Opdenakker, G., Van Damme, J., Geboes, K., and Struyf, S. (2015). Myofibroblasts in proliferative diabetic retinopathy can originate from infiltrating fibrocytes and through endothelial-to-mesenchymal transition (EndoMT). Exp Eye Res *132*, 179-189.

Adamis, A.P., Miller, J.W., Bernal, M.T., D'Amico, D.J., Folkman, J., Yeo, T.K., and Yeo, K.T. (1994). Increased vascular endothelial growth factor levels in the vitreous of eyes with proliferative diabetic retinopathy. Am J Ophthalmol *118*, 445-450.

Aiello, L.P., Avery, R.L., Arrigg, P.G., Keyt, B.A., Jampel, H.D., Shah, S.T., Pasquale, L.R., Thieme, H., Iwamoto, M.A., Park, J.E*., et al.* (1994). Vascular endothelial growth factor in ocular fluid of patients with diabetic retinopathy and other retinal disorders. N Engl J Med *331*, 1480-1487.

Aikens, D., Bunce, S., Onasch, F., Parker, R., 3rd, Hurwitz, C., and Clemans, S. (1983). The interactions between nucleic acids and polyamines. II. Protonation constants and 13C-NMR chemical shift assignments of spermidine, spermine, and homologs. Biophys Chem *17*, 67-74.

Aldini, G., Orioli, M., and Carini, M. (2011). Protein modification by acrolein: relevance to pathological conditions and inhibition by aldehyde sequestering agents. Mol Nutr Food Res *55*, 1301-1319.

Amin, R., Puklin, J.E., and Frank, R.N. (1994). Growth factor localization in choroidal neovascular membranes of age-related macular degeneration. Invest Ophthalmol Vis Sci *35*, 3178-3188.

Ashcroft, G.S., Yang, X., Glick, A.B., Weinstein, M., Letterio, J.L., Mizel, D.E., Anzano, M., Greenwell-Wild, T., Wahl, S.M., Deng, C*., et al.* (1999). Mice lacking Smad3 show accelerated wound healing and an impaired local inflammatory response. Nat Cell Biol *1*, 260-266.

Babbar, N., and Casero, R.A., Jr. (2006). Tumor necrosis factor-alpha increases reactive oxygen species by inducing spermine oxidase in human lung epithelial cells: a potential mechanism for inflammation-induced carcinogenesis. Cancer Res *66*, 11125-11130.

Biedermann, B., Skatchkov, S.N., Brunk, I., Bringmann, A., Pannicke, T., Bernstein, H.G., Faude, F., Germer, A., Veh, R., and Reichenbach, A. (1998). Spermine/spermidine is expressed by retinal glial (Muller) cells and controls distinct K+ channels of their membrane. Glia *23*, 209-220.

Bloch, S.B., Lund-Andersen, H., Sander, B., and Larsen, M. (2013). Subfoveal fibrosis in eyes with neovascular age-related macular degeneration treated with intravitreal ranibizumab. Am J Ophthalmol *156*, 116-124 e111.

Bringmann, A., Pannicke, T., Grosche, J., Francke, M., Wiedemann, P., Skatchkov, S.N., Osborne, N.N., and Reichenbach, A. (2006). Muller cells in the healthy and diseased retina. Prog Retin Eye Res *25*, 397-424.

Camby, I., Le Mercier, M., Lefranc, F., and Kiss, R. (2006). Galectin-1: a small protein with major functions. Glycobiology *16*, 137R-157R.

Cao, J., Zhao, L., Li, Y., Liu, Y., Xiao, W., Song, Y., Luo, L., Huang, D., Yancopoulos, G.D.,

Wiegand, S.J., *et al.* (2010). A subretinal matrigel rat choroidal neovascularization (CNV) model and inhibition of CNV and associated inflammation and fibrosis by VEGF trap. Invest Ophthalmol Vis Sci *51*, 6009-6017.

Casero, R.A., and Pegg, A.E. (2009). Polyamine catabolism and disease. Biochem J *421*, 323-338.

Cervelli, M., Bellavia, G., Fratini, E., Amendola, R., Polticelli, F., Barba, M., Federico, R., Signore, F., Gucciardo, G., Grillo, R., *et al.* (2010). Spermine oxidase (SMO) activity in breast tumor tissues and biochemical analysis of the anticancer spermine analogues BENSpm and CPENSpm. BMC Cancer *10*, 555.

Chae, Y.B., and Kim, M.M. (2014). Activation of p53 by spermine mediates induction of autophagy in HT1080 cells. Int J Biol Macromol *63*, 56-63.

Chang, H.J., Park, J.S., Kim, M.H., Hong, M.H., Kim, K.M., Kim, S.M., Shin, B.A., Ahn, B.W., and Jung, Y.D. (2006). Extracellular signal-regulated kinases and AP-1 mediate the up-regulation of vascular endothelial growth factor by PDGF in human vascular smooth muscle cells. Int J Oncol *28*, 135-141.

Chao, H.H., Chen, P.Y., Hao, W.R., Chiang, W.P., Cheng, T.H., Loh, S.H., Leung, Y.M., Liu, J.C., Chen, J.J., and Sung, L.C. (2017). Lipopolysaccharide pretreatment increases protease-activated receptor-2 expression and monocyte chemoattractant protein-1 secretion in vascular endothelial cells. J Biomed Sci *24*, 85.

Cheon, H., Yu, S.J., Yoo, D.H., Chae, I.J., Song, G.G., and Sohn, J. (2002). Increased expression of pro-inflammatory cytokines and metalloproteinase-1 by TGF-beta1 in synovial fibroblasts from rheumatoid arthritis and normal individuals. Clin Exp Immunol *127*, 547-552.

Chung, L.Y., Tang, S.J., Sun, G.H., Chou, T.Y., Yeh, T.S., Yu, S.L., and Sun, K.H. (2012). Galectin-1 promotes lung cancer progression and chemoresistance by upregulating p38 MAPK, ERK, and cyclooxygenase-2. Clin Cancer Res *18*, 4037-4047.

Clifford, R.L., Deacon, K., and Knox, A.J. (2008). Novel regulation of vascular endothelial growth factor-A (VEGF-A) by transforming growth factor (beta)1: requirement for Smads, (beta)-CATENIN, AND GSK3(beta). The Journal of biological chemistry *283*, 35337-35353.

Congdon, N., O'Colmain, B., Klaver, C.C., Klein, R., Munoz, B., Friedman, D.S., Kempen, J., Taylor, H.R., Mitchell, P., and Eye Diseases Prevalence Research, G. (2004). Causes and prevalence of visual impairment among adults in the United States. Arch Ophthalmol *122*, 477-485.

Croci, D.O., Cerliani, J.P., Dalotto-Moreno, T., Mendez-Huergo, S.P., Mascanfroni, I.D., Dergan-Dylon, S., Toscano, M.A., Caramelo, J.J., Garcia-Vallejo, J.J., Ouyang, J., *et al.* (2014). Glycosylation-dependent lectin-receptor interactions preserve angiogenesis in anti-VEGF refractory tumors. Cell *156*, 744-758.

Dai, Y., Wu, Z., Wang, F., Zhang, Z., and Yu, M. (2014). Identification of chemokines and growth factors in proliferative diabetic retinopathy vitreous. Biomed Res Int *2014*, 486386.

Daniel, E., Toth, C.A., Grunwald, J.E., Jaffe, G.J., Martin, D.F., Fine, S.L., Huang, J., Ying, G.S., Hagstrom, S.A., Winter, K., *et al.* (2014). Risk of scar in the comparison of age-related macular degeneration treatments trials. Ophthalmology *121*, 656-666.

DeJarnett, N., Conklin, D.J., Riggs, D.W., Myers, J.A., O'Toole, T.E., Hamzeh, I., Wagner, S., Chugh, A., Ramos, K.S., Srivastava, S.*, et al.* (2014). Acrolein exposure is associated with increased cardiovascular disease risk. J Am Heart Assoc *3*.

Del Rio, B., Redruello, B., Linares, D.M., Ladero, V., Ruas-Madiedo, P., Fernandez, M., Martin, M.C., and Alvarez, M.A. (2018). Spermine and spermidine are cytotoxic towards intestinal cell cultures, but are they a health hazard at concentrations found in foods? Food Chem *269*, 321-326.

Dong, Y., Noda, K., Murata, M., Yoshida, S., Saito, W., Kanda, A., and Ishida, S. (2017). Localization of Acrolein-Lysine Adduct in Fibrovascular Tissues of Proliferative Diabetic Retinopathy. Curr Eye Res *42*, 111-117.

Duan, D., and Derynck, R. (2019). Transforming growth factor-beta (TGF-beta)-induced up-regulation of TGF-beta receptors at the cell surface amplifies the TGF-beta response. J Biol Chem *294*, 8490-8504.

Dumont, N., Bakin, A.V., and Arteaga, C.L. (2003). Autocrine transforming growth factor-beta signaling mediates Smad-independent motility in human cancer cells. J Biol Chem *278*, 3275-3285.

Dziembowska, M., Danilkiewicz, M., Wesolowska, A., Zupanska, A., Chouaib, S., and Kaminska, B. (2007). Cross-talk between Smad and p38 MAPK signalling in transforming growth factor beta signal transduction in human glioblastoma cells. Biochemical and biophysical research communications *354*, 1101-1106.

Elad-Sfadia, G., Haklai, R., Ballan, E., Gabius, H.J., and Kloog, Y. (2002). Galectin-1 augments Ras activation and diverts Ras signals to Raf-1 at the expense of phosphoinositide 3-kinase. J Biol Chem *277*, 37169-37175.

Fang, L., Li, Y., Wang, S., Li, Y., Chang, H.M., Yi, Y., Yan, Y., Thakur, A., Leung, P.C.K., Cheng, J.C.*, et al.* (2020). TGF-β1 induces VEGF expression in human granulosa-lutein cells: a potential mechanism for the pathogenesis of ovarian hyperstimulation syndrome. Experimental & molecular medicine *52*, 450-460.

Feroe, A.G., Attanasio, R., and Scinicariello, F. (2016). Acrolein metabolites, diabetes and insulin resistance. Environ Res *148*, 1-6.

Ferris, F.L., 3rd, Fine, S.L., and Hyman, L. (1984). Age-related macular degeneration and blindness due to neovascular maculopathy. Arch Ophthalmol *102*, 1640-1642.

Finger, R.P., Fimmers, R., Holz, F.G., and Scholl, H.P. (2011). Incidence of blindness and severe visual impairment in Germany: projections for 2030. Invest Ophthalmol Vis Sci *52*, 4381-4389.

Forsythe, J.A., Jiang, B.H., Iyer, N.V., Agani, F., Leung, S.W., Koos, R.D., and Semenza, G.L. (1996). Activation of vascular endothelial growth factor gene transcription by hypoxia-inducible factor 1. Mol Cell Biol *16*, 4604-4613.

Friedlander, M. (2007). Fibrosis and diseases of the eye. J Clin Invest *117*, 576-586.

Gawandi, V., and Fitzpatrick, P.F. (2007). The synthesis of deuterium-labeled spermine, N-acetylspermine and N-acetylspermidine. J Labelled Comp Radiopharm *50*, 666-670.

Goodwin, A.C., Jadallah, S., Toubaji, A., Lecksell, K., Hicks, J.L., Kowalski, J., Bova, G.S., De Marzo, A.M., Netto, G.J., and Casero, R.A., Jr. (2008). Increased spermine oxidase expression in human prostate cancer and prostatic intraepithelial neoplasia tissues. Prostate *68*, 766-772.

Guidry, C., Bradley, K.M., and King, J.L. (2003). Tractional force generation by human muller cells: growth factor responsiveness and integrin receptor involvement. Invest Ophthalmol Vis Sci *44*, 1355-1363.

Guidry, C., King, J.L., and Mason, J.O., 3rd (2009). Fibrocontractive Muller cell phenotypes in proliferative diabetic retinopathy. Invest Ophthalmol Vis Sci *50*, 1929-1939.

Heby, O. (1981). Role of polyamines in the control of cell proliferation and differentiation. Differentiation *19*, 1-20.

Hirasawa, M., Noda, K., Noda, S., Suzuki, M., Ozawa, Y., Shinoda, K., Inoue, M., Ogawa, Y., Tsubota, K., and Ishida, S. (2011). Transcriptional factors associated with epithelial-mesenchymal transition in choroidal neovascularization. Mol Vis *17*, 1222-1230.

Hong, S.K., Chaturvedi, R., Piazuelo, M.B., Coburn, L.A., Williams, C.S., Delgado, A.G., Casero, R.A., Jr., Schwartz, D.A., and Wilson, K.T. (2010). Increased expression and cellular localization of spermine oxidase in ulcerative colitis and relationship to disease activity. Inflamm Bowel Dis *16*, 1557-1566.

Hsieh, S.H., Ying, N.W., Wu, M.H., Chiang, W.F., Hsu, C.L., Wong, T.Y., Jin, Y.T., Hong, T.M., and Chen, Y.L. (2008). Galectin-1, a novel ligand of neuropilin-1, activates VEGFR-2 signaling and modulates the migration of vascular endothelial cells. Oncogene *27*, 3746-3753.

Huang, Y.J., Jin, M.H., Pi, R.B., Zhang, J.J., Ouyang, Y., Chao, X.J., Chen, M.H., Liu, P.Q., Yu, J.C., Ramassamy, C*., et al.* (2013). Acrolein induces Alzheimer's disease-like pathologies in vitro and in vivo. Toxicol Lett *217*, 184-191.

Ip, M.S., Domalpally, A., Sun, J.K., and Ehrlich, J.S. (2015). Long-term effects of therapy with ranibizumab on diabetic retinopathy severity and baseline risk factors for worsening retinopathy. Ophthalmology *122*, 367-374.

Ishida, S., Shinoda, K., Kawashima, S., Oguchi, Y., Okada, Y., and Ikeda, E. (2000). Coexpression of VEGF receptors VEGF-R2 and neuropilin-1 in proliferative diabetic retinopathy. Invest Ophthalmol Vis Sci *41*, 1649-1656.

Ishida, S., Usui, T., Yamashiro, K., Kaji, Y., Amano, S., Ogura, Y., Hida, T., Oguchi, Y., Ambati, J., Miller, J.W*., et al.* (2003). VEGF164-mediated inflammation is required for pathological, but not physiological, ischemia-induced retinal neovascularization. J Exp Med *198*, 483-489.

Ishikawa, K., Kannan, R., and Hinton, D.R. (2016). Molecular mechanisms of subretinal fibrosis in age-related macular degeneration. Exp Eye Res *142*, 19-25.

Iwanishi, H., Fujita, N., Tomoyose, K., Okada, Y., Yamanaka, O., Flanders, K.C., and Saika, S. (2016). Inhibition of development of laser-induced choroidal neovascularization with suppression of infiltration of macrophages in Smad3-null mice. Lab Invest *96*, 641-651.

Jiang, S.J., Hsu, S.Y., Deng, C.R., Huang, H.C., Liu, S.L., Shi, G.Y., and Wu, H.L. (2013). Dextromethorphan attenuates LPS-induced adhesion molecule expression in human endothelial cells. Microcirculation *20*, 190-201.

Kalluri, R., and Weinberg, R.A. (2009). The basics of epithelial-mesenchymal transition. J Clin Invest *119*, 1420-1428.

Kanda, A., Dong, Y., Noda, K., Saito, W., and Ishida, S. (2017). Advanced glycation endproducts link inflammatory cues to upregulation of galectin-1 in diabetic retinopathy. Sci Rep *7*, 16168.

Kanda, A., Hirose, I., Noda, K., Murata, M., and Ishida, S. (2020). Glucocorticoid-transactivated TSC22D3 attenuates hypoxia- and diabetes-induced Muller glial galectin-1 expression via HIF-1alpha destabilization. Journal of cellular and molecular medicine *24*, 4589-4599.

Kanda, A., Noda, K., Hirose, I., and Ishida, S. (2019). TGF-beta-SNAIL axis induces Muller glial-mesenchymal transition in the pathogenesis of idiopathic epiretinal membrane. Sci Rep *9*, 673.

Kanda, A., Noda, K., Saito, W., and Ishida, S. (2015). Aflibercept Traps Galectin-1, an Angiogenic Factor Associated with Diabetic Retinopathy. Sci Rep *5*, 17946.

Kaneko, S., Ueda-Yamada, M., Ando, A., Matsumura, S., Okuda-Ashitaka, E., Matsumura, M., Uyama, M., and Ito, S. (2007). Cytotoxic effect of spermine on retinal pigment epithelial cells. Invest Ophthalmol Vis Sci *48*, 455-463.

Kathiriya, J.J., Nakra, N., Nixon, J., Patel, P.S., Vaghasiya, V., Alhassani, A., Tian, Z., Allen-Gipson, D., and Dave, V. (2017). Galectin-1 inhibition attenuates profibrotic signaling in hypoxia-induced pulmonary fibrosis. Cell Death Discov *3*, 17010.

Kim, I., Moon, S.O., Kim, S.H., Kim, H.J., Koh, Y.S., and Koh, G.Y. (2001). Vascular endothelial growth factor expression of intercellular adhesion molecule 1 (ICAM-1), vascular cell adhesion molecule 1 (VCAM-1), and E-selectin through nuclear factor-kappa B activation in endothelial cells. J Biol Chem *276*, 7614-7620.

Koberlein, J., Beifus, K., Schaffert, C., and Finger, R.P. (2013). The economic burden of visual impairment and blindness: a systematic review. BMJ Open *3*, e003471.

Kuiper, E.J., Van Nieuwenhoven, F.A., de Smet, M.D., van Meurs, J.C., Tanck, M.W., Oliver, N., Klaassen, I., Van Noorden, C.J., Goldschmeding, R., and Schlingemann, R.O. (2008). The angio-fibrotic switch of VEGF and CTGF in proliferative diabetic retinopathy. PLoS One *3*, e2675.

Lamouille, S., Xu, J., and Derynck, R. (2014). Molecular mechanisms of epithelial-mesenchymal transition. Nat Rev Mol Cell Biol *15*, 178-196.

Lasbury, M.E., Merali, S., Durant, P.J., Tschang, D., Ray, C.A., and Lee, C.H. (2007). Polyamine-mediated apoptosis of alveolar macrophages during Pneumocystis pneumonia. J Biol Chem *282*, 11009-11020.

Le, Y.Z. (2017). VEGF production and signaling in Muller glia are critical to modulating vascular function and neuronal integrity in diabetic retinopathy and hypoxic retinal vascular diseases. Vision Res *139*, 108-114.

Li, C., Miao, X., Li, F., Wang, S., Liu, Q., Wang, Y., and Sun, J. (2017). Oxidative Stress-Related Mechanisms and Antioxidant Therapy in Diabetic Retinopathy. Oxid Med Cell Longev *2017*, 9702820.

Lim, M.J., Ahn, J., Yi, J.Y., Kim, M.H., Son, A.R., Lee, S.L., Lim, D.S., Kim, S.S., Kang, M.A., Han, Y.*, et al.* (2014). Induction of galectin-1 by TGF-beta1 accelerates fibrosis through enhancing nuclear retention of Smad2. Exp Cell Res *326*, 125-135.

Limb, G.A., Salt, T.E., Munro, P.M., Moss, S.E., and Khaw, P.T. (2002). In vitro characterization of a spontaneously immortalized human Muller cell line (MIO-M1). Invest Ophthalmol Vis Sci *43*, 864-869.

Liu, C.H., Wang, Z., Sun, Y., and Chen, J. (2017). Animal models of ocular angiogenesis: from development to pathologies. FASEB J *31*, 4665-4681.

Liu, F., Saul, A.B., Pichavaram, P., Xu, Z., Rudraraju, M., Somanath, P.R., Smith, S.B., Caldwell, R.B., and Narayanan, S.P. (2020). Pharmacological Inhibition of Spermine Oxidase Reduces Neurodegeneration and Improves Retinal Function in Diabetic Mice. J Clin Med *9*.

Liu, S.C., Chuang, S.M., Hsu, C.J., Tsai, C.H., Wang, S.W., and Tang, C.H. (2014). CTGF increases vascular endothelial growth factor-dependent angiogenesis in human synovial fibroblasts by increasing miR-210 expression. Cell Death Dis *5*, e1485.

Loureiro, R.M., and D'Amore, P.A. (2005). Transcriptional regulation of vascular endothelial growth factor in cancer. Cytokine & growth factor reviews *16*, 77-89.

Mahabir, R., Tanino, M., Elmansuri, A., Wang, L., Kimura, T., Itoh, T., Ohba, Y., Nishihara, H., Shirato, H., Tsuda, M.*, et al.* (2014). Sustained elevation of Snail promotes glial-mesenchymal transition after irradiation in malignant glioma. Neuro Oncol *16*, 671-685.

Marhoffer, W., Stein, M., Schleinkofer, L., and Federlin, K. (1994). Monitoring of polymorphonuclear leukocyte functions in diabetes mellitus--a comparative study of conventional radiometric function tests and low-light imaging systems. J Biolumin Chemilumin *9*, 165-170.

Marumo, T., Schini-Kerth, V.B., and Busse, R. (1999). Vascular endothelial growth factor activates nuclear factor-kappaB and induces monocyte chemoattractant protein-1 in bovine retinal endothelial cells. Diabetes *48*, 1131-1137.

Massague, J. (1998). TGF-beta signal transduction. Annu Rev Biochem *67*, 753-791.

Miele, C., Rochford, J.J., Filippa, N., Giorgetti-Peraldi, S., and Van Obberghen, E. (2000). Insulin and insulin-like growth factor-I induce vascular endothelial growth factor mRNA expression via different signaling pathways. J Biol Chem *275*, 21695-21702.

Miller, J.W., Le Couter, J., Strauss, E.C., and Ferrara, N. (2013). Vascular endothelial growth factor a in intraocular vascular disease. Ophthalmology *120*, 106-114.

Murata, M., Noda, K., Kawasaki, A., Yoshida, S., Dong, Y., Saito, M., Dong, Z., Ando, R., Mori, S., Saito, W.*, et al.* (2017). Soluble Vascular Adhesion Protein-1 Mediates Spermine Oxidation as Semicarbazide-Sensitive Amine Oxidase: Possible Role in Proliferative Diabetic Retinopathy. Curr Eye Res *42*, 1674-1683.

Murata, M., Noda, K., Yoshida, S., Saito, M., Fujiya, A., Kanda, A., and Ishida, S. (2019). Unsaturated Aldehyde Acrolein Promotes Retinal Glial Cell Migration. Invest Ophthalmol Vis Sci *60*, 4425-4435.

Narayanan, S.P., Shosha, E., and C, D.P. (2019). Spermine oxidase: A promising therapeutic target for neurodegeneration in diabetic retinopathy. Pharmacol Res *147*, 104299.

Nicoletti, R., Venza, I., Ceci, G., Visalli, M., Teti, D., and Reibaldi, A. (2003). Vitreous polyamines spermidine, putrescine, and spermine in human proliferative disorders of the retina. Br J Ophthalmol *87*, 1038-1042.

Niwa, H., Yamamura, K., and Miyazaki, J. (1991). Efficient selection for high-expression transfectants with a novel eukaryotic vector. Gene *108*, 193-199.

Noda, K., Ishida, S., Shinoda, H., Koto, T., Aoki, T., Tsubota, K., Oguchi, Y., Okada, Y., and Ikeda, E. (2005). Hypoxia induces the expression of membrane-type 1 matrix metalloproteinase in retinal glial cells. Invest Ophthalmol Vis Sci *46*, 3817-3824.

Nork, T.M., Wallow, I.H., Sramek, S.J., and Anderson, G. (1987). Muller's cell involvement in proliferative diabetic retinopathy. Arch Ophthalmol *105*, 1424-1429.

O'Connor, J.W., and Gomez, E.W. (2014). Biomechanics of TGFbeta-induced epithelial-mesenchymal transition: implications for fibrosis and cancer. Clin Transl Med *3*, 23.

Ohira, A., and de Juan, E., Jr. (1990). Characterization of glial involvement in proliferative diabetic retinopathy. Ophthalmologica *201*, 187-195.

Pages, G., and Pouyssegur, J. (2005). Transcriptional regulation of the Vascular Endothelial Growth Factor gene--a concert of activating factors. Cardiovascular research *65*, 564-573.

Pegg, A.E. (2013). Toxicity of polyamines and their metabolic products. Chem Res Toxicol *26*, 1782-1800.

Penn, J.S., Madan, A., Caldwell, R.B., Bartoli, M., Caldwell, R.W., and Hartnett, M.E. (2008). Vascular endothelial growth factor in eye disease. Prog Retin Eye Res *27*, 331-371.

Piek, E., Ju, W.J., Heyer, J., Escalante-Alcalde, D., Stewart, C.L., Weinstein, M., Deng, C., Kucherlapati, R., Bottinger, E.P., and Roberts, A.B. (2001). Functional characterization of transforming growth factor beta signaling in Smad2- and Smad3-deficient fibroblasts. J Biol Chem *276*, 19945-19953.

Pignatti, C., Tantini, B., Stefanelli, C., and Flamigni, F. (2004). Signal transduction pathways linking polyamines to apoptosis. Amino Acids *27*, 359-365.

Praidou, A., Papakonstantinou, E., Androudi, S., Georgiadis, N., Karakiulakis, G., and Dimitrakos, S. (2011). Vitreous and serum levels of vascular endothelial growth factor and platelet-derived growth factor and their correlation in patients with non-proliferative diabetic retinopathy and clinically significant macula oedema. Acta Ophthalmol *89*, 248-254.

Qian, D., Lin, H.Y., Wang, H.M., Zhang, X., Liu, D.L., Li, Q.L., and Zhu, C. (2004). Involvement of ERK1/2 pathway in TGF-beta1-induced VEGF secretion in normal human cytotrophoblast cells. Mol Reprod Dev *68*, 198-204.

Radisavljevic, Z., Avraham, H., and Avraham, S. (2000). Vascular endothelial growth factor up-regulates ICAM-1 expression via the phosphatidylinositol 3 OH-kinase/AKT/Nitric oxide pathway and modulates migration of brain microvascular endothelial cells. J Biol Chem *275*, 20770-20774.

Ridano, M.E., Subirada, P.V., Paz, M.C., Lorenc, V.E., Stupirski, J.C., Gramajo, A.L., Luna, J.D., Croci, D.O., Rabinovich, G.A., and Sanchez, M.C. (2017). Galectin-1 expression imprints a neurovascular phenotype in proliferative retinopathies and delineates responses to anti-VEGF. Oncotarget *8*, 32505-32522.

Saiki, R., Nishimura, K., Ishii, I., Omura, T., Okuyama, S., Kashiwagi, K., and Igarashi, K. (2009). Intense correlation between brain infarction and protein-conjugated acrolein. Stroke *40*, 3356-3361.

Sakurai, E., Anand, A., Ambati, B.K., van Rooijen, N., and Ambati, J. (2003a). Macrophage depletion inhibits experimental choroidal neovascularization. Invest Ophthalmol Vis Sci *44*, 3578-3585.

Sakurai, E., Taguchi, H., Anand, A., Ambati, B.K., Gragoudas, E.S., Miller, J.W., Adamis, A.P., and Ambati, J. (2003b). Targeted disruption of the CD18 or ICAM-1 gene inhibits choroidal neovascularization. Invest Ophthalmol Vis Sci *44*, 2743-2749.

Seghieri, G., Gironi, A., Niccolai, M., Mammini, P., Alviggi, L., De Giorgio, L.A., Caselli, P., and Bartolomei, G. (1990). Serum spermidine oxidase activity in patients with insulin-dependent diabetes mellitus and microvascular complications. Acta Diabetol Lat *27*, 303-

308.
Seystahl, K., Tritschler, I., Szabo, E., Tabatabai, G., and Weller, M. (2015). Differential regulation of TGF-beta-induced, ALK-5-mediated VEGF release by SMAD2/3 versus SMAD1/5/8 signaling in glioblastoma. Neuro Oncol *17*, 254-265.
Shi, Y., and Massague, J. (2003). Mechanisms of TGF-beta signaling from cell membrane to the nucleus. Cell *113*, 685-700.
Skiest, D.J. (1999). Cytomegalovirus retinitis in the era of highly active antiretroviral therapy (HAART). Am J Med Sci *317*, 318-335.
Snead, D.R., James, S., and Snead, M.P. (2008). Pathological changes in the vitreoretinal junction 1: epiretinal membrane formation. Eye (London, England) *22*, 1310-1317.
Snezhkina, A.V., Krasnov, G.S., Lipatova, A.V., Sadritdinova, A.F., Kardymon, O.L., Fedorova, M.S., Melnikova, N.V., Stepanov, O.A., Zaretsky, A.R., Kaprin, A.D.*, et al.* (2016). The Dysregulation of Polyamine Metabolism in Colorectal Cancer Is Associated with Overexpression of c-Myc and C/EBPbeta rather than Enterotoxigenic Bacteroides fragilis Infection. Oxid Med Cell Longev *2016*, 2353560.
Sommer, A., Tielsch, J.M., Katz, J., Quigley, H.A., Gottsch, J.D., Javitt, J.C., Martone, J.F., Royall, R.M., Witt, K.A., and Ezrine, S. (1991). Racial differences in the cause-specific prevalence of blindness in east Baltimore. N Engl J Med *325*, 1412-1417.
Stevens, J.F., and Maier, C.S. (2008). Acrolein: sources, metabolism, and biomolecular interactions relevant to human health and disease. Mol Nutr Food Res *52*, 7-25.
Stone, J., Itin, A., Alon, T., Pe'er, J., Gnessin, H., Chan-Ling, T., and Keshet, E. (1995). Development of retinal vasculature is mediated by hypoxia-induced vascular endothelial growth factor (VEGF) expression by neuroglia. J Neurosci *15*, 4738-4747.
Swaroop, A., Chew, E.Y., Rickman, C.B., and Abecasis, G.R. (2009). Unraveling a multifactorial late-onset disease: from genetic susceptibility to disease mechanisms for age-related macular degeneration. Annu Rev Genomics Hum Genet *10*, 19-43.
Tamaki, K., Usui-Ouchi, A., Murakami, A., and Ebihara, N. (2016). Fibrocytes and Fibrovascular Membrane Formation in Proliferative Diabetic Retinopathy. Invest Ophthalmol Vis Sci *57*, 4999-5005.
Tang, D., Wu, Q., Zhang, J., Zhang, H., Yuan, Z., Xu, J., Chong, Y., Huang, Y., Xiong, Q., Wang, S.*, et al.* (2018). Galectin-1 expression in activated pancreatic satellite cells promotes fibrosis in chronic pancreatitis/pancreatic cancer via the TGF-beta1/Smad pathway. Oncol Rep *39*, 1347-1355.
Thijssen, V.L., Barkan, B., Shoji, H., Aries, I.M., Mathieu, V., Deltour, L., Hackeng, T.M., Kiss, R., Kloog, Y., Poirier, F.*, et al.* (2010). Tumor cells secrete galectin-1 to enhance endothelial cell activity. Cancer Res *70*, 6216-6224.
Thijssen, V.L., Postel, R., Brandwijk, R.J., Dings, R.P., Nesmelova, I., Satijn, S., Verhofstad, N., Nakabeppu, Y., Baum, L.G., Bakkers, J.*, et al.* (2006). Galectin-1 is essential in tumor angiogenesis and is a target for antiangiogenesis therapy. Proc Natl Acad Sci U S A *103*, 15975-15980.
Tomi, M., Funaki, T., Abukawa, H., Katayama, K., Kondo, T., Ohtsuki, S., Ueda, M., Obinata, M., Terasaki, T., and Hosoya, K. (2003). Expression and regulation of L-cystine transporter, system xc-, in the newly developed rat retinal Muller cell line (TR-MUL). Glia *43*, 208-217.

Tomitori, H., Usui, T., Saeki, N., Ueda, S., Kase, H., Nishimura, K., Kashiwagi, K., and Igarashi, K. (2005). Polyamine oxidase and acrolein as novel biochemical markers for diagnosis of cerebral stroke. Stroke *36*, 2609-2613.

Tsai, J.C., Goldman, C.K., and Gillespie, G.Y. (1995). Vascular endothelial growth factor in human glioma cell lines: induced secretion by EGF, PDGF-BB, and bFGF. J Neurosurg *82*, 864-873.

Tsutsumi, C., Sonoda, K.H., Egashira, K., Qiao, H., Hisatomi, T., Nakao, S., Ishibashi, M., Charo, I.F., Sakamoto, T., Murata, T.*, et al.* (2003). The critical role of ocular-infiltrating macrophages in the development of choroidal neovascularization. J Leukoc Biol *74*, 25-32.

Uehara, F., Ohba, N., and Ozawa, M. (2001). Isolation and characterization of galectins in the mammalian retina. Invest Ophthalmol Vis Sci *42*, 2164-2172.

Vander Ark, A., Cao, J., and Li, X. (2018). TGF-beta receptors: In and beyond TGF-beta signaling. Cell Signal *52*, 112-120.

Wang, G.L., Jiang, B.H., Rue, E.A., and Semenza, G.L. (1995). Hypoxia-inducible factor 1 is a basic-helix-loop-helix-PAS heterodimer regulated by cellular O2 tension. Proc Natl Acad Sci U S A *92*, 5510-5514.

Wang, J., He, C., Zhou, T., Huang, Z., Zhou, L., and Liu, X. (2016). NGF increases VEGF expression and promotes cell proliferation via ERK1/2 and AKT signaling in Muller cells. Mol Vis *22*, 254-263.

Wang, L., Kwak, J.H., Kim, S.I., He, Y., and Choi, M.E. (2004). Transforming growth factor-beta1 stimulates vascular endothelial growth factor 164 via mitogen-activated protein kinase kinase 3-p38alpha and p38delta mitogen-activated protein kinase-dependent pathway in murine mesangial cells. J Biol Chem *279*, 33213-33219.

Wang, X., Ma, W., Han, S., Meng, Z., Zhao, L., Yin, Y., Wang, Y., and Li, J. (2017). TGF-β participates choroid neovascularization through Smad2/3-VEGF/TNF-α signaling in mice with Laser-induced wet age-related macular degeneration. Scientific reports *7*, 9672.

Willbold, E., and Layer, P.G. (1998). Muller glia cells and their possible roles during retina differentiation in vivo and in vitro. Histol Histopathol *13*, 531-552.

Willems-Widyastuti, A., Vanaudenaerde, B.M., Vos, R., Dilisen, E., Verleden, S.E., De Vleeschauwer, S.I., Vaneylen, A., Mooi, W.J., de Boer, W.I., Sharma, H.S.*, et al.* (2013). Azithromycin attenuates fibroblast growth factors induced vascular endothelial growth factor via p38(MAPK) signaling in human airway smooth muscle cells. Cell Biochem Biophys *67*, 331-339.

Wong, W.L., Su, X., Li, X., Cheung, C.M., Klein, R., Cheng, C.Y., and Wong, T.Y. (2014). Global prevalence of age-related macular degeneration and disease burden projection for 2020 and 2040: a systematic review and meta-analysis. Lancet Glob Health *2*, e106-116.

Wu, D., Kanda, A., Liu, Y., Kase, S., Noda, K., and Ishida, S. (2019). Galectin-1 promotes choroidal neovascularization and subretinal fibrosis mediated via epithelial-mesenchymal transition. FASEB J *33*, 2498-2513.

Xu, F., Liu, C., Zhou, D., and Zhang, L. (2016). TGF-beta/SMAD Pathway and Its Regulation in Hepatic Fibrosis. J Histochem Cytochem *64*, 157-167.

Yamada, M., Hiratsuka, Y., Roberts, C.B., Pezzullo, M.L., Yates, K., Takano, S., Miyake, K., and Taylor, H.R. (2010). Prevalence of visual impairment in the adult Japanese population

by cause and severity and future projections. Ophthalmic Epidemiol *17*, 50-57.

Yang, N., Zhang, W., He, T., and Xing, Y. (2017). Silencing of galectin-1 inhibits retinal neovascularization and ameliorates retinal hypoxia in a murine model of oxygen-induced ischemic retinopathy. Exp Eye Res *159*, 1-15.

Zamudio, S., Wu, Y., Ietta, F., Rolfo, A., Cross, A., Wheeler, T., Post, M., Illsley, N.P., and Caniggia, I. (2007). Human placental hypoxia-inducible factor-1alpha expression correlates with clinical outcomes in chronic hypoxia in vivo. Am J Pathol *170*, 2171-2179.

Zhang, M., Fraser, D., and Phillips, A. (2006). ERK, p38, and Smad signaling pathways differentially regulate transforming growth factor-beta1 autoinduction in proximal tubular epithelial cells. Am J Pathol *169*, 1282-1293.

Zheng, L., Xu, C., Guan, Z., Su, X., Xu, Z., Cao, J., and Teng, L. (2016). Galectin-1 mediates TGF-beta-induced transformation from normal fibroblasts into carcinoma-associated fibroblasts and promotes tumor progression in gastric cancer. Am J Transl Res *8*, 1641-1658.

Zhong, H., De Marzo, A.M., Laughner, E., Lim, M., Hilton, D.A., Zagzag, D., Buechler, P., Isaacs, W.B., Semenza, G.L., and Simons, J.W. (1999). Overexpression of hypoxia-inducible factor 1alpha in common human cancers and their metastases. Cancer Res *59*, 5830-5835.

Zhong, X., Li, X., Liu, F., Tan, H., and Shang, D. (2012). Omentin inhibits TNF-alpha-induced expression of adhesion molecules in endothelial cells via ERK/NF-kappaB pathway. Biochem Biophys Res Commun *425*, 401-406.

Zozulinska, D.A., Wierusz-Wysocka, B., Wysocki, H., Majchrzak, A.E., and Wykretowicz, A. (1996). The influence of insulin-dependent diabetes mellitus (IDDM) duration on superoxide anion and hydrogen peroxide production by polymorphonuclear neutrophils. Diabetes Res Clin Pract *33*, 139-144.

Zudaire, E., Gambardella, L., Kurcz, C., and Vermeren, S. (2011). A computational tool for quantitative analysis of vascular networks. PLoS One *6*, e27385.